STABILITY ANALYSIS OF VIRTUAL SYNCHRONOUS MACHINE CONTROL STRATEGY IN POWER SYSTEM

by

MIN ZHAO

A thesis submitted to the University of Birmingham for the degree of

DOCTOR OF PHILOSOPHY

Department of Electronic, Electrical

and Systems Engineering

School of Engineering

The University of Birmingham

June 2021

Dedicated to

My Family

ACKNOWLEDGEMENT

First and foremost, I would like to express my sincere gratitude to my supervisor Prof. Xiao-Ping Zhang, for his patience, guidance and encouragement during my PhD study. His invaluable support greatly helped me to overcome the difficulties in my research period and to continue with my research. It is a great honour for me to be a student of Prof. Zhang.

I appreciate the financial support from Chinese Scholarship Council (CSC). I would like to thank Dr. Ying Xue for his inspiring academic discussions and suggestions. I would also like to express my appreciation to my colleagues Dr. Jianing Li, Dr. Hao Fu, Dr. Zuanhong Yan, Dr. Xianxian Zhao, Dr. Conghuan Yang, Dr. Rui Guan Dr. Jiajie Luo, Mr. Cong Wu, Mr. Kai Lin, Mr. Longmao Fan, Mr. Nan Chen, Miss Xin Ma and all my other colleagues in the Power and Control Group for their kind advice and assistance. It was an enjoyable experience to work with them.

Finally, I must express my greatest appreciation to my family, for their endless love and support throughout my life so far.

ABSTRACT

With massive integration of power electronic interfaced renewables including wind and solar power, one of the big challenges is the continuous reduction in power system inertia. In order to deal with this issue, virtual synchronous machine (VSM) control is proposed. Associated with such a solution, it is of great interest to know the impacts of VSM on power system stability, in particular, power system oscillations. Hence, the focus of this doctoral research work is to investigate the effects of VSM control on power system oscillations including sub-synchronous oscillations (SSO), low-frequency oscillation (LFO) and forced power oscillation.

The sub-synchronous oscillation (SSO) of wind farm with series compensated network has attracted increasing attention from researchers. Considering the potential risk of phase-locked loop (PLL) on system sub-synchronous stability, VSM control is implemented which can synchronise power converters to AC grid without PLL-related issues. The permanent magnetic synchronous generator (PMSG)-based wind farm with series-compensated network controlled by vector current control (VCC) and VSM are studied in the first section. The small signal stability and time-domain simulations are compared to show the superiority of VSM on system stability in the sub-synchronous frequency range.

Then a coordinated supplementary damping control (SDC) design for multiple VSMs is proposed to enhance system damping performance. As VSM control emulates the dynamic behaviour of traditional synchronous generator (SG), it may introduce LFO similar to the interaction between multiple SGs. The supplementary channel is added to the reactive power loop of VSM to avoid undesired mechanical vibration when prime mover power comes from a

wind turbine. The design process is based on Prony method which is utilised to obtain system modes information. The decentralised sequential design, which can reduce the dependency on communication and the adverse interactions between auxiliary controllers, is implemented to make multiple VSMs to work cooperatively.

Finally, the probability of electro-mechanical interactions between VSMs and other devices especially SGs in power system is higher because of the mentioned reason before. Besides, the renewable energy will suffer some sustained disturbances and thus is prone to exciting forced oscillation due to the resonance between natural LFO mode and external disturbances. Therefore, the impacts of VSM control on forced oscillation is investigated in the last section. The analytical results of infinite bus system with VSM and multi-machines system with VSM are explicitly conducted.

CONTENTS

LIST OF FIGURES

LIST OF TABLES

LIST OF ABBREVIATIONS

B2B	Back-to-Back
CO_2	Carbon Dioxide
DFIG	Doubly Fed Induction Generator
DG	Distributed Generation
ERA	Eigenvalue Realization Algorithm
ESS	Energy Storage System
EVs	Electric Vehicles
FACTS	Flexible AC Transmission System
FFT	Fast-Fourier-Transformation
GFL	Grid-Following
GFM	Grid-Forming
GSC	Grid Side Converter
Gt	Gigatons
HHT	Hilbert-Huang Transformation
HVAC	High Voltage Alternative Current
HVDC	High Voltage Direct Current
LCC	Line Commutated Converter
LFAC	Low Frequency AC Transmission
LFO	Low-Frequency Oscillation
LHP	Left Half Plane
MMC	Modular Multi-Level Converter
M3C	Modular Multilevel Matrix Converter
MIMO	Multi-Input-Multi-Output

MTDC	Multi-Terminal DC
PCC	Point of Common Coupling
PLL	Phase-Locked Loop
PMSG	Permanent Magnetic Synchronous Generator
PMU	Phasor Measurement Unit
PSD	Power Spectrum Density
PSS	Power System Stabiliser
PV	Photovoltaic
RHP	Right Half Plane
RSC	Rotor Side Converter
SCIB	Single Converter Infinite Bus
SDC	Supplementary Damping Control
SG	Synchronous Generator
SISO	Single-Input-Single-Output
SPC	Synchronous Power Controller
SRF	Synchronous Reference Frame
SSCI	Sub-Synchronous Controller Interaction
SSO	Sub-Synchronous Oscillation
SSR	Sub-Synchronous Resonance
SSTI	Sub-Synchronous Torsional Interaction
VCC	Vector Current Control
VPSS	Virtual PSS
VSC	Voltage Source Converter
VSM/VSG	Virtual Synchronous Machine/Generator

CHAPTER 1 INTRODUCTION

1.1 Research Background

1.1.1 The Development of Power Electronic Interfaced Devices

To pursue sustainable development of ecological environment, the carbon neutrality has been promoted to achieve net-zero carbon dioxide (CO_2) emission [1]. The greenhouse gases, especially CO_2, are mainly produced by fossil fuel combustion. As illustrated in Figure 1-1 [2, 3], there is a positive correlation between fossil fuel consumption and CO_2 emission. The recorded global annual emission of CO_2 reaches to nearly 33.5 gigatons (Gt) in 2019. And it is believed that the emission level is going to be tripled in 2040 if no positive actions are implemented [4]. Fortunately, most countries in the world, including the largest three contributors to CO_2 emission as shown in Figure 1-2 [5], have committed to propose ambitious plans to facilitate the reduction of carbon footprints. UK has set a target to reduce greenhouse gas emissions by 78% by 2035 (based on 1990 baseline) through emission reduction and removal technologies [6, 7].

Renewable energy is a promising alternative to achieve the de-carbonization objective. The penetration of green energy experiences a notable growth which can be attributed to the innovation of technologies and supportive policies from governments. Many countries worldwide have been making their utmost effort to increase the capacity of renewables in their energy structure [8]. UK has developed advanced wind generation technologies to utilise abundant wind sources and it has deployed the largest offshore wind farms in the world. The

proportion of electricity from offshore and onshore wind rises to 24% in 2020 [9]. Denmark has the highest penetration level of wind and solar power and 50% electricity is directly from these two renewable sources in 2019 [10]. In addition, a 100% renewable energy-driven community is built in Bornholm island of Denmark. This pilot project is a frontrunner to investigate the mechanisms and operation of such green transition. The global electricity

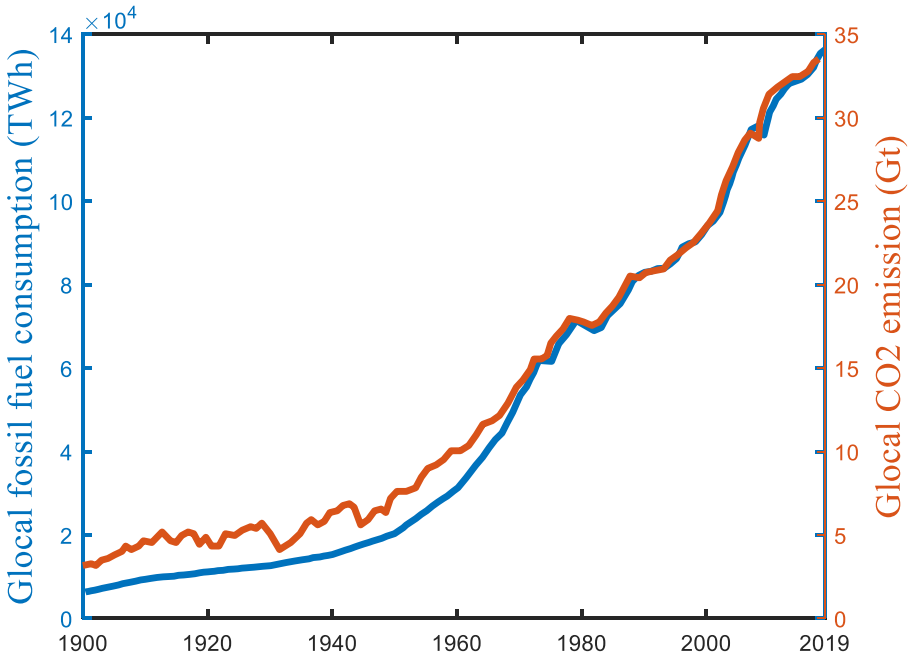

Figure 1-1 Global fossil fuel consumption and CO_2 emission [2, 3].

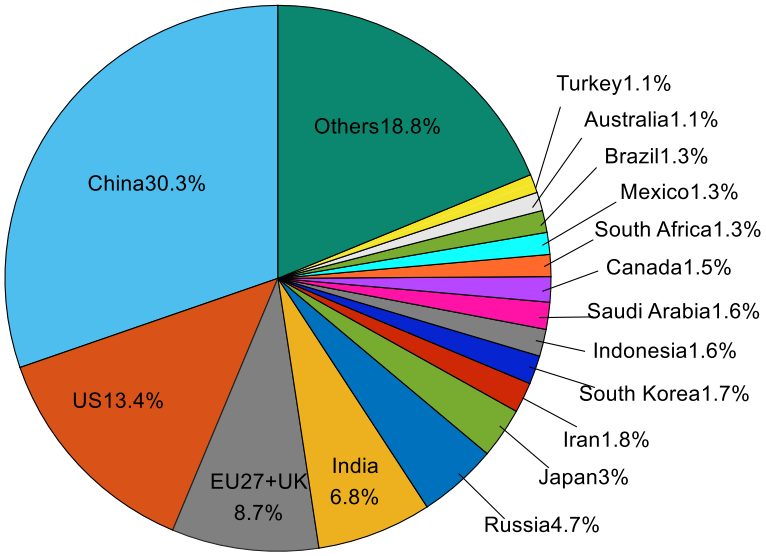

Figure 1-2. Global CO_2 emission share in 2019 [5].

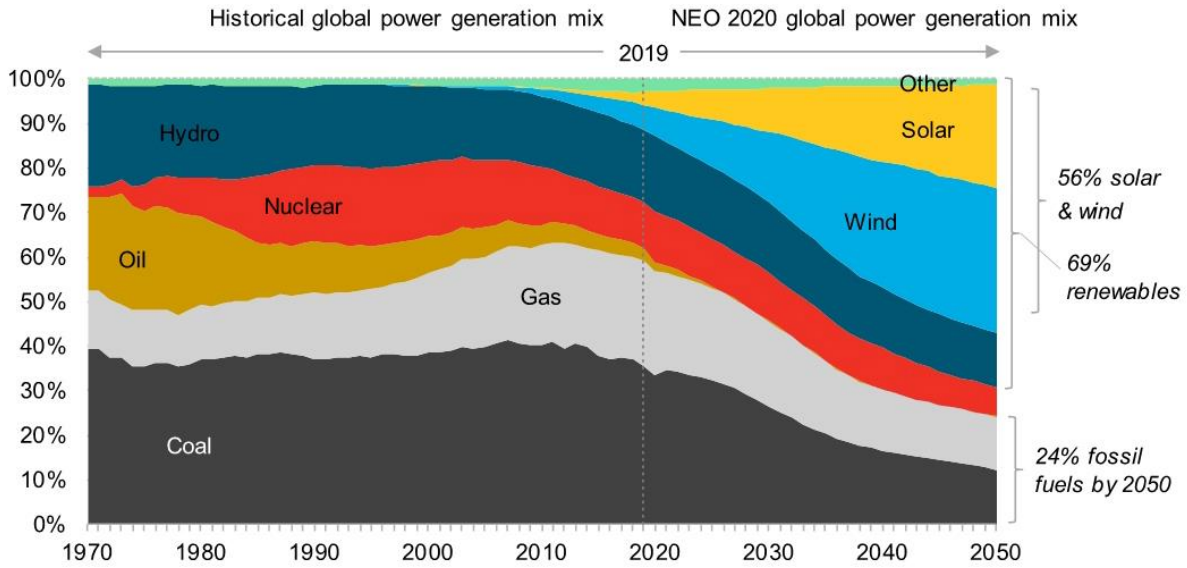

Figure 1-3. Global power generation [11].

generation is depicted in Figure 1-3. As observed in this figure, the share of power generation from renewables shows a continuous upward trend. It is also anticipated that solar and wind-powered energy constitutes more than half in the middle of this century.

Currently, most renewables are interfaced into power system based on power electronic devices. Two typical structures of wind generation, type 3 (doubly fed induction generator (DFIG)) and type 4 wind turbine generators (full size converter generator) are shown in Figure 1-4. The permanent magnetic synchronous generator (PMSG) and squirrel-cage induction generator (SCIG) are generally implemented for type 4 wind model [12, 13]. The stator of DFIG is directly connected to grid while the rotor is interfaced into network through a back-to-back (B2B) converter. The B2B converter physically decouples the turbine of type 4 wind generators and AC network. All the extracted power from wind is fed into system through the converter. Therefore, the requirement of converter capacity is usually larger than that of DFIG. Figure 1-5 illustrates the topology of two-stage photovoltaic (PV) system. The output power from solar cells is maximised through a commonly used DC-DC converter and the PV inverter exports the power to grid.

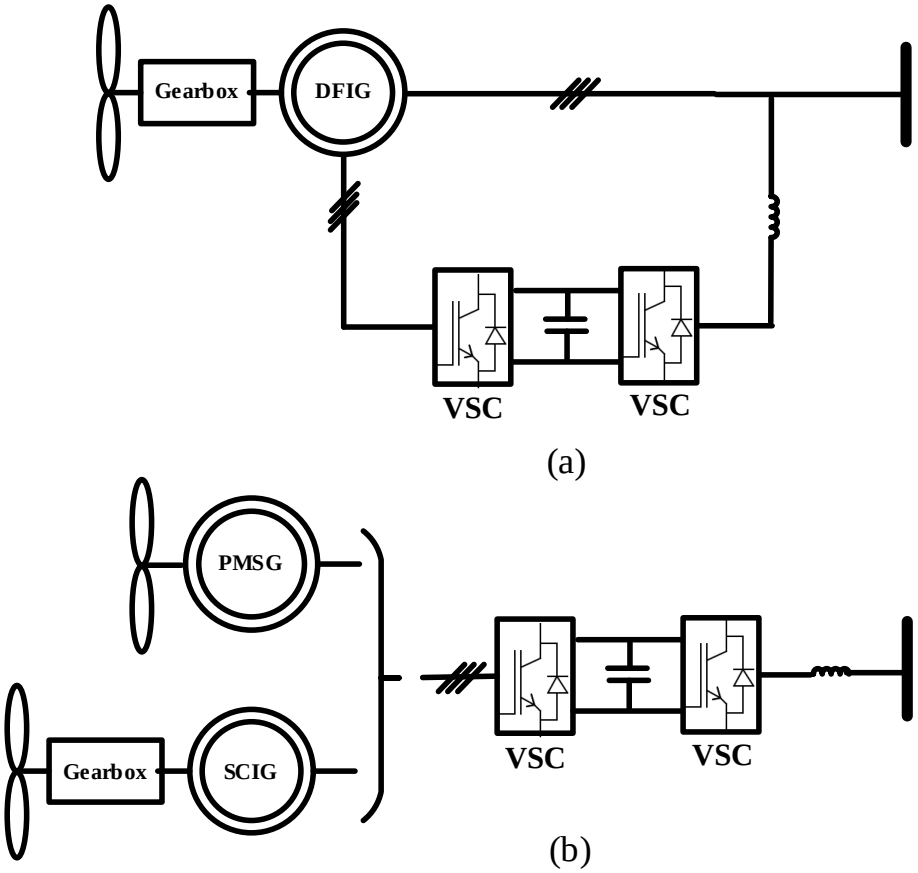

Figure 1-4. Schematic diagram of wind generation [12, 14]. (a) Type 3. (b) Type 4.

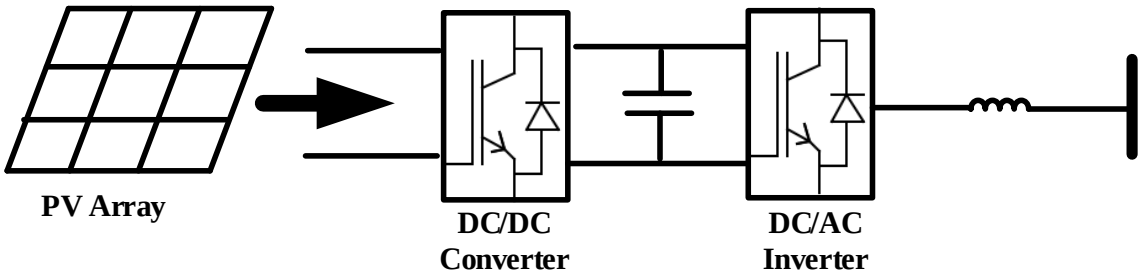

Figure 1-5 Schematic diagram of PV generation.

Apart from the structure change in generation side, more power electronics are also introduced into transmission system. Due to the disadvantages of High Voltage Alternative Current

(HVAC) transmission technologies concerning the increasing power losses and reactive compensation under long-distance transmission condition [15], more and more High Voltage Direct Current (HVDC) projects have been carried out since the first commercial application in 1954. The total HVDC projects in operation and under construction/planning by 2020 are demonstrated in Figure 1-6. The advanced controllability of Voltage Source Converter (VSC) HVDC in terms of active and reactive power makes it more preferred than Line Commutated Converter (LCC) HVDC [16]. The VSC HVDC also shows it superiority for remote offshore wind power transfer as such large wind farms are always far away from main

Description	Africa	Australia Oceania	Asia	Europe	North America	South America	Total
No. of HVDC Systems	4	5	60	69	22	5	165
In Operation	3	5	52	49	12	5	126
Refurbished/Upgraded	2	2	1	3	3	0	11
No. of LCC	3	3	51	28	17	5	107
No. of VSC	1	2	8	41	5	0	57
No. of Hybrid (LCC+VSC)	0	0	1	0	0	0	1
No. of Multi-Terminal	0	0	4	1	1	0	6
Voltage Level (kV)	350-533	80-400	30-1100	9-600	150-600	600-800	2-1100
Power Rating (MW)	300-2000	180-735	18-10000	3-2200	312-3500	3150-7100	3-10000
OHL (No./max km)	4/1700	n.a.	43/3333	1/10	12/1362	5/2439	65/3333
Cable (No./max km)	n.a.	2/176	9/134	53/740	5/248	n.a.	69/1928
OHL+Cable (No./max km)	n.a.	3/611	8/451	15/623	5/1135	n.a.	31 6.6-1100/7-570

Figure 1-6. Summary of HVDC Projects in 2020 [17].

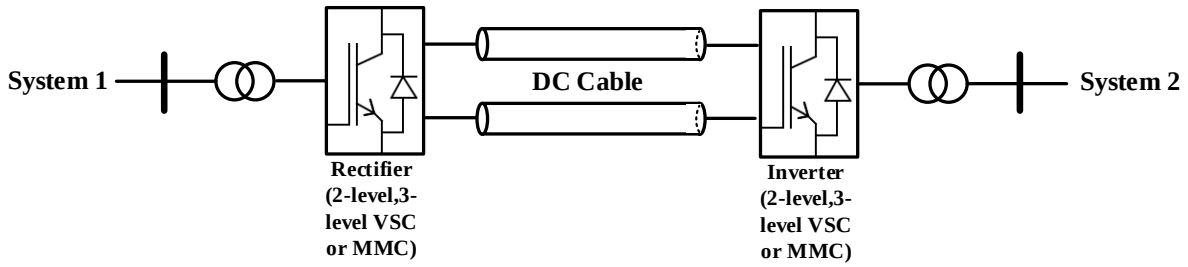

Figure 1-7. Schematic diagram of VSC HVDC.

grid and VSC HVDC can provide grid support [18, 19]. The typical topology of VSC HVDC is demonstrated in Figure 1-7 and it can be utilised to interconnect two asynchronous systems. Besides, the implementation of Flexible AC Transmission System (FACTS) is capable of strengthening network and increasing transferred power [20-22]. The development and evolution of HVDC technology also makes it viable to form a multi-terminal DC (MTDC) transmission grid. Some MTDC demonstration projects have been conducted in China [23, 24].

It is expected that massive loads like household and industrial devices will be interfaced to grid with power electronic converters in the future [25]. The incentive polices and cost reduction of electricity from renewables make transport sector less dependent on fossil fuel energy. Figure 1-8 depicts the significant growth of electric vehicles (EVs) and new passengers are more likely to buy EVs in the long term as shown in Figure 1-9. These aggregated EVs can be considered as smart loads which can be charged or discharged through power converters. Besides, distributed generation (DG) like city renewables [26] and energy storage system

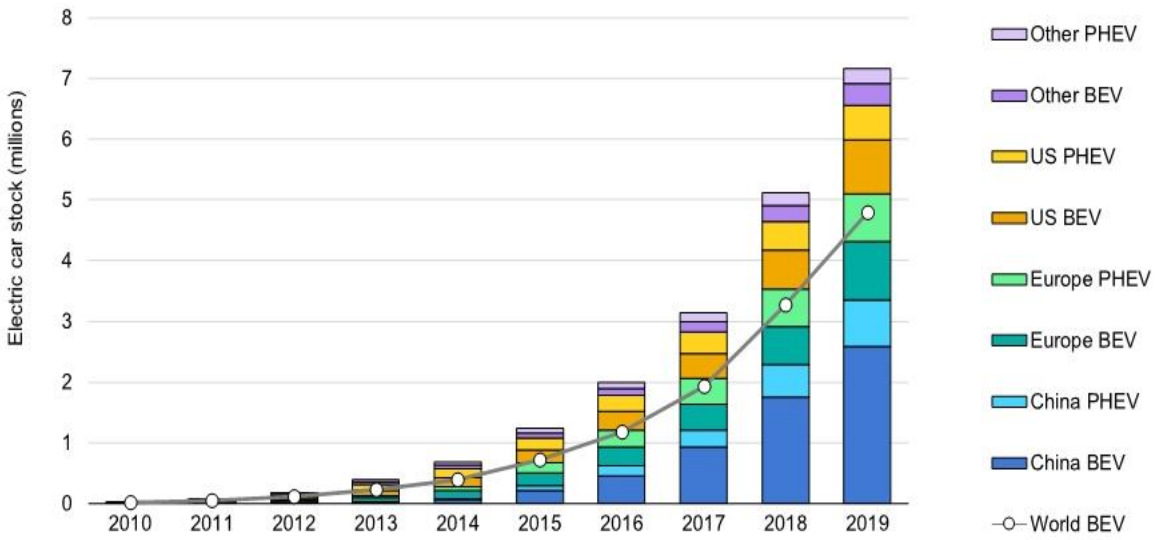

Figure 1-8. Global electric vehicle stock [27].

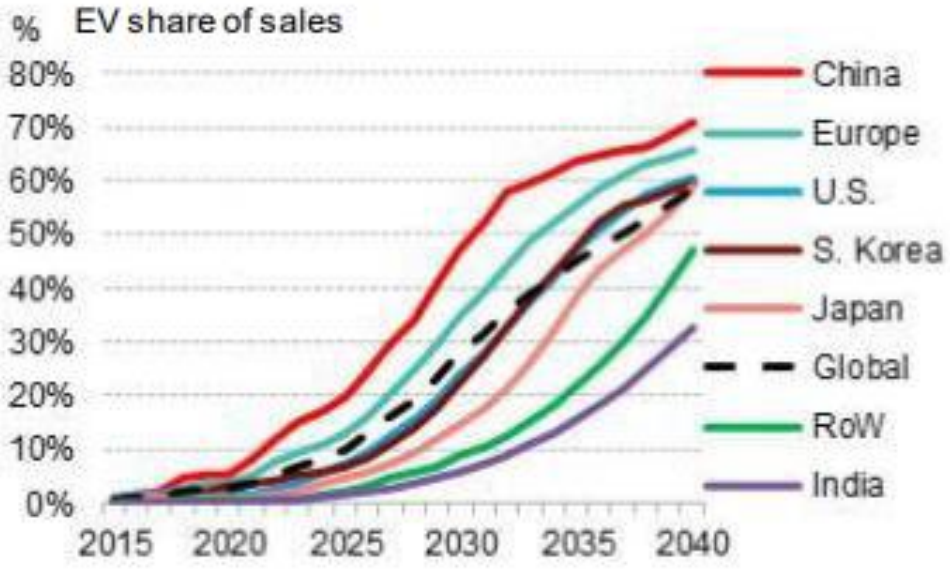

Figure 1-9. Global long-term passenger EV adoption [28].

(ESS) can be regarded as generalised flexible converter-based loads [29]. These non-conventional loads introduce changes of structure and characteristics to electrical demand.

Therefore, power grid is experiencing the transition to a power electronics dominated system from the perspectives of generation, transmission and load. However, the increasing permeability of power electronics will result in a decline of system inertia level. This leads to a weak grid caused by the phase-out of SGs [30, 31] and systems become more susceptible to disturbances. For traditional SG, the stored kinetic energy in rotor can afford reasonable inertia to resist frequency variations. The converter-interfaced units (wind and solar plants) are generally operated in a way that is independent on system frequency and they have limited contribution to system inertia [32-34]. Consequently, the inertia-less devices will degrade frequency stability and introduce large frequency excursions [35, 36]. Besides, the challenges on the rate of change of frequency (ROCOF) and frequency nadir under extreme conditions will activate protection systems more frequently which may result in load shedding and

generator trip [31, 35, 37]. The Australia system blackout in 2016 and recent UK system disruption event in August 2019 reveal that low inertia level may degrade system resilience to disturbances[33, 38]. To address these critical inadequate inertia issues, virtual synchronous machine (VSM) or virtual synchronous generator (VSG) [39, 40] control was proposed to equip converters with inertia provision capability by emulating the swing equation of traditional synchronous generator (SG). The architecture of a VSM controlled power electronic system is demonstrated in Figure 1-10.

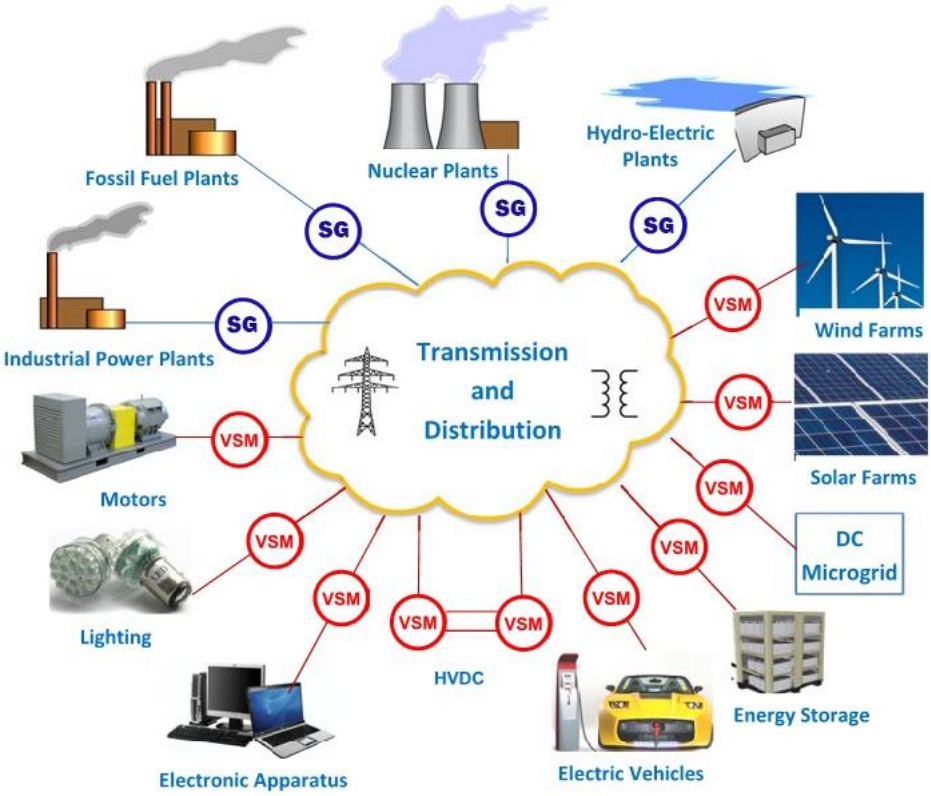

Figure 1-10. Power electronic dominated system with VSM control [41].

1.1.2 The Sub-synchronous Oscillation of Wind Farms in Series Compensated Network

The global initiative to create a low-carbon environment promotes substantial integration of renewable energy. The total worldwide installed capacity of wind generation reaches to 733.3 GW in 2020 [42]. However, renewable generations especially large-scale wind farms or solar plants are usually located in remote areas and are far away from load centre. Therefore, renewables are weakly connected to main grid. The electricity from wind and solar resources in Three-North region of China needs to be transmitted to Southeast demand centre and the transmission length is even over 3000 km [43, 44]. The great potential of wind energy from sea facilitates the development of offshore wind farms and the distance to onshore main grid is expected to be longer because of more favourable wind conditions. The distance of North Sea offshore wind plants can reach to 200 km from shore [45].

The series compensation technology is widely implemented to transmission network to improve power transfer capability which is limited by weak grid [46]. However, there is a potential risk of sub-synchronous oscillation (SSO) caused by the interaction between wind farms and series compensated network [47-52]. It is found that converter controllers take main responsibilities for this sub-synchronous controller interaction (SSCI) phenomenon. The unexpected sub-synchronous resonance from phase-locked loop (PLL) may excite SSO and such adverse effect will deteriorate system stability [49-52].

Alternatively, the power converters can be also synchronised to grid based on regulating active power, (e.g., VSM control) rather than using PLL [53]. The typical control structures of these two methodologies are depicted in Figure 1-11. Comparing to DFIG-based wind farm, PMSG-based wind farm is taking an increasingly share especially in larger offshore wind farms due to its superiority of on-grid performance and generation efficiency [54-57]. Therefore, the sub-

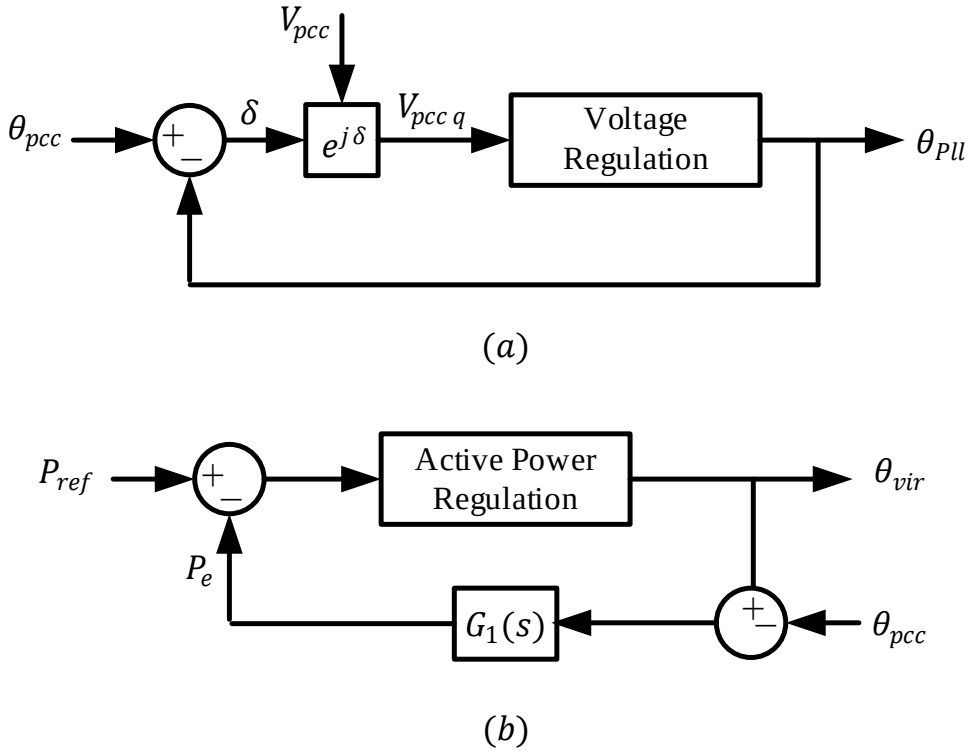

Figure 1-11. Schematic diagram of synchronization technologies. (a) Voltage-based synchronization - PLL. (b) Power-based synchronization - VSM.

synchronous stability analysis of PMSG-based wind farm with these two synchronization technologies in series compensated network should be explored.

1.1.3 The Low Frequency Oscillation in Power System

Low-frequency oscillation (LFO) is one of the main concerns in power system especially for large inter-connected areas. This inherent phenomenon in traditional power system is caused by power imbalance between SGs. When the equilibrium between electrical torque and mechanical torque is disturbed, power systems will suffer a long-period oscillation without adequate damping. The local mode (1~2Hz) includes oscillatory devices in the same area while inter-area mode (0.1~1.0 Hz) is related to coherent generator groups in different areas. The

electro-mechanical oscillation can degrade system stability margin e.g., limiting power transfer capability of cross-reginal grids or leading to blackout events [58-60].

The increasing renewable generation which replaces rotational generators will reduce system inertia and thus pose challenges to LFOs (why not damping) [61]. It is found that high penetration of PV plants or wind farms has adverse impact on supressing electro-mechanical oscillatory modes [62, 63]. VSM control has been extensively studied for renewable energy to improve system inertia under external disturbances. However, new LFOs related to VSM will be inevitably introduced since VSM emulates the behaviour of SG. Therefore, the coordinated control of multiple VSMs to damp LFOs should be investigated.

1.1.4 The Forced Oscillation in Power System

The forced power oscillation has attracted increasing attention due to recorded occurrences in real power system and its severer perniciousness than traditional LFOs [64-68]. Different from natural LFOs which are mainly caused by inadequate system damping, the forced power oscillation can be excited when there is sustained external disturbance. And the oscillation magnitude is more prominent if disturbance frequency is in the proximity of natural mode [64, 65, 69-71].

Many external persistent perturbations can induce forced oscillation. The perturbation from hydro plant mechanical turbine can lead to an undesired forced power oscillation [71]. An forced oscillation phenomenon was also observed due to the malfunction of power system stabiliser (PSS) [72]. [73] indicates a serious forced oscillation event caused by interaction between a sustained disturbance from incorrect manipulation of steam extractor control and an inter-area mode. Apart from main forced oscillation sources from traditional generators, the

increasing integrated renewables also pose significant challenges on system operation in terms of forced oscillation. The wind shear and tower shadow effects lead to mechanical torque fluctuation [74-77] which brings negative effect to system stability and even introduces forced power oscillation. Additionally, the turbine vibration of floating wind farm can also be a potential power fluctuation source [78]. The periodic power variation caused by solar radiation and its effects on system forced oscillation are studied in [79].

Due to the inherited oscillation characteristics from SGs, the impacts of VSM-controlled converters on system forced oscillation should be studied.

1.2 Research Aim, Objectives and Contributions

1.2.1 Project Aim and Objectives

Based on the literature review and research gaps identified in Chapter 2, the aim of this PhD thesis is focused on the analysis of VSM control strategy on power system stability, and the main research objectives of this doctoral thesis are to:

- Develop a PMSG-based wind farm with VCC scheme and VSM control respectively in series compensated grid for SSO analysis.
- Investigate and compare the sub-synchronous stability of PMSG-based wind farm with PLL-based and PLL-less methodologies, respectively.
- Investigate the impacts of multiple VSMs on system LFOs.
- Develop Prony based modelling approach for large scale power system.
- Develop a coordinated supplementary damping control (SDC) for multiple VSMs to improve system damping performance.

- Develop mathematical model of forced oscillation in power system with VSM.
- Investigate the impacts of VSM on forced oscillation characteristics and validate the analytical results.

1.2.2 Technical Contributions of The Thesis

The main contributions of this research work are summarised as follows:

- The mathematical modelling of PMSG-based wind farm with series compensated transmission lines is developed in detail. The system performance with VCC and VSM control are compared by modal analysis and time-domain simulations. The eigenvalue locus and participation factor reveal that the SSO mode of PLL-based system is dominated by the interactions between PLL and series compensated network. On the contrary, VSM is not actively engaged in this mode. Therefore, the virtual inertia and damping from VSM can be flexibly designed without compromising the system sub-synchronous stability.
- The decentralised sequential approach is proposed to make supplementary damping controllers of multiple VSMs to work cooperatively. It is revealed that VSMs participate in low-frequency modes significantly. The auxiliary damping is achieved by equipping VSM with virtual PSS (VPSS). The Prony method is utilised to extract system low-frequency modes which facilitates the estimation of oscillatory pattern in large power systems. The undesired interactions between supplementary damping controllers can be reduced with sequential approach. The proposed control can improve system damping performance and it even can accommodate the application of high virtual inertia from VSM.

- The impacts of VSM on power system forced oscillation are thoroughly investigated with mathematical analysis and time-domain simulations. The mathematical analysis based on infinite bus system and multi-machine system is conducted to demonstrate how the characteristics of forced oscillation are affected by VSM. Increasing system damping or separating disturbance frequency and natural mode frequency can suppress oscillation magnitude. Comparing to VCC, VSM may exaggerate forced oscillation due to the resonance effect between natural LFO and external sustained disturbance.

1.3 Thesis Outline

Based on the introduction above, the outline of this thesis is described as follows.

Chapter 2: A literature review concerning VSM control is presented in this chapter. The research focus related to VSM is reviewed in detail.

Chapter 3: This chapter aims to conduct sub-synchronous stability analysis of PMSG-based wind farm in series-compensated network. The PMSG with VCC and VSM schemes are developed based on detailed modelling. The small signal analysis is carried out to analyse system stability under different conditions. The time-domain simulation is provided to validate relevant analysis.

Chapter 4: The coordinated supplementary damping controller design of multiple VSMs is investigated in this chapter. The principles of decentralised sequential approach are explained first and then simulation results are presented to validate the effectiveness of proposed method.

Chapter 5: The focus of this chapter is analysing the impacts of VSM on power system forced oscillation. The mathematical analysis is conducted based on an infinite bus system and a multi-machine system. In addition, simulation results are demonstrated to verify the analytical results.

Chapter 6: This chapter concludes the doctoral research and indicates possible work that could be conducted in the future.

The thesis structure and technical roadmap are presented in Figure 1-12. Chapter 1 and Chapter 2 explain the motivations of this research and give a brief introduction about VSM-related issues. Then system oscillations with VSM are investigated in the sub-synchronous frequency range and electro-mechanical range which are presented in Chapter 3, Chapter 4 and Chapter 5, respectively. Based on the research of Chapter 4, the resonance between natural LFO and sustained disturbance which is also called forced oscillation is explored in Chapter 5.

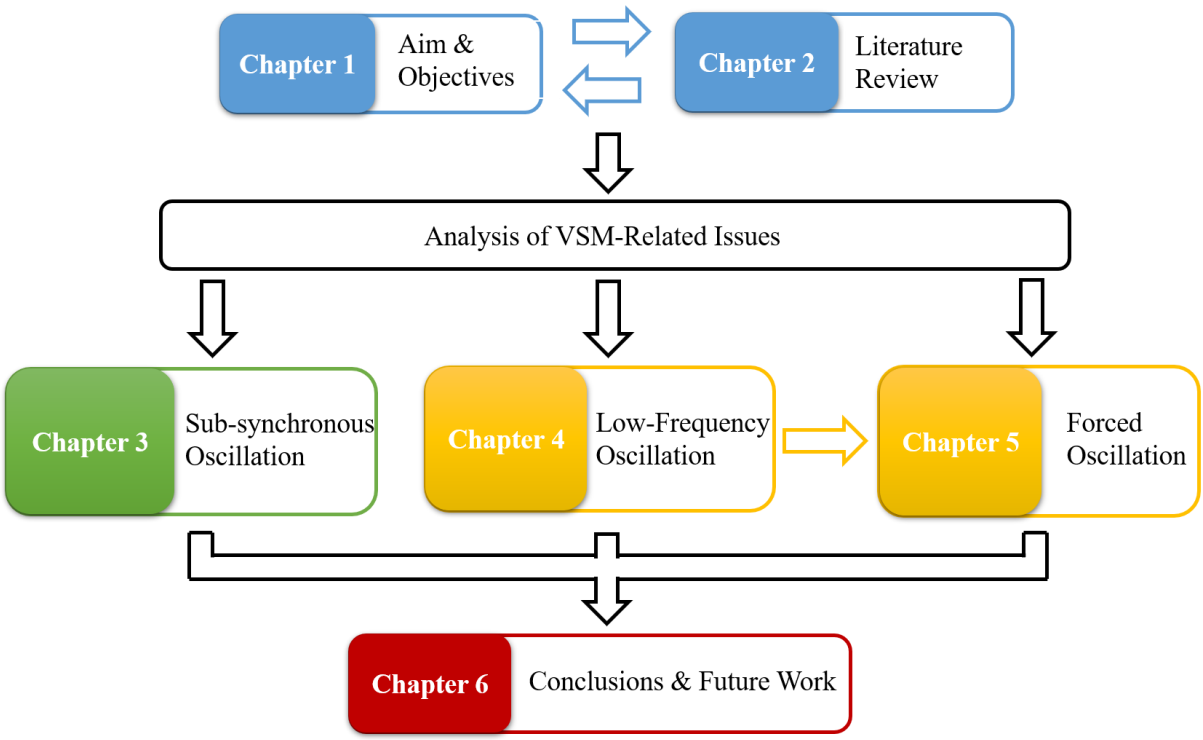

Figure 1-12. Structure and roadmap of the thesis.

CHAPTER 2 LITERATURE REVIEW

2.1 Virtual Synchronous Machine Control

The necessary inertia and damping from mechanical rotor and amortissuer windings of traditional SG can guarantee the stable operation of power system. Different scenarios of emulating electro-mechanical and electromagnetic dynamics of SG have been discussed in [80]. The core of VSM control is incorporating the second-order rotor dynamics of SG into VSC active power control loop [39, 40, 81]. Although there is no physical rotational unit in converters, the imitation of swing equation can be achieved with the utilization of energy storage elements (e.g. rotor of generators [82, 83], energy storage system [84] and DC-link capacitor [85]). The equivalent emulation is demonstrated in Figure 2-1 and can be represented using following equation (The system quantities are given in per unit if not specified).

$$\begin{cases} 2H\frac{d\omega_{vir}}{dt} = P_m - P_e + K_d(\omega_n - \omega) \\ \frac{d\delta_{vir}}{dt} = \omega_b\omega_{vir} \end{cases} \tag{2-1}$$

where P_m and P_e are the virtual prime mover power from DC side and converter output active power; H and K_d are the virtual inertia constant and virtual damping coefficient. The virtual inertia contributes to regulating the rate of change of frequency within acceptable range [86]. Virtual inertia constant H represents the per-unit value of inertia [34, 37]. The typical values of H are chosen in the same level with conventional SGs (0~10s) [83, 87]. ω_b and ω_{vir} are the base frequency and generated virtual angular frequency; and δ_{vir} is the virtual phase angle which is used for synchronous reference frame (SRF) transformation. It is claimed in [88] that the use of nominal frequency ω_n will lead to steady-state deviation if grid frequency changes.

Therefore, the detected frequency ω_g from PLL is fed into the active power loop as PLL-related instability is not introduced with this alternation [85]. Instead of imitating the damping function based on swing equation, the virtual damping can be provided analogous to the dynamics of SG's transient/sub-transient reactance [89].

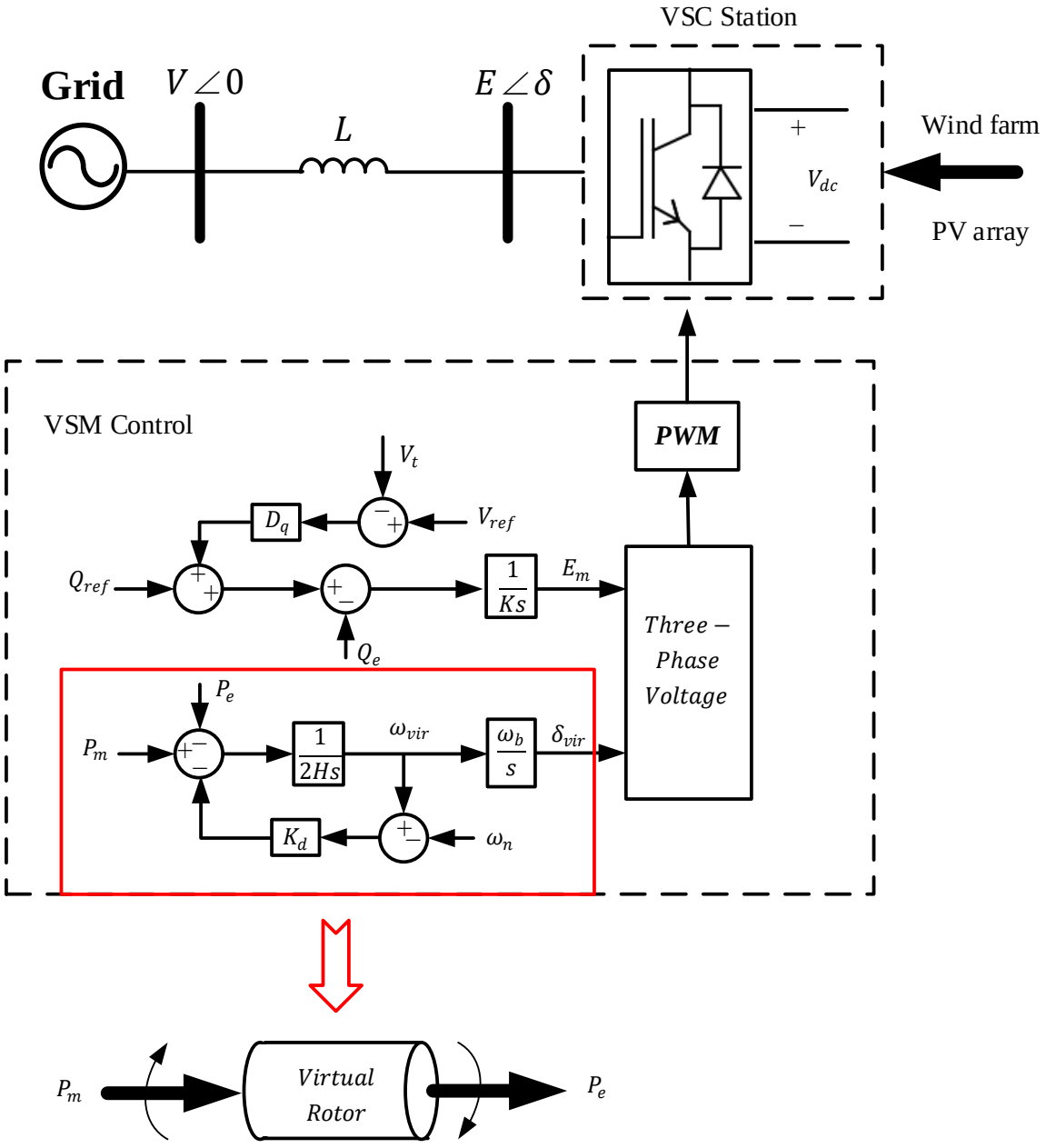

Figure 2-1 Emulation of SG.

In this thesis, the virtual excitation control which can enhance system transient performance [90] is implemented for the reactive power loop and this can be represented as below,

$$K\frac{dE_m}{dt} = D_q\left(V_{ref} - V_t\right) + \left(Q_{ref} - Q_e\right) \tag{2-2}$$

where V_{ref}, V_t and E_m are the voltage reference, terminal voltage and generated virtual voltage magnitude; D_q and K are the virtual droop coefficient and virtual excitation coefficient.

Besides, the implementation of virtual impedance is to improve controller flexibility and enhance system performance. The VSM control with algebraic virtual impedance [91, 92] is shown in Figure 2-2. where i_{dq} is the measured system current, and the virtual impedance is equal to $Z_v = (R_v + j\omega L_v)$.

Apart from virtual impedance, the cascaded control structure [40] which considers the dynamics of LC filter is also applied to achieve fast voltage or current tracking. The control structure is depicted in Figure 2-3. If the dynamics of capacitors are not considered in the control loop, then the control structure is rearranged as illustrated in Figure 2-4. This scenario

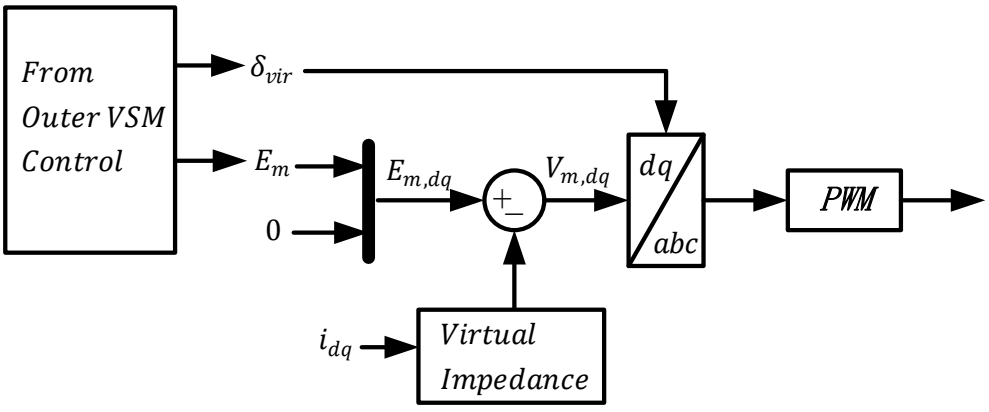

Figure 2-2. VSM control with algebraic virtual impedance.

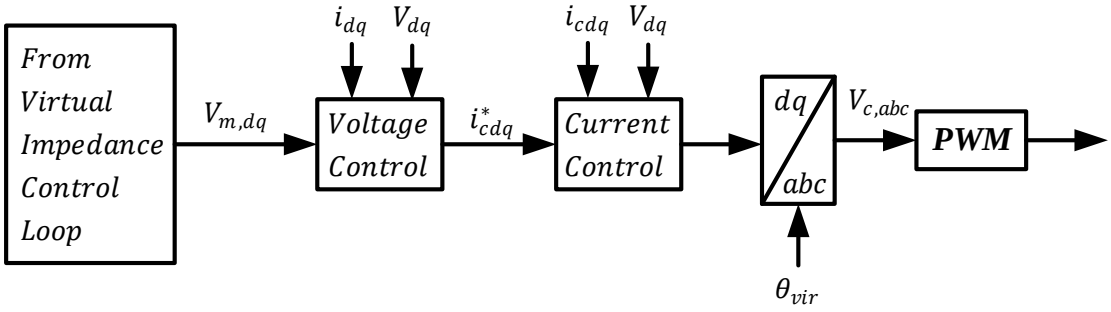

Figure 2-3. VSM control with cascaded voltage-current loop.

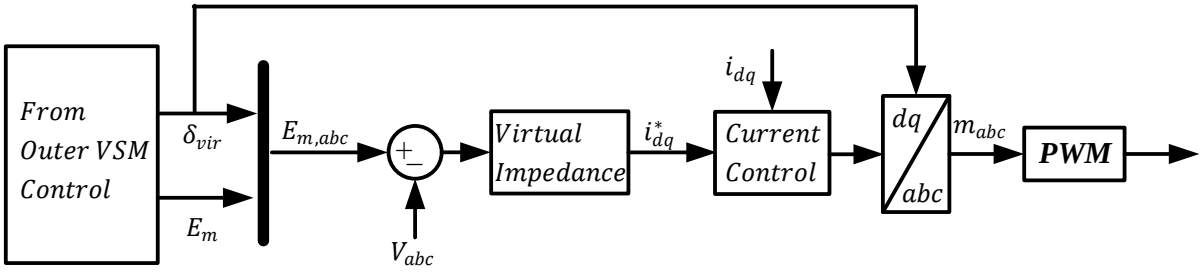

Figure 2-4. VSM control with cascaded current loop.

is also called as synchronous power controller (SPC) [93].

In addition to these described VSM control structures which will be used in this thesis, there are different control schemes studied in massive research work. The well-known synchroverter emulates the electrical and mechanical characteristics of SG in stationary reference frame. The related control structure is illustrated in Figure 2-5 and more details can be found in [94].

The control schemes described above can achieve grid synchronization with aforementioned active power loop and converters are regulated with generated voltage magnitude and phase angle commands. These control methodologies are also categorised as grid-forming (GFM) control since they can be regarded as a controlled voltage source [53, 90].

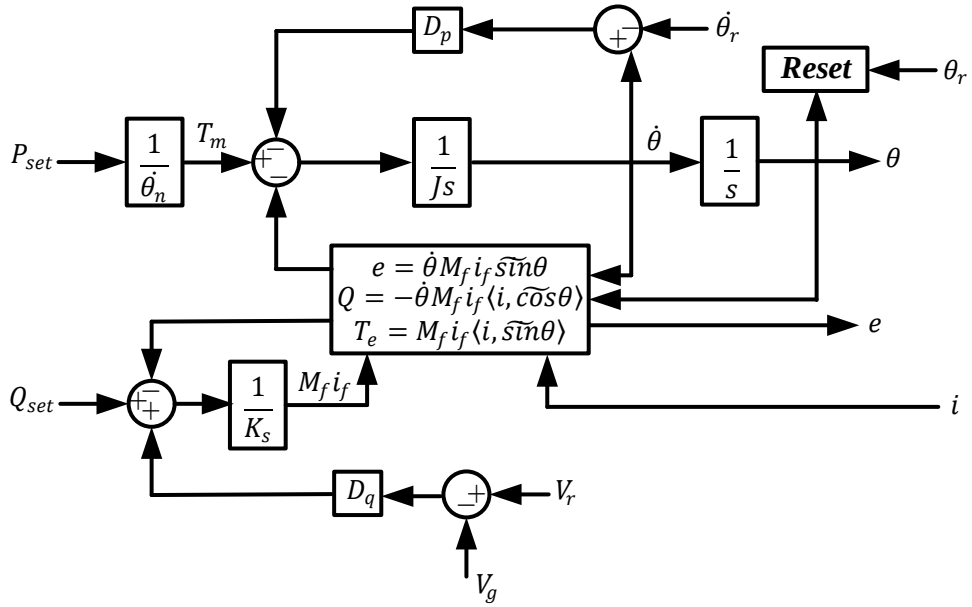

Figure 2-5 Synchroverter control strategy [94].

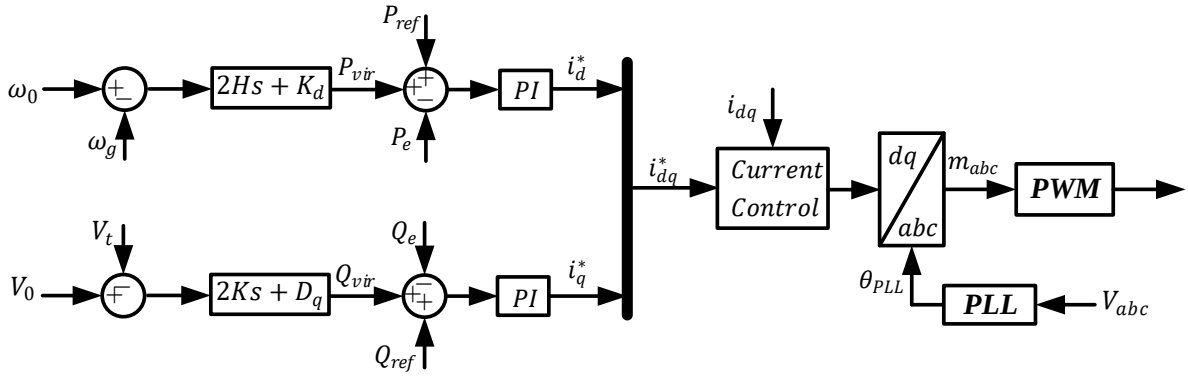

Figure 2-6 GFL-type VSM control.

The other VSM control methods [95-97] which still rely on a PLL unit are classified into grid-following (GFL) group and they are categorised into a controlled current source. Figure 2-6 demonstrates the basic structure of such control. An additional channel which achieves inertia and damping provision is added to the active power loop. Although there are few modifications

required for existing converter control, the system frequency from PLL is required and the converter cannot work independently (e.g., the islanding mode).

The VSM control has been extensively studied for power converters. For generation system, the VSM control equips DFIGs with frequency support capability to stabilise system when suffering frequency disturbances [82]. A method which combines multiple virtual inertia loop was proposed to improve the maximum power tracking of PMSG without compromising the inertial response under various wind speed [83]. The VSM control is applied to the DC/AC converter of PV generation and enables PV system to have grid-forming capability [98]. At transmission level, the secondary frequency regulation is incorporated into VSM and this control is implemented for a VSC HVDC system [99]. It is claimed in [100] that VSM control with adaptive droop for MTDC network can improve system inertia level and decrease frequency deviation. The VSM is also examined for a low frequency ac transmission (LFAC) system with modular multilevel matrix converters (M3C) [101]. As more power electronic loads are connected to grid, the implementation of VSM enables loads to actively participate in frequency regulation. The ‘plug and play’ feature makes loads more friendly and reliable to power system [80, 102-104].

2.2 The Sub-Synchronous Stability of PMSG-Based Wind Farm

Wind farms are normally geographically far away from consumer side, therefore, the power from wind generation needs to be transferred via long-distance transmission lines [54, 105]. However, unsatisfactory power transfer capability under this condition limits further expansion of wind farms. The construction of new transmission lines is an option to accommodate power transfer from increasing installations of wind farms. Nevertheless, the investment on new

infrastructure is non-economical scheme [106]. The alternative, fixed-series capacitor, is popularly applied in long transmission system to decrease the electrical distance and thus to increase power transfer capability [105].

However, the interactions between wind farms and series compensated network may adversely affect system stability by introducing SSO. Generally, the frequency of SSO ranges from 5 to 55Hz with a grid frequency of 60 Hz [107]. The traditional SSO can be classified into sub-synchronous resonance (SSR), sub-synchronous torsional interaction (SSTI) and SSCI [106]. The wind farm-based SSCI is an emerging focus and the first real-world SSO event is observed in south Texas power grid where the DFIG-based wind farm is radially connected to a line with 50% compensation level after a line fault. Similar oscillations are then reported in Buffalo Ridge area of Minesota and Guyuan power system of China [48, 108]. Since then, the SSO which potentially threats the reliable operation of wind farms has attracted increasing attention from researchers.

The previous SSO accidents recorded are mainly from DFIG-based wind farm, however, this oscillation was also investigated for PMSG-based wind farm. It is claimed that the PMSG is immune to SSO with stiff grid [50, 109] while the connected grid is not always strong enough. The PMSG-based wind farm in Xinjiang, China experiences a SSO event [54] and it is revealed that the passive characteristics of PMSG lead to such oscillation. The resonance effect from phase-locked loop (PLL) may excite SSO which will degrade system stability [49]. [50] investigated the sub-synchronous stability of PMSG in a series compensated network and it is found that grid-side controllers dominate the SSO mode. The interaction between weak grid mode which is affected by PLL and RLC transmission line mode will introduce unstable sub-

synchronous power oscillation [51]. It was also implied that the synchronization loop based on PLL may impose stress on system stability in the sub-synchronous frequency range [52].

Since there is a potential risk of sub-synchronous instability caused by PLL's dynamics, the alternative VSM control is introduced [39, 40]. Such PLL-less methodology can provide virtual inertia support to system whose inertia level is lowered by the integration of power-electronics interfaced devices. On the other hand, the VSM makes power converters to synchronise with AC grid by emulating the behaviour of SG without introducing instability caused by PLL. The power synchronization technique was proposed for VSC-HVDC in [46, 110] and it is reported that it has stronger voltage support and higher stability margin under weak grid condition. The dynamics of DC-link capacitor was utilised to achieve grid synchronization rather than using PLL [85, 96, 111]. Such synchronization technique is also implemented to DFIG- and PMSG-based wind farms by utilizing the energy stored in rotors and the VSM controlled wind farm permits better performance even in weak grid [82, 83].

There are multiple methods to analyse the SSO of wind farm. The sub-synchronous stability of converter-based devices under different conditions can be evaluated with small-signal analysis method. The system dynamics are described with explicit state-space model and then linearised at the equilibrium point of interest. The modal analysis including eigenvalue locus, participation factor and sensitivity analysis [112-114] can be utilised to accurately explore the factors which will affect system stability in the sub-synchronous frequency range [50, 105, 115]. The impedance-based modelling in phasor domain or dq domain can also be utilised to analyse system stability from the perspective of the interaction between equivalent converter impedance and grid impedance. The system stability is evaluated based on Nyquist criterion or General Nyquist criterion [51, 116, 117] which provides an insight into the passive

characteristics of converter impedance [118, 119]. In addition, the sub-synchronous stability of wind farm can be assessed with complex torque method which has been widely used for analysing the stability of SG [120]. The equivalent negative damping contributed by the interaction of control loops in converters can destabilise power system [121-123].

Based on the literature review above, following research gaps and research opportunities are identified.

- Due to the fact that undesired SSO may be induced by PLL, the sub-synchronous stability of PMSG-based wind farm with VSM will be a research topic of interest.
- As few papers focus on comparing the sub-synchronous stability of PMSG with different control strategies, a detailed model for VSM-controlled wind farm in series compensated network is established and hence its performance can be compared with PLL-based system.
- It will be useful to carry out modal analysis to provide comprehensive information and reveal the dominant factors responsible for system stability in the sub-synchronous frequency range.

2.3 Low-Frequency Oscillation Related to VSM

VSM control can provide frequency support for power system by emulating the inertial responses of SG. Notwithstanding, undesired power oscillation issues are also inherited. The power oscillation is prone to occurring during load transients between VSM and SG devices due to inertia difference [124]. It was reported in [125] that the system suffers from undamped low-frequency instability because of considerable grid resistance and the undesired coupling

between active power and reactive power. [126] explained the resonance instability among parallel operated SG and VSM in the vicinity of natural frequency and stated that it is caused by the combination of governor and inertia characteristics.

However, most of existing studies are mainly focused on small systems [124-127]. On the other hand, LFO is one of the major concerns for large power systems [88] especially under bulk power transfer between weakly connected power grids. The oscillatory behaviour is more prominent when the capacity of VSM controlled devices, e.g. VSC-HVDC, is similar to SGs [88, 128]. Generally, there are several methods to suppress system power oscillations in the low-frequency range. Reducing the stress of critical tie-lines by limiting transferred power can effectively mitigate LFOs [129]. However, this uneconomical method leads to the under-utilization of transmission paths [130]. The damping of LFOs contributed by aggregated loads was investigated in [129] while this technique requires significant participation and frequent controller reconfiguration from abundant loads at the instant of needs. The adjustment of VSM internal control parameters such as inertia and damping/droop coefficients are investigated in [125, 131] to improve system damping performance. However, it is also described that adjusting such parameters have limited impacts on system oscillation damping [132] and smaller inertia constant or larger damping coefficients can even degrade system behaviour [127, 133, 134]. The virtual reactance was introduced to improve system damping performance [81], however, the virtual reactance can lead to reactive power calculation error and the research works were demonstrated with limited simulation studies [134].

In addition, some other methods were also proposed by employing additional stabilizing signal into controllers to improve system damping [133, 135-137]. The auxiliary damping can be provided via active power modulation or reactive power/voltage modulation. These schemes

have been extensively studied for renewables. [138] proposed a supplementary controller by regulating active power commands to provide additional damping. On the contrary, the supplementary signal is added to the reactive power reference to achieve LFOs damping [139]. A double-channel damping controller which combines the two supplementary algorithms above are added to the active power and reactive power control loops of DFIG's rotor side converter to suppress LFOs [140]. Similarly, the application of SDC was also presented for VSMs. An improved damping control by modifying the voltage magnitude loop was introduced to VSM [133]. [136] proposed a strategy which implements the combination of power feedback signal and derivative of virtual frequency feedback signal into active power loop to enhance the damping of VSM. The implementation of identification-based hierarchical control was investigated in [135] and this supplementary signal was also added into the real power loop. However, considering the potential risk of introducing torsional oscillation when injecting supplementary signal into active power loop if the prime mover power of VSM comes from wind turbines [130, 141], the additional damping signal is applied to reactive loop in this thesis. As virtual excitation control is implemented, the supplementary signal is employed to voltage droop loop rather than directly regulating the internal voltage magnitude like [133]. Therefore, it equips the VSM with a VPSS. This PSS-based control can provide one more degree of freedom to enhance system damping performance and it is easy to be implemented in practice.

The coordinated damping control for multiple VSMs is particularly useful to reduce the undesired coupling between them and also increase the damping of multiple dominant system oscillation modes [142-144]. Generally, the coordinated control can be categorised into a multi-input-multi-output (MIMO) centralised control or a decentralised control [145] which usually decouples the system into multiple loops of single-input-single-output (SISO) one . Re-

organizing a MIMO control problem into SISO control issue makes it more viable and attractive for practical power system. Besides, the centralised control is highly dependent on communication, therefore, it increases the system investment, system control complexity and decreases system reliability when there is a loss of communication [146]. The communication-less decentralised coordination control with a local structure is therefore more preferable. The sequential approach is generally implemented to design controllers for a group of devices. A series of coordinated controllers for multiple FACTS devices are designed and studied with sequential strategy in [144]. Similarly, the sequential design method is utilised to ensure multiple damping controllers of VSMs to work cooperatively.

Generally, there are two mainstream techniques, viz., eigenvalue-based approach and measurement-based method which can be implemented to obtain modal properties of power system [147]. The modal analysis is subject to system modelling details which is not practical for large power systems. Fortunately, with the application of phasor measurement unit (PMU), it is possible to timely record the dynamic behaviours of power system and sample data for further processing. The measurement-based approach identifies system modes by the approximate linear reconstruction of a system from sampled data. The Matrix Pencil method, Eigenvalue Realization Algorithm (ERA), Hilbert-Huang Transformation (HHT) and Prony method can be utilised to analyse system modes information from ring-down measurements [148-151].

The research gaps and challenges based on aforementioned literature review are identified as below:

- Due to the potential massive application of VSMs and limited research work revealing the

impacts of multiple VSMs on system LFOs, the interactions between multiple VSMs and power systems will be of great interest.

- Considering the complexity of modelling large-scale power system in detail, the measurement-based approach is developed to identify system characteristics, i.e., Prony method is implemented to equivalently model system with VSMs in the frequency range of interest.

- In this situation, the coordinated design of SDCs for multiple VSMs becomes an important yet challenging research topic. To achieve the coordination, a decentralised sequential approach combined with Prony based modelling approach becomes attractive due to its merit of simple and feasible implementation vs centralised design and this will be investigated in this section.

2.4 Forced Oscillation Related to VSM

The forced oscillation is a resonance phenomenon between natural LFO modes of power grid and external periodic disturbance. This interaction between forced oscillation source and natural oscillatory modes in bulk power system will highly magnify the resonance [66] which may jeopardise system stability. A forced oscillation accident was recorded in power grid of southern China as shown in Figure 2-7. Based on the component analysis of real-world forced oscillation event, the frequency of forced oscillation is near the intrinsic LFO modes, ranging from 0.1~2 Hz. The damping ratio of forced oscillation near zero or even negative [64, 65]. The forced oscillation will persist continuously which even lasts more than one hour [152] unless the disturbance source is removed.

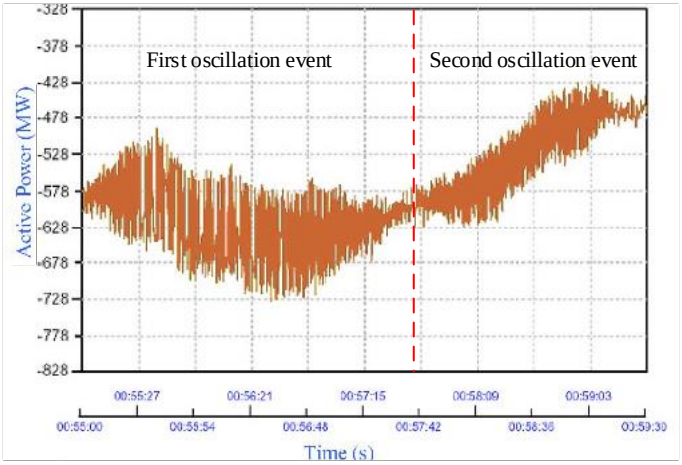

(a)

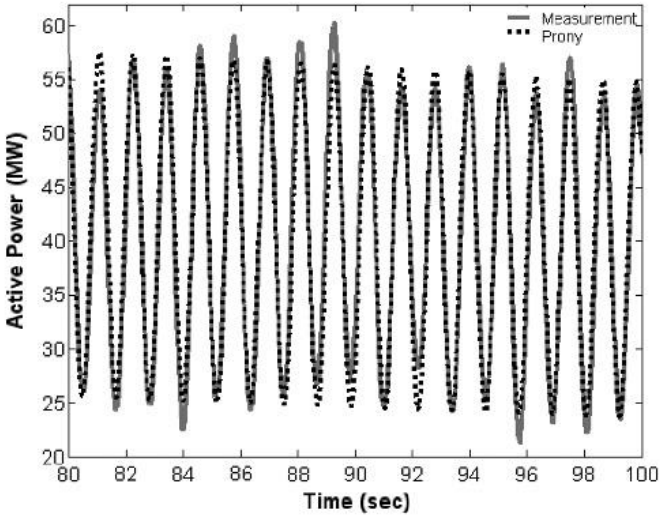

(b)

Figure 2-7 Recorded forced oscillation in China Southern Power Grid. (a) Oscillation from Luoping to TSQ. (b) Selected data of first oscillation [64].

The adverse effects from forced oscillation accidents which have been reviewed in [66] can lead to significant power loss, equipment damages or even system break-down. In order to reduce the risk of forced oscillation, necessary measures should be taken to lighten such stress. The most efficient method is accurately locating the oscillation source and removing it [152]. Some methods have been proposed which aim to identify the forced oscillation characteristics

and locate the perturbation source with PMU. The power spectrum density (PSD) can be utilised to estimate the sinusoidal characteristics of forced oscillation [152]. The oscillation mode angle which indicates the direction of power flow is adopted as an index to justify the source location [66]. A Bayesian approach was proposed to identify the location of forced oscillation source and it was designed to address the noise of data and uncertainties of generators [153]. A comprehensive review summarises existing methods to locate the oscillation source in power system [154].

Considering the challenges to locate original forced oscillation source in a timely manner [66], some remedial methods which can provide more time for source location are researched to supress forced oscillation magnitude. The utilisation of extra energy from ESS was investigated to attenuate forced oscillation energy [66, 68, 155]. The dynamics of DC-link capacitor in PMSG and VSC-HVDC are directly incorporated into control systems to supress the amplitude of forced power oscillation without additional investment [77, 156]. However, the effectiveness of such method is not evident due to the limited size of DC capacitor.

Based on the literature review above, it has been found that current studies of forced oscillation are mainly based on SGs and renewables with traditional VCC. Since VSM is prone to participating in LFO, the interaction between VSM and external sustained disturbance may cause serious resonance and excite forced oscillation. However, the impacts of VSM on forced oscillation are rarely studied and this leads to the research objective which aims to investigate the forced oscillation of power system with VSM.

CHAPTER 3 SUB-SYNCHRONOUS STABILITY ANALYSIS OF PMSG-BASED WIND FARM IN SERIES COMPENSATED AC NETWORK

3.1 Introduction

This chapter investigates the sub-synchronous stability of PMSG-based wind farm in series compensated network using VSM and compares its control performance with that of PLL-based VCC. The detailed mathematical model of PMSG-based wind farm with series compensated network is established in Section 3.2. The state-space model is developed in Section 3.3 and the impacts of compensation level and number of wind turbines are investigated via modal analysis. Relevant time-domain simulations are also carried out to validate the analytical results. The major findings are summarised in Section 3.4.

3.2 Mathematical Model of PMSG-Based Wind Farm with Series Compensated Transmission Network

The schematic diagram of studied system is illustrated in Figure 3-1. The total capacity of wind farm is 100MW (2.5MW×40) and its power is transferred into 220 kV AC system through a series compensated transmission line. An aggregated model is built to represent the whole wind farm [115].

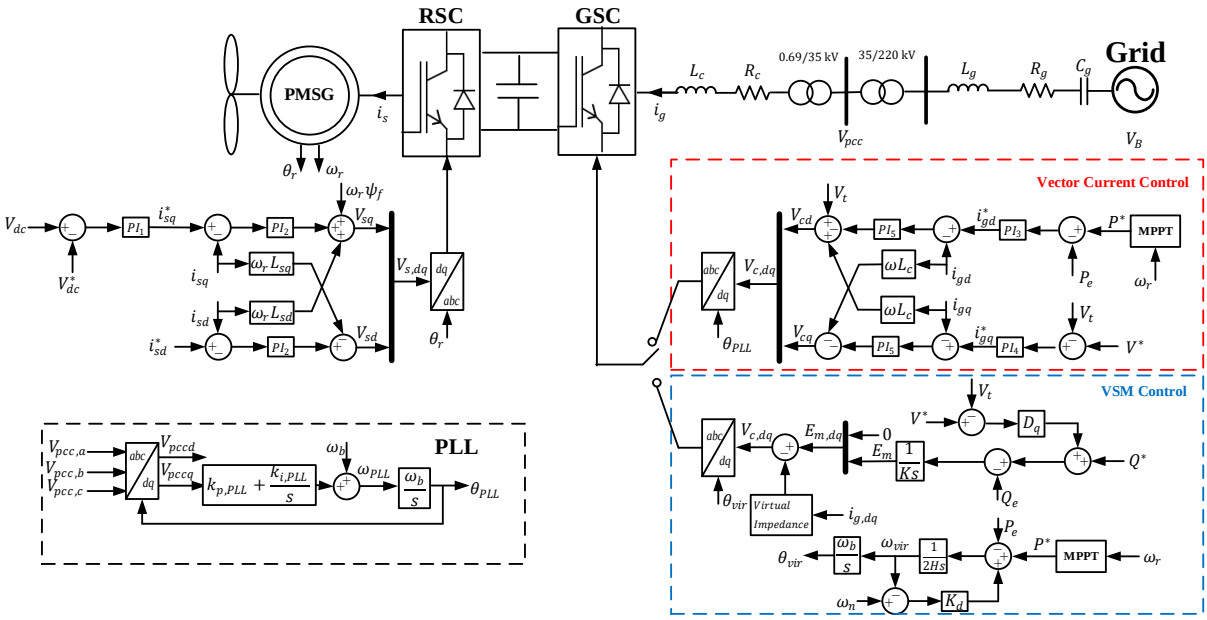

Figure 3-1 Schematic diagram of PMSG-based wind farm.

3.2.1 Modelling of Wind Turbine and Drive Train

The wind energy is converted into electricity through a wind turbine system. The extracted mechanical power through wind turbine is presented as:

$$P_m = C_P(\lambda, \beta)\frac{\rho A}{2}V_w^3 \tag{3-1}$$

where $C_P(\lambda, \beta)$ is the utilization coefficient, λ is the speed ratio ($\lambda = \omega_r R/V_w$), ω_r is the rotor speed, R is the radius of blade, β is the pitch angel ($\beta = 0^o$ if the wind speed is below rated value), ρ is the air density, A is the swept area of wind blade and V_w is the wind speed. And $C_P(\lambda, \beta)$ can be further expressed as [157]:

$$\begin{cases} C_P(\lambda,\beta) = c_1\left(\frac{c_2}{\lambda_i} - c_3\beta - c_4\right)e^{-\frac{c_5}{\lambda_i}} + c_6\lambda \\ \frac{1}{\lambda_i} = \frac{1}{\lambda+0.08\beta} - \frac{0.035}{\beta^3+1} \end{cases} \tag{3-2}$$

where $c_1 \sim c_6$ are the characteristic coefficients and they are dependent on the wind turbine structure. The characteristics of $C_P(\lambda, \beta)$ and P_m ($\beta = 0^\circ$) are depicted in Figure 3-2.

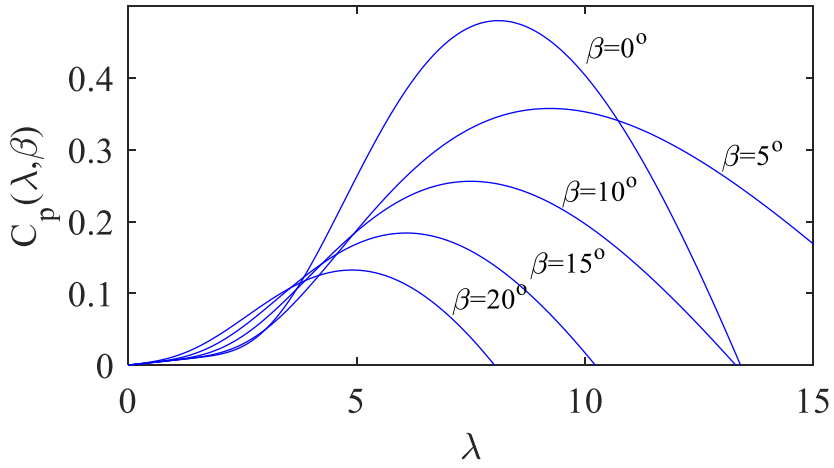

(a)

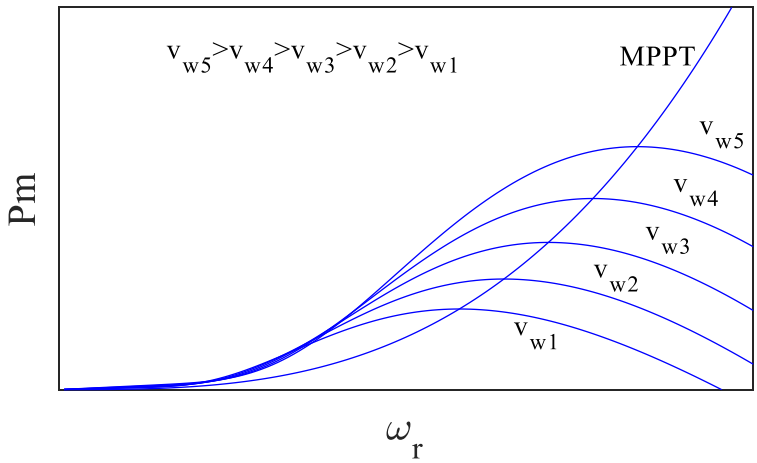

(b)

Figure 3-2 Diagram of wind turbine characteristics. (a) $C_P(\lambda, \beta)$. (b) P_m ($\beta = 0^\circ$).

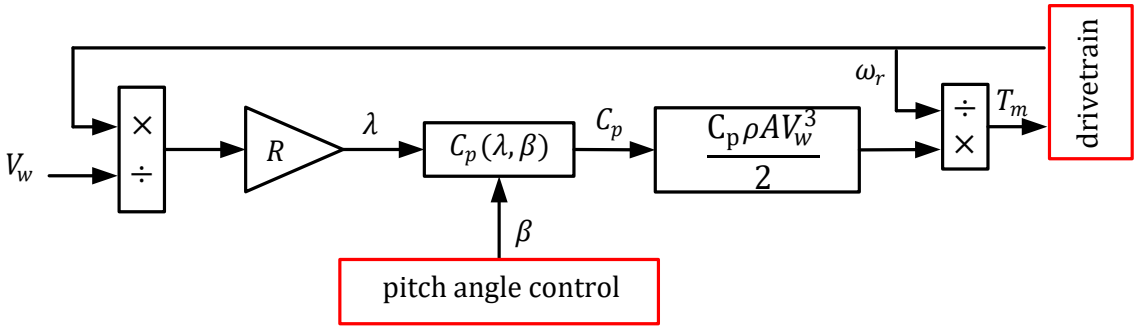

Figure 3-3 Schematic diagram of wind turbine.

The pitch angle control is given as:

$$T_{pitch}\frac{d\beta}{dt} = k_{p,pitch}(\omega_r - \omega_r^*) - \beta \tag{3-3}$$

where $k_{p,pitch}$ and T_{pitch} are pitch control coefficients, ω_r^* is the reference. The model of wind turbine is illustrated in Figure 3-3.

The wind turbine rotor is directly connected to generator and therefore the dynamics of drive train can be established as [158]:

$$2H_g\frac{d\omega_r}{dt} = T_m - T_e \tag{3-4}$$

where T_m and T_e are the mechanical and electrical torque, H_g is the inertia constant.

3.2.2 Modelling of Generator

The motor convention is adopted (The current flows from grid to machine) and generator is modelled in synchronous rotating dq reference frame. The equations are based on the following Park Transformation matrix [159].

$$\boldsymbol{T_{abc-dq}} = \frac{2}{3}\begin{bmatrix} cos\,\theta & cos\,(\theta - \frac{2\pi}{3}) & cos\,(\theta + \frac{2\pi}{3}) \\ -sin\,\theta & -sin\,(\theta - \frac{2\pi}{3}) & -sin\,(\theta + \frac{2\pi}{3}) \\ \frac{1}{2} & \frac{1}{2} & \frac{1}{2} \end{bmatrix} \tag{3-5}$$

If d-axis is aligned with rotor flux linkage, the equation of generator is developed as:

$$\begin{cases} V_{sd}^r = R_s i_{sd}^r - \omega_r L_{sq} i_{sq}^r + L_{sd}\frac{di_{sd}^r}{dt} \\ V_{sq}^r = R_s i_{sq}^r + \omega_r\left(L_{sd} i_{sd}^r + \psi_f\right) + L_{sq}\frac{di_{sq}^r}{dt} \\ T_e = \psi_f i_{sq}^r + \left(L_{sd} - L_{sq}\right) i_{sd}^r i_{sq}^r \end{cases} \tag{3-6}$$

where $i_{sd}^r, i_{sq}^r, V_{sd}^r, V_{sq}^r$ are the d-axis and q-axis current and voltage of stator windings. L_{sd} and L_{sq} are the stator inductance, R_s is the stator resistance. ψ_f is rotor flux linkage (this value is usually a constant). The equivalent circuit is shown in Figure 3-4. The superscript 'r' represents variables which are in rotor-side dq reference frame.

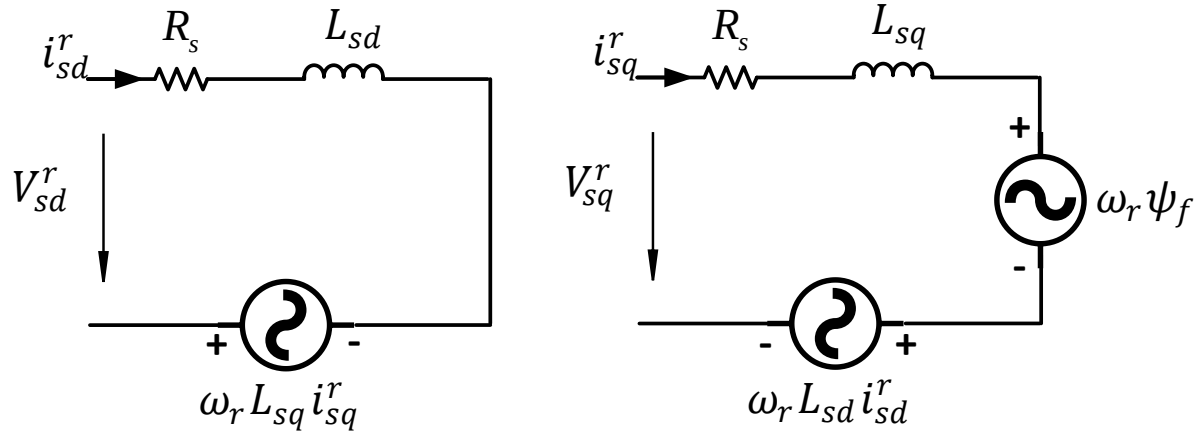

Figure 3-4 Equivalent circuit of generator. (a) d-axis. (b) q-axis.

3.2.3 Modelling of Back-to-Back Converter

The B2B converter is assumed to be ideal and therefore the converter loss is not considered. The power balance equation of DC capacitor is established as:

$$\begin{cases} C_{dc}V_{dc}\frac{dV_{dc}}{dt} = P_g - P_s \\ P_s = T_e\omega_r \\ P_g = V_{cd}^g i_{gd}^g + V_{cq}^g i_{gq}^g \end{cases} \tag{3-7}$$

where C_{dc} is the DC capacitance, V_{dc} is the DC voltage of capacitor, P_g and P_s are the power from grid side converter (GSC) and rotor side converter (RSC), $i_{gd}^g, i_{gq}^g, V_{cd}^g, V_{cq}^g$ are the current and voltage at GSC. The superscript 'g' represents variables which are in grid-side dq reference frame.

(1) Model of Rotor Side Converter

According to generator equations, the block diagram of RSC controller is illustrated in Figure 3-1. The RSC aims to maintain DC voltage balance due to its superiority in terms of fault ride through capability and torsional damping [160-162]. The *d*-axis current is controlled to zero and *q*-axis current is controlled by the dynamics of DC voltage. The controller equations are developed as:

$$\frac{dx_1}{dt} = V_{dc} - V_{dc}^* \tag{3-8}$$

$$\begin{cases} {i_{sd}^*}^r = 0 \\ {i_{sq}^*}^r = \left(k_{p1} + \frac{k_{i1}}{s}\right)(V_{dc} - V_{dc}^*) \end{cases} \tag{3-9}$$

$$\begin{cases} V_{sd}^r = k_{p2}\left({i_{sd}^*}^r - i_{sd}^r\right) + k_{i2}x_2 - \omega_r L_{sq} i_{sq}^r \\ V_{sq}^r = k_{p2}\left({i_{sq}^*}^r - i_{sq}^r\right) + k_{i2}x_3 + \omega_r L_{sd} i_{sd}^r + \omega_r \psi_f \end{cases} \tag{3-10}$$

where ${i_{sd}^*}^r$, ${i_{sq}^*}^r$ and V_{dc}^* are the stator current references and DC voltage reference. k_{p1}, k_{i1} and k_{p2}, k_{i2} are the PI controller parameters.

(2) Model of Grid Side Converter (GSC)

For GSC, the PLL-based VCC and PLL-less VSM schemes are introduced respectively. The control block diagram for both types of controllers is also presented in Figure 3-1. The GSC is responsible for achieving maximum power point tracking (MPPT) and controlling AC side voltage.

If grid voltage oriented VCC is implemented to GSC, then the controller equations can be written as:

$$\begin{cases} \frac{dx_4}{dt} = P^* - P_e \\ \frac{dx_5}{dt} = V^* - V_t \end{cases} \tag{3-11}$$

$$\begin{cases} {i_{gd}^*}^g = k_{p3}(P^* - P_e) + k_{i3}x_4 \\ {i_{gq}^*}^g = k_{p4}(V^* - V_t) + k_{i4}x_5 \end{cases} \tag{3-12}$$

$$\begin{cases} \frac{dx_6}{dt} = {i_{gd}^*}^g - i_{gd}^g \\ \frac{dx_7}{dt} = {i_{gq}^*}^g - i_{gq}^g \end{cases} \tag{3-13}$$

$$\begin{cases} V_{cd}^g = -k_{p5}\left({i_{gd}^*}^g - i_{gd}^g\right) - k_{i5}x_6 + \omega_b L_c i_{gq}^g + V_t \\ V_{cq}^g = -k_{p5}\left({i_{gq}^*}^g - i_{gq}^g\right) - k_{i5}x_7 - \omega_b L_c i_{gd}^g \end{cases} \tag{3-14}$$

where $P^*(P^* = K_{opt}\omega_r^3)$ and V^* are the power reference and voltage reference, $K_{opt}$is optimal coefficient for maximum power extraction, P_e and V_t are the power and voltage at point of common coupling (PCC), ${i_{gd}^*}^g$ and ${i_{gq}^*}^g$ are current reference from outer loop, i_{gd}^g and i_{gq}^g are

the grid side current, V_{cd}^{g} and V_{cq}^{g} are the converter voltage, L_c is the grid side reactor, $k_{p3}, k_{i3}, k_{p4}, k_{i4}$ and k_{p5}, k_{i5} are the PI controller parameters.

As the synchronization of vector control is dependent on PLL, the control block of PLL [114] is presented in Figure 3-1 and its dynamics are derived as:

$$\begin{cases} \frac{d\gamma_{PLL}}{dt} = V_{pccq}^{g} \\ \frac{d\theta_{PLL}}{dt} = \omega_b(k_{p,PLL}V_{pccq}^{g} + k_{i,PLL}\gamma_{PLL}) \end{cases} \tag{3-15}$$

where ω_{PLL} and θ_{PLL} are the detected grid frequency and phase angle, $k_{p,PLL}, k_{i,PLL}$ are the PI controller parameters of PLL.

If GSC adopts VSM control, then the controller equation can be defined as (2-1) and (2-2).

If algebraic virtual impedance is considered as well [91], the following equation can be obtained as:

$$\begin{cases} V_{cd}^{g} = E_{md}^{g} - R_v i_{gd}^{g} + \omega_{vir} L_v i_{gq}^{g} \\ V_{cq}^{g} = E_{mq}^{g} - R_v i_{gq}^{g} - \omega_{vir} L_v i_{gd}^{g} \end{cases} \tag{3-16}$$

As the controller equations are developed based on their local reference frame, it is necessary to transfer the variables into a unified reference frame. Figure 3-5 illustrates the relationship between two rotating dq reference frames.

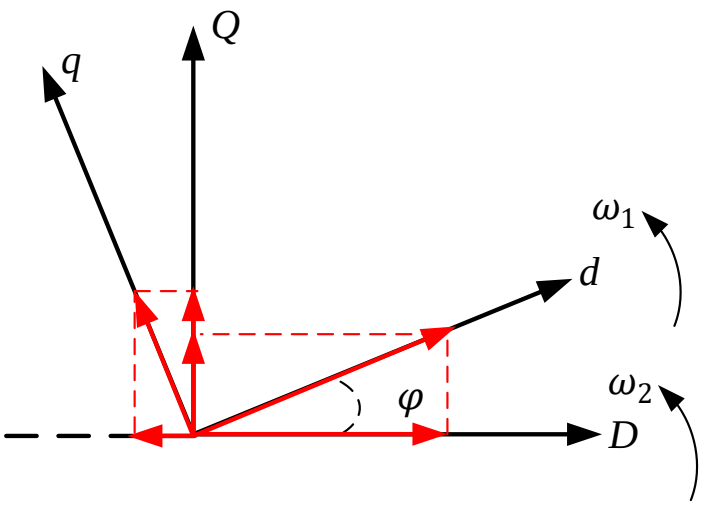

Figure 3-5 Relationship between local and unified dq reference frame.

$$\begin{bmatrix} f_D \\ f_Q \end{bmatrix} = \begin{bmatrix} cos\varphi & -sin\varphi \\ sin\varphi & cos\varphi \end{bmatrix} \begin{bmatrix} f_d \\ f_q \end{bmatrix} \tag{3-17}$$

$$\begin{bmatrix} f_d \\ f_q \end{bmatrix} = \begin{bmatrix} cos\varphi & sin\varphi \\ -sin\varphi & cos\varphi \end{bmatrix} \begin{bmatrix} f_D \\ f_Q \end{bmatrix} \tag{3-18}$$

where φ is the angle difference, f_d, f_q and f_D, f_Q are the variables in local and unified reference frame, respectively.

3.2.4 Modelling of Series-Compensated Network

The dynamics of series compensated network are established as:

$$\begin{cases} L_g \frac{di_{gD}}{dt} = \omega_b \left(V_{BD} - V_{scD} - V_{pccD}\right) - \omega_b R_g i_{gD} + \omega_b L_g i_{gQ} \\ L_g \frac{di_{gQ}}{dt} = \omega_b \left(V_{BQ} - V_{scQ} - V_{pccQ}\right) - \omega_b R_g i_{gQ} - \omega_b L_g i_{gD} \\ \frac{C_g}{\omega_b} \frac{dV_{scD}}{dt} = i_{gD} + C_g V_{scQ} \\ \frac{C_g}{\omega_b} \frac{dV_{scQ}}{dt} = i_{gQ} - C_g V_{scD} \end{cases} \tag{3-19}$$

where L_g, R_g and C_g are the network inductance, resistance and fixed series capacitor. V_{BD}, V_{BQ}, V_{scD}, V_{scQ} and are V_{pccD}, V_{pccQ} the infinite bus voltage, capacitor voltage and PCC voltage.

3.3 Small Signal Analysis and Simulations

Linearizing previously described non-linear state-space equations at specified operating points, the small signal model of entire system can be presented as:

$$\frac{d\Delta \boldsymbol{x}}{dt} = \boldsymbol{A}\Delta \boldsymbol{x} + \boldsymbol{B}\Delta \boldsymbol{u} \tag{3-20}$$

where $\boldsymbol{A}$ and $\boldsymbol{B}$ are the state matrix and input matrix. The state variables are defined as:

$$\Delta \boldsymbol{x_{VCC}} = [\Delta i_{sd}^{r}, \Delta i_{sq}^{r}, \Delta\beta, \Delta\omega_r, \Delta x_1, \Delta x_2, \Delta x_3, \Delta V_{dc}, \Delta x_4, \Delta x_5, \Delta x_6, \Delta x_7, \Delta x_{pll}, \Delta\theta_{pll}, \Delta i_{gD}, \Delta i_{gQ}, \Delta V_{scD}, \Delta V_{scQ}]^T$$

or

$$\Delta \boldsymbol{x_{VSM}} = [\Delta i_{sd}^{r}, \Delta i_{sq}^{r}, \Delta\beta, \Delta\omega_r, \Delta x_1, \Delta x_2, \Delta x_3, \Delta V_{dc}, \Delta E_m, \Delta\omega_{vir}, \Delta\theta_{vir}, \Delta i_{gD}, \Delta i_{gQ}, \Delta V_{scD}, \Delta V_{scQ}]^T$$

The system stability can be evaluated by eigenvalues obtaining from small signal model. The participation factor [159] is also utilised to indicate which states are highly involved in related modes.

$$P_{k,i} = \phi_{ki}\psi_{ik} \tag{3-21}$$

where ϕ_{ki} and ψ_{ik} are the elements of right eigenvector and left eigenvector.

3.3.1 The Impacts of Compensation Level

The eigenvalue locus of wind farm as depicted in Figure 3-1 (The system parameters are listed in Table A1-3 in the Appendix) with different compensation level ($CL = \frac{X_{Cg}}{X_{Lg}}$) [163] varying from 10% to 75% is plotted in Figure 3-6. It can be seen from Figure 3-6 that increasing compensation level will weaken system sub-synchronous stability. As shown in Figure 3-6 (a) that the SSO mode of vector current controlled wind farm shifts to the right half plane (RHP) if compensation level increases to 32.5%, which brings sub-synchronous instability to system.

In contrast, the eigenvalues of VSM-controlled system stay in the left half plane (LHP) within varied compensation level, which means the system remains stable under this situation.

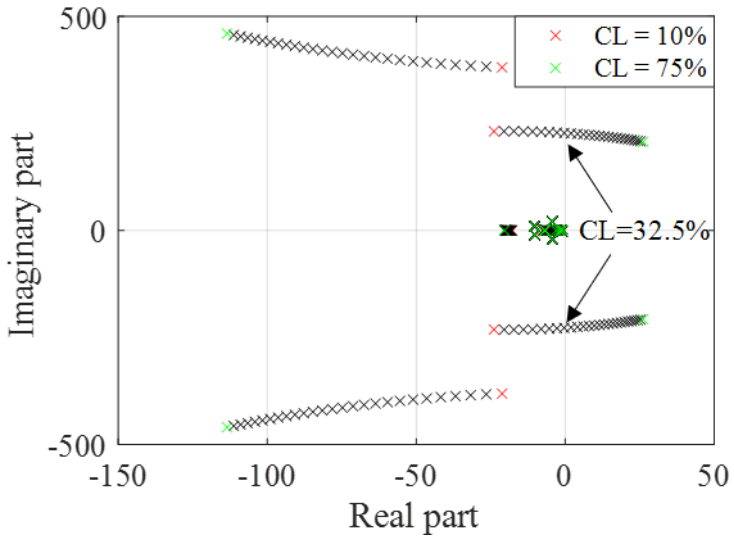

(a)

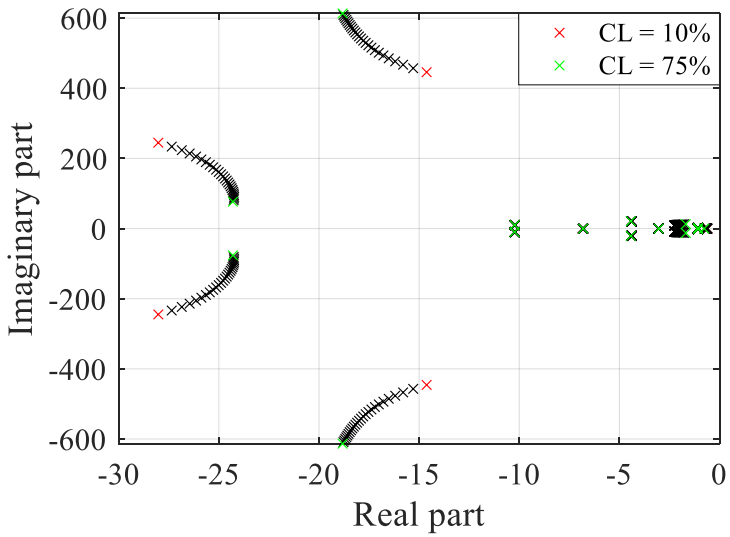

(b)

Figure 3-6 Eigenvalue locus of system under compensation level variation. (a) VCC. (b) VSM.

TABLE 3-1
EIGENVALUE ANALYSIS RESULTS OF VECTOR-CURRENT CONTROLLED PMSG

Modes	Eigenvalue	Frequency (Hz)	Damping ratio
1	$-65.2 \pm j405.4$	64.5	0.159
2	$\mathbf{1.7 \pm j228.3}$	**36.3**	$\mathbf{-0.007}$
3	$-4.3 + j20.7$	3.3	0.204
4	$-1.1 \pm j1.7$	0.3	0.529
5	$-6.8 \pm j0.05$	0.008	1.000
6	$-10.2 \pm j10.0$	1.6	0.716

TABLE 3-2
EIGENVALUE ANALYSIS RESULTS OF VSM CONTROLLED PMSG

Modes	Eigenvalue	Frequency (Hz)	Damping ratio
1	$-9.3 \pm j486.0$	77.3	0.019
2	$\mathbf{-12.0 \pm j236.5}$	**37.6**	**0.050**
3	$-4.4 \pm j20.8$	3.3	0.206
4	$-2.4 + j2.2$	0.3	0.749
5	$-1.0 \pm j2.0$	0.3	0.436
6	$-10.2 \pm j10.0$	1.6	0.716

The detailed modes information of system with VCC in marginal condition ($CL = 32.5\%$) is presented in Table 3-1 and VSM controlled one with the same compensation level is shown in Table 3-2. The damping ratio of SSO mode (in bold) in PLL-based wind farm is negative which means the system becomes unstable especially suffering disturbances. The SSO mode

information in Table 3-2 implies that VSM-controlled system is stable although the damping ratio is not very strong.

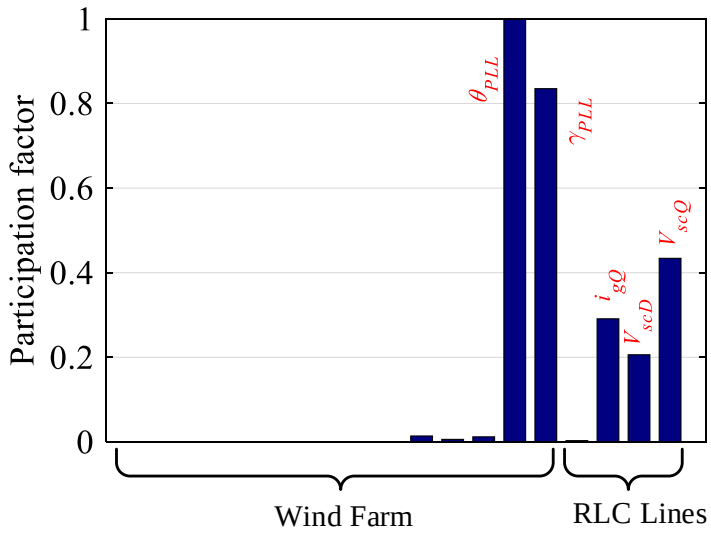

(a)

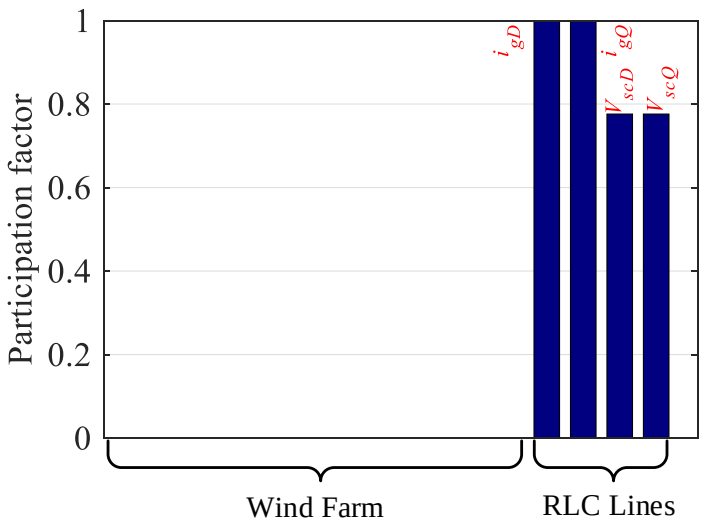

(b)

Figure 3-7 Participation factor of SSO mode. (a) VCC. (b) VSM.

In addition, the participation factor is calculated to identify the dominant contribution from system states for SSO and it is illustrated in Figure 3-7. The x-axis indicates two main parts of studied system – the wind farm and series compensated transmission line. The blue bar implies the level of involvement of each state in SSO. It can be observed in Figure 3-7 (a) that the states of PLL (θ_{PLL} and γ_{PLL}) and RLC transmission lines (i_{gQ}, V_{scD} and V_{scQ}) have noticeable participation factor values. Therefore, the SSO mode of wind farm with PLL-based control is significantly affected by PLL and series compensated transmission lines. On the contrary, as depicted in Figure 3-7 (b), the participation factor values of VSM controller states are negligible compared to that of transmission lines. Therefore, the SSO mode of VSM controlled system is dominated by RLC transmission lines and the states related to VSM are not actively engaged in this mode.

The impacts of different parameters in virtual rotor and virtual excitation loops are further explored in Figure 3-8. It is obviously depicted that SSO mode is barely affected by the variation of these four parameters. Therefore, it can be inferred that the system sub-synchronous stability can still be guaranteed when considering virtual inertia or virtual damping provision from VSM.

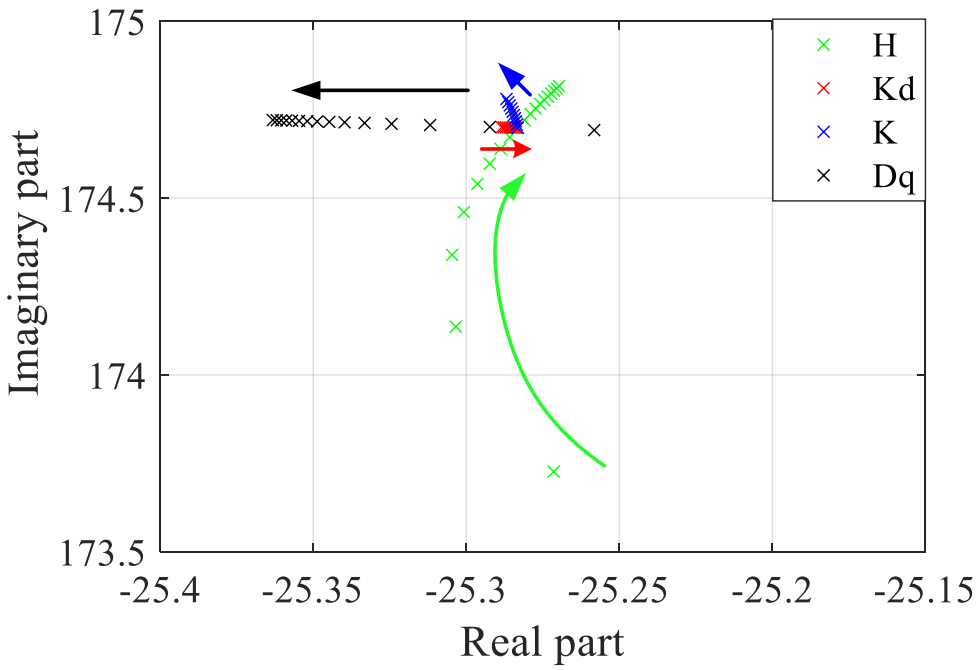

Figure 3-8 Eigenvalue locus of virtual rotor and virtual excitation parameters variation. H changing from 1s to 10s; K_d changing from $10pu$ to $50pu$; K changing from $5pu$ to $50pu$; D_q changing from $5pu$ to $50pu$.

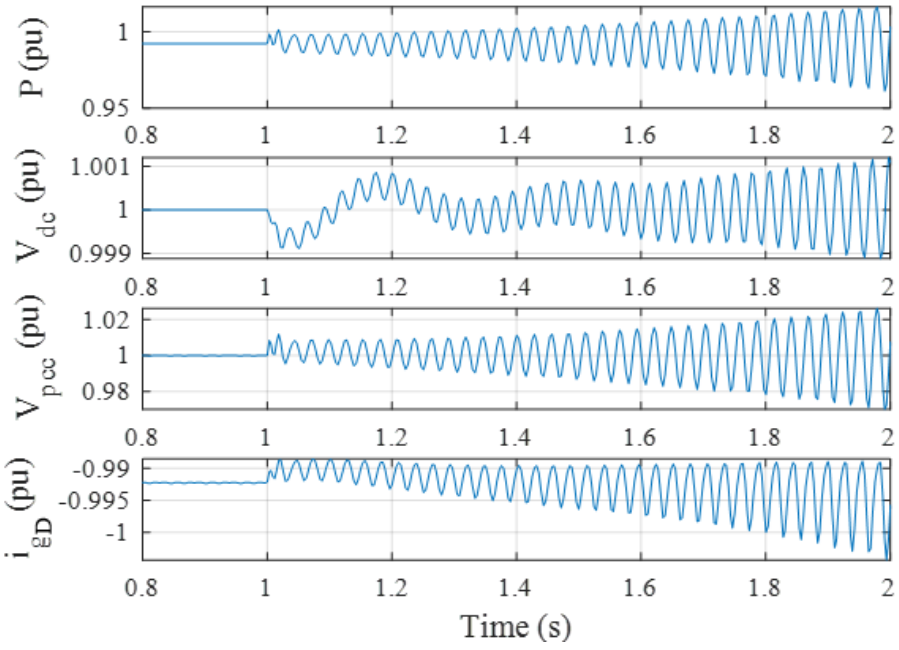

(a)

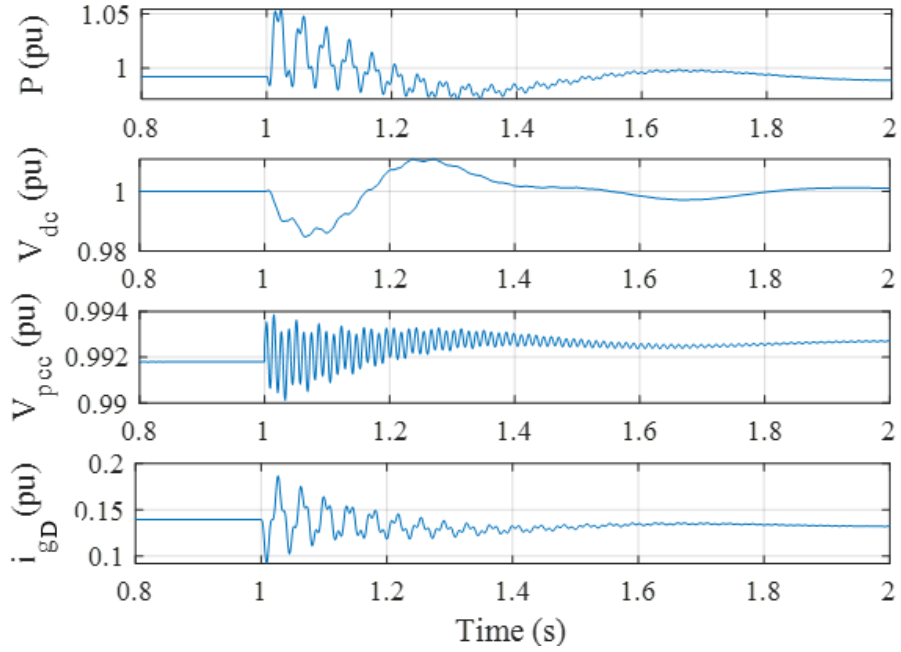

(b)

Figure 3-9 Dynamic response. (a) VCC. (b) VSM.

The time-domain simulations are further conducted based on MATLAB/Simulink to validate aforementioned analysis. A step disturbance of compensation level in transmission line which changes from 30% to 32.5% is applied at 1s and the simulation results are demonstrated in Figure 3-9. It can be observed that the wind farm with VCC experiences a sustained oscillation with higher compensation level while the system stability is maintained with VSM control under the same disturbance. This implies that VSM controlled system can accommodate higher compensation level.

The time-frequency analysis of active power in system with VCC is illustrated in Figure 3-10. The sub-synchronous component with frequency at 36 Hz is observed in active power and this matches the modal analysis results in Table 3-1. Therefore, the developed system model in this chapter reveals that there is a potential risk of unstable SSO in vector current controlled wind farm with higher compensation level.

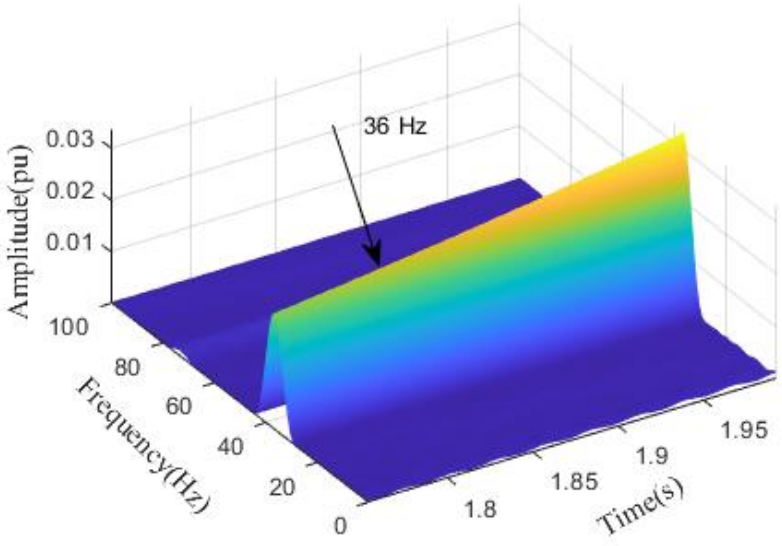

Figure 3-10 Time-frequency analysis of active power in vector current controlled system.

3.3.2 The Impacts of Number of Wind Turbines

The number of wind turbines which are on-service can also affect system sub-synchronous stability [54]. In this situation, the compensation level of the system is 20%, the eigenvalue locus considering the varied number of on-line wind turbines is depicted in Figure 3-11. It demonstrates that increasing the number of on-service wind turbines makes the SSO mode to move towards right which indicates a negative relationship between SSO stability and the number of on-line wind turbines. The increasing number of wind turbines can be equally considered to weaken grid strength [54]. For system with VCC, the SSO mode becomes unstable when the number of on-line wind turbines are larger than 105 with compensation level 20%. The VSM controlled system, by contrast, ensures reliable operation of wind farm without losing sub-synchronous stability.

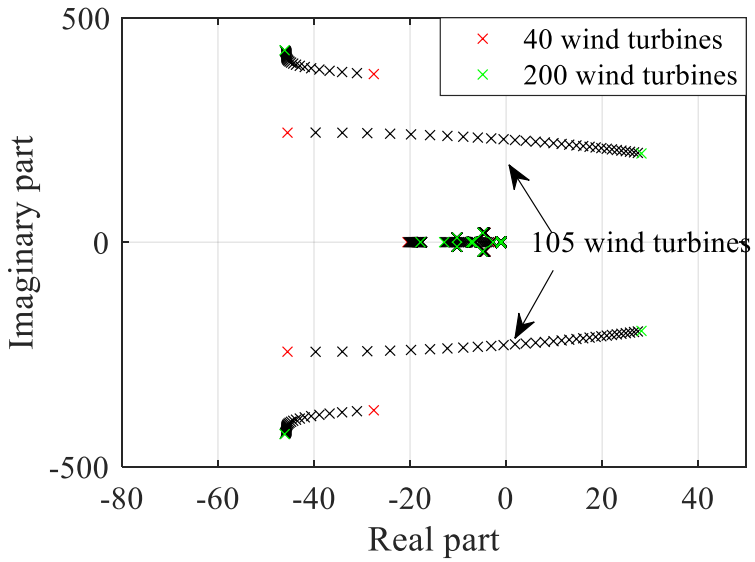

(a)

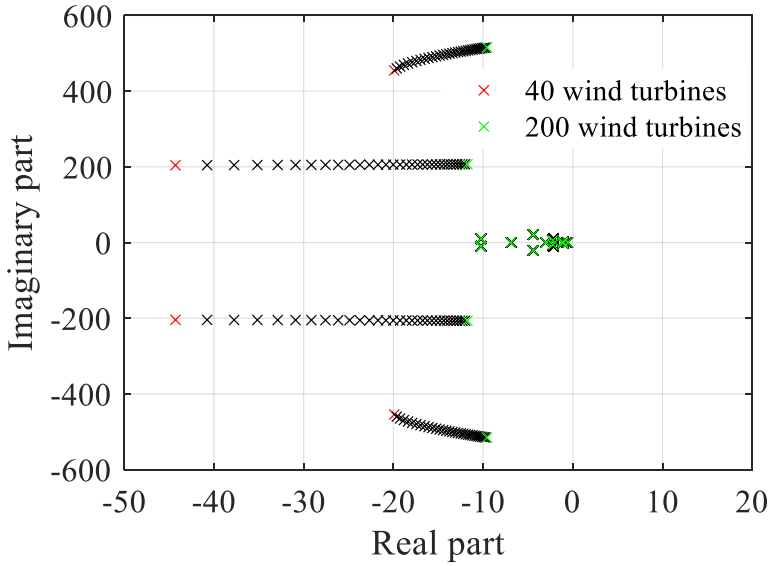

(b)

Figure 3-11 Eigenvalue locus of system with varied on-line wind turbines. (a) VCC. (b) VSM.

The time-domain simulation results are provided and they are illustrated in Figure 3-12. The number of on-service wind turbines changes from 100 to 105 at 1s. It is obviously revealed that the vector current controlled system will lose stability with larger number of wind turbines connecting to grid. Conversely, the system with VSM control remains stable with higher wind output power. The analysis results above indicate that VSM control can accommodate more wind energy integrated to power system.

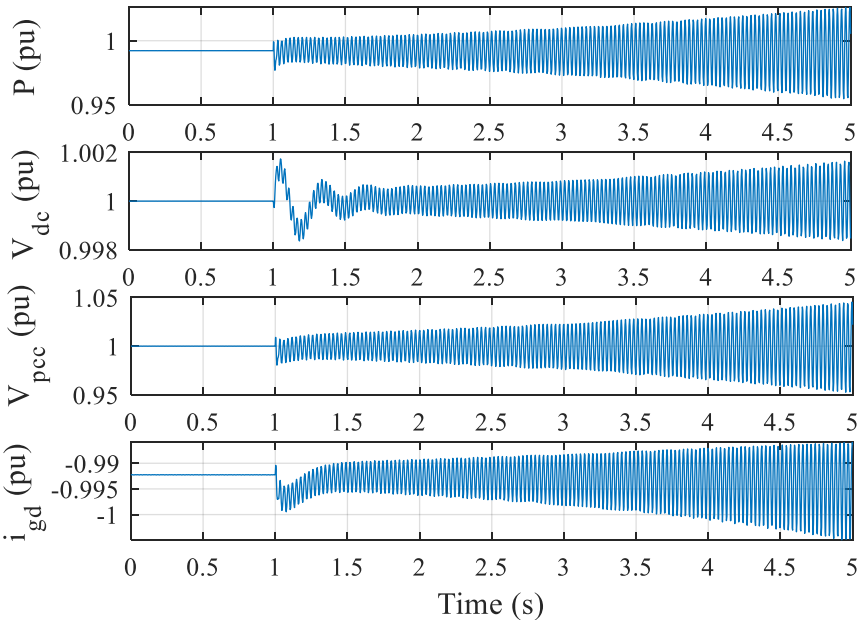

(a)

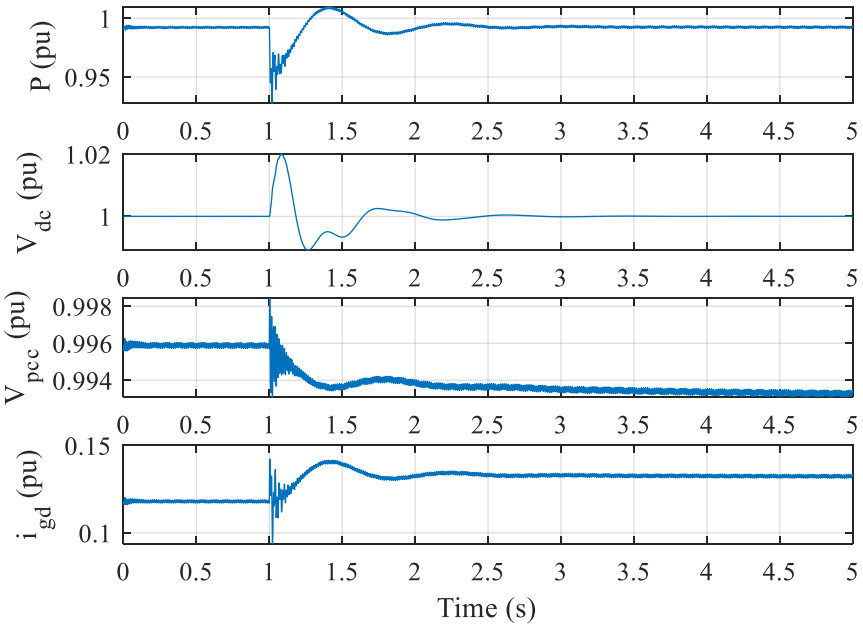

(b)

Figure 3-12 Dynamic response. (a) VCC. (b) VSM.

3.3.3 Two Aggregated Wind Farms

Since most wind power plant is equipped with vector control, to further investigate the impacts of VSM control on system sub-synchronous stability, the wind farm in Figure 3-1 is rearranged as two-aggregated system. The developed new system topology is demonstrated in Figure 3-13. Two wind farms are connected to the same bus and each wind farm have a rated power of 50 MW. The traditional VCC is implemented for wind farm 1 while wind farm 2 adopts aforementioned PLL-based and PLL-less control schemes

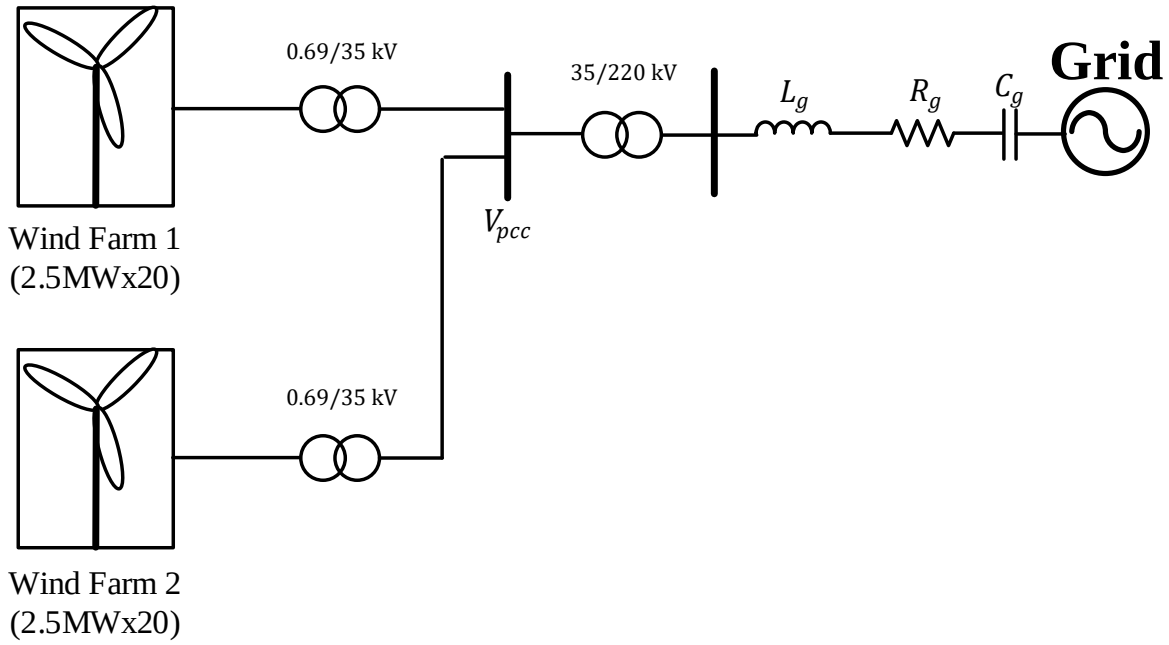

Figure 3-13 Equivalent circuit of two aggregated wind farms.

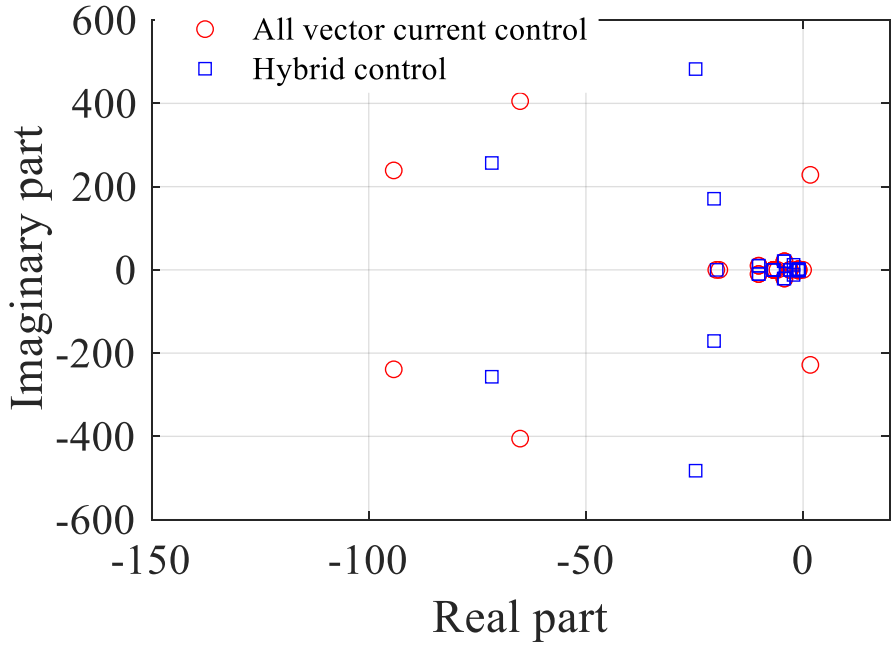

Figure 3-14 Eigenvalues of two aggregated wind farms.

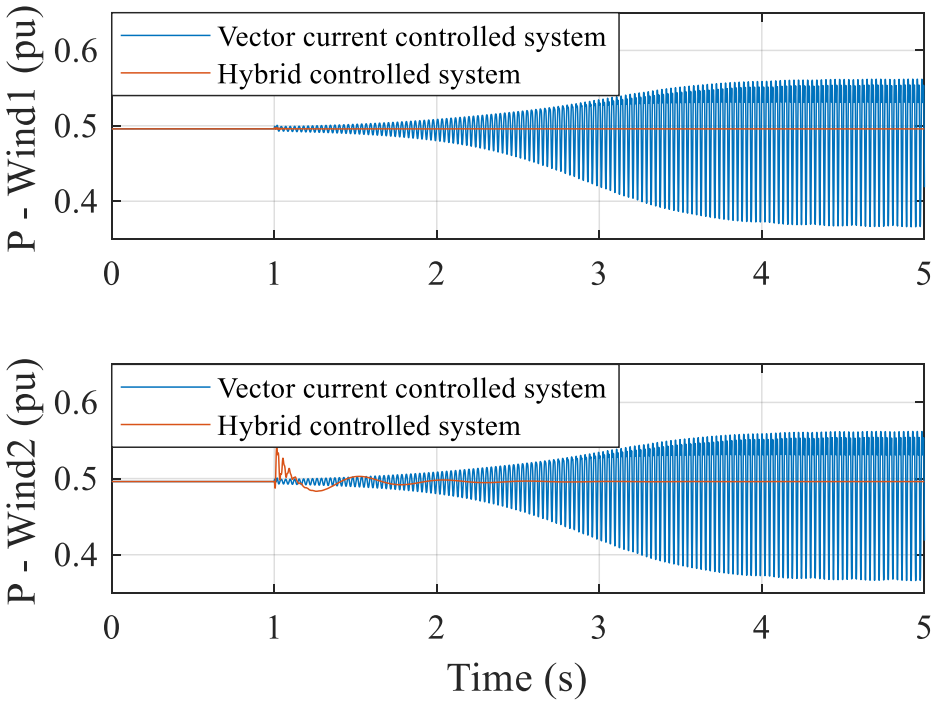

Figure 3-15 Dynamic response.

(all vector current controlled system and hybrid controlled system) to test the impacts of VSM on system SSO. The parameters are the same with the system in Figure 3-1.

The eigenvalues of aforementioned vector current controlled system and hybrid controlled system with CL equal to 32.5 % are illustrated in Figure 3-14. It is clear that all the eigenvalues of system with hybrid control are in the LHP which means they are stable. However, there is an unstable SSO mode in all vector current controlled system which represents the system stability is deteriorated. The simulation results with the same disturbance as mentioned in Section 3.3.1 are depicted in Figure 3-15. It can be seen that the system with hybrid control keeps stable when suffering such disturbance. Therefore, it implies that VSM control positively contributes to stabilizing the system in the sub-synchronous frequency range. And it also indicates that system stability can be improved by partly modifying the conventional control of PMSG-based wind farms.

3.4 Summary

This chapter has investigated the sub-synchronous stability of PMSG-based wind farm in series compensated AC network with VSM control. The wind farm with VCC is studied as well to compare system stability in the sub-synchronous frequency range. Modal analysis based on detailed small signal modelling is carried out to identify the SSO characteristics. For wind farm with VCC, the system is prone to suffering unstable SSO with higher compensation level and larger number of on-line wind turbines. The instability is caused by undesired interaction between PLL and RLC transmission lines. On the contrary, the VSM control is not actively participating in system SSO and this mode is lightly affected by VSM. Therefore, it can provide more flexibility to afford virtual inertia and damping services without compromising the sub-synchronous stability of system.

CHAPTER 4 COORDINATED DAMPING CONTROL DESIGN FOR POWER SYSTEM WITH MULTIPLE VIRTUAL SYNCHRONOUS MACHINES BASED ON PRONY METHOD

4.1 Introduction

A coordinated supplementary damping controller design for multiple VSMs is proposed in this chapter. The VSM control with VPSS is developed in Section 4.2. Sections 4.3 discusses the methods to identify system modes and Prony analysis is further utilised for VSM controller design in following sections. Then the general description of decentralised sequential control scheme is provided in Section 4.4. The implementation of proposed control is based on a revised two-area systema and a modified 39-bus system. It starts by revealing that the system low-frequency oscillatory modes are affected by multiple VSMs. And various cases are studied to validate the effectiveness of designed controller.

4.2 VSM Control with Supplementary Damping Controller

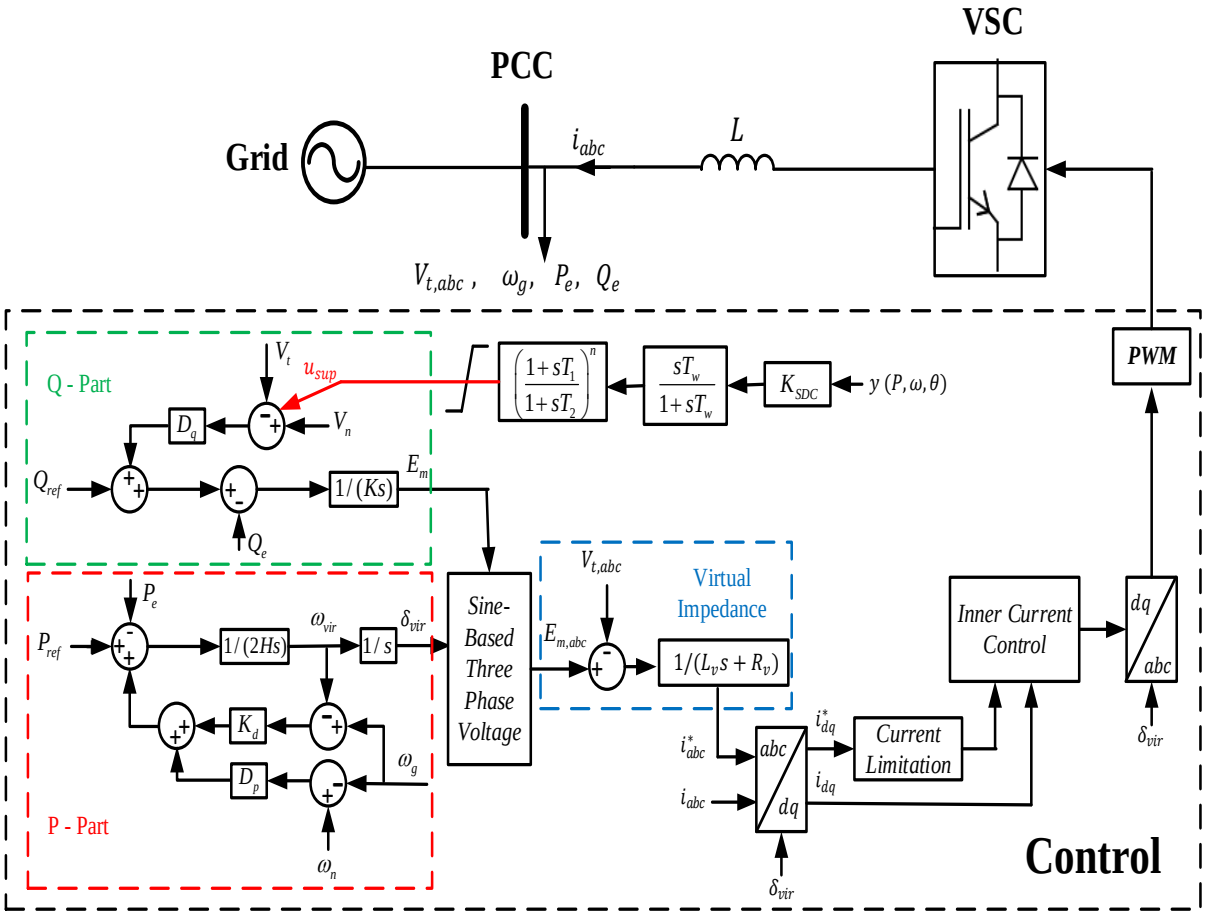

Figure 4-1 Diagram of converter with VSM control.

The VSM control implemented in this chapter is shown in Figure 4-1. For active power loop of VSM control, it is slightly different from Figure 3-1 where the $P-f$ droop is also included. The active power control is rewritten as:

$$2H\frac{d\omega_{vir}}{dt} = P_{ref} - P_e + D_p(\omega_n - \omega_g) + K_d(\omega_g - \omega_{vir}) \tag{4-1}$$

where D_p is the active droop coefficient and ω_g is the detected frequency from PLL. The supplementary damping controller added to reactive power control is explained as following.

Referring to the structure of PSS in conventional SG, which is originally utilised to counteract the adverse effect of fast excitation control, the dynamic model of exciter with PSS is represented as [164]:

$$E_m = G_{ex}(s)(V_{ref} - V_t + u_{sup}) \tag{4-2}$$

where u_{sup} is the supplementary signal and $G_{ex}(s)$ is the virtual excitation transfer function. If V_t can track the reference value without static error, then an integration block should be included in $G_{ex}(s)$. If $V - Q$ droop is considered as well,

$$V_{ref} = V_n + (Q_{ref} - Q_e)/D_q \tag{4-3}$$

where V_n is the nominal voltage. Combining (4-2) and (4-3) together, the following can be developed:

$$E_m = \frac{G_{ex}(s)\left(D_q(V_n - V_t + u_{sup}) + (Q_{ref} - Q_e)\right)}{D_q} \tag{4-4}$$

If $\frac{G_{ex}(s)}{D_q} = \frac{1}{Ks}$, (4-4) is rearranged as:

$$K\frac{dE_m}{dt} = D_q\left(V_n - V_t + u_{sup}\right) + \left(Q_{ref} - Q_e\right) \tag{4-5}$$

This explains how the supplementary control is implemented to VSM and it behaves like a VPSS.

The inner current control loop is adopted to achieve fast current control. The virtual impedance which emulates the output impedance of SG generates current reference and then feeds into current loop [93].

$$i^*_{abc} = \frac{E_{m,abc} - V_{t,abc}}{(L_v s + R_v)} \tag{4-6}$$

To secure the operation of converters, the current limitation [165] is also considered.

$$\begin{cases} |i_d^*| = min\,(I_{max}, |i_d^*|) \\ |i_q^*| = min\,(\sqrt{I_{max}^2 - i_d^{*\,2}}, |i_q^*|) \end{cases} \tag{4-7}$$

4.3 Oscillation Mode Identification Methods

A brief description of two mainstream methodologies, viz., the modal analysis and Prony method for system modes identification is presented in this section.

4.3.1 Modal Analysis

The modal analysis is subject to detailed system information and the modelling of system components is introduced respectively as below:

(1) Synchronous Generator and Exciter

The six-order model of SG and IEEE type-1 excitation system are modelled [166].

(2) Virtual Synchronous Machine

The mathematical modelling of VSM control has been presented in Chapter 3 and Section 4.2. Similarly, the transformation between local dq-reference frame and unified system DQ-reference frame should be considered.

(3) Overall System

Combining all the system differential equations above and power flow algebraic equations, the system oscillation modes can be identified with eigenvalue analysis based on linearised model.

4.3.2 Prony Method

The aforementioned modal analysis is dependent on system modelling details and operating points, which may not be suitable for practical large-scale power systems. On the other hand, a measurement-based methodology, i.e., Prony analysis, which does not require detailed system information, is used in this chapter to estimate system modal features. Prony analysis reconstructs the signal with a set of complex exponential functions [167],

$$\hat{y}_n = \sum_{i=1}^{p} M_i e^{j\theta_i} e^{(\alpha_i + j2\pi f_i)T_s n} = \sum_{i=1}^{p} H_i e^{\lambda_i t} \tag{4-8}$$

where $\hat{y}_{\mathrm{n}}$ is the estimated signal of a data sequence $\hat{\boldsymbol{y}} = [\hat{y}_0, \hat{y}_1 \dots \hat{y}_{\mathrm{N}-1}]$, p is the order of the fitting model, M_i is the magnitude of i_{th} mode, θ_i is the phase angle, α_i is the damping coefficient, f_i is the frequency, T_s is the time interval of sampling and H_i is the i_{th} output residue including the input signal (rather than the transfer function residue).

Considering the system is represented in Laplace domain ($Y(s) = G(s)U(s)$), the transfer function can be represented in residue form as:

$$G(s) = \sum_{i=1}^{p} \frac{R_i}{s - \lambda_i} \tag{4-9}$$

The residue H_i contains input signal information, which is not specified in (4-8). If input *U(s)* is given and it is assumed as a step signal, then the transfer function residue can be calculated as [149]:

$$\begin{cases} U(s) = \sum_{i=0}^{k} c_i \dfrac{e^{-sD_i} - e^{-sD_{i+1}}}{s} \\ R_j = \dfrac{H_j \lambda_j}{\sum_{i=0}^{k} c_i e^{\lambda_j (D_k - D_i)}} \quad j = 1,2 \dots p \end{cases} \tag{4-10}$$

After applying a known input disturbance to power system and then performing Prony analysis using corresponding output, the transfer function residue can be obtained. The estimated system information from Prony method can be utilised to guide system controller design.

4.4 Decentralised Sequential Damping Controller Design

As described before, the decentralized control is less dependent on communication compared to centralized control [146]. Besides, the coordinated sequential control can simplify the controller design process and reduce undesired interactions between controllers [142, 144].Therefore, a decentralised coordinated sequential design approach for the system with multiple VSMs is presented in this part. The proposed scheme is based on identified system transfer function with Prony method. A general description is demonstrated in this section.

In order to obtain the identified model, a probing signal is injected to VSM (e.g., a step voltage reference with small magnitude is applied to Q-part loop of VSM) as shown in Figure 4-2, the corresponding output related to power oscillation such as active power and virtual angular frequency, etc., is used to extract system oscillatory modes with Prony method. The obtained oscillatory pattern is then utilised to develop a reduced-order system.

The structure of supplementary damping controller is depicted in Figure 4-1 where y is the selected feedback signal from VSM. K_{SDC} is the supplementary controller gain; T_w is

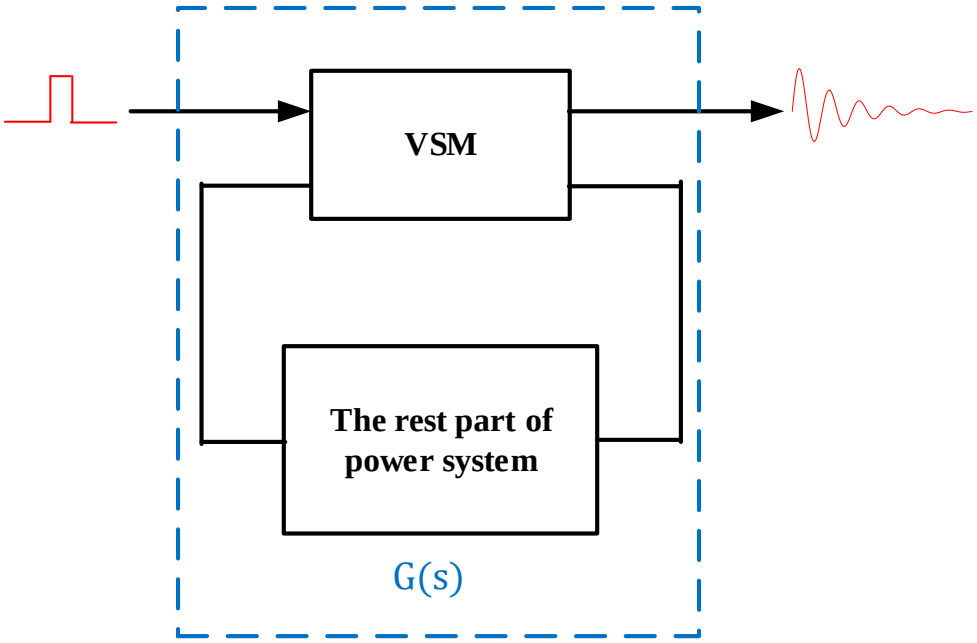

Figure 4-2 Data sampling process.

the time constant of wash-out block and typical values are 1~20s [159]; T_1 and T_2 are the time constants of lead-lag block. After obtaining system oscillation information, the residue method is utilised to calculate lead-lag block parameters. With the identified system transfer function $G(s)$ and obtained SDC parameters, the gain K_{SDC} can be determined with root-locus method.

To coordinate damping controllers for multiple VSMs, the sequential approach depicted in Figure 4-3 is implemented. The power grid is first treated as a SISO system and the damping controller for first VSM is designed with preceding steps. After obtaining the damping controller for first VSM, a closed-loop system model including the designed controller is formed (as highlighted in Figure 4-3) and it is regarded as a new open-loop system for next VSM damping controller design. With such method, undesired adverse interactions among

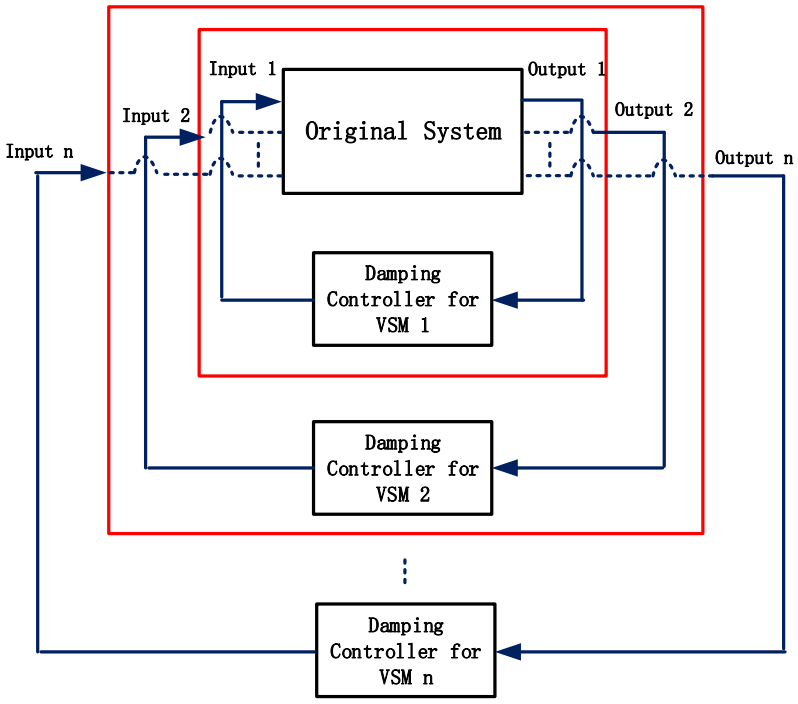

Figure 4-3 Sequential design approach.

different VSM units in damping controller design can be reduced and the design process of multiple damping controllers can be simplified as well.

The complete controller design process can be summarised as following:

(1) Step 1: Injecting a specified input disturbance to first VSM and extracting system oscillatory information with Prony method;

(2) Step 2: Designing the damping controller with obtained system information and testing system performance. More specifically, the parameters of lead-lag block are obtained based on residue method and the stabilizing gain is determined with root-locus method;

(3) Step 3: Repeating Step 1 and Step 2 to design damping controller for next VSM;

(4) Step 4: Validating the effectiveness of designed controller after finishing the decentralised sequential damping controllers for multiple VSMs.

4.5 Stability Analysis and Simulation Results

In this section, a revised two-area system is first analysed with modal analysis which reveals the impacts of VSMs on system LFOs. Then Prony method is applied to extract system modes which are subsequently for SDC design. A decentralised sequential control method is proposed for the coordinated damping controller design of multiple VSMs. A more complex power system based on New-England 39-bus system is modelled as well to confirm the effectiveness of designed controller. The phasor-type model in MATLAB/Simulink are developed for conducting relevant simulations.

4.5.1 Modal Analysis, Controller Design and Simulations of Two-Area System

A modified case based on the two-area benchmark system [159] is developed to analyse the impacts of multiple VSMs on power system LFO modes. The schematic diagram of two-area

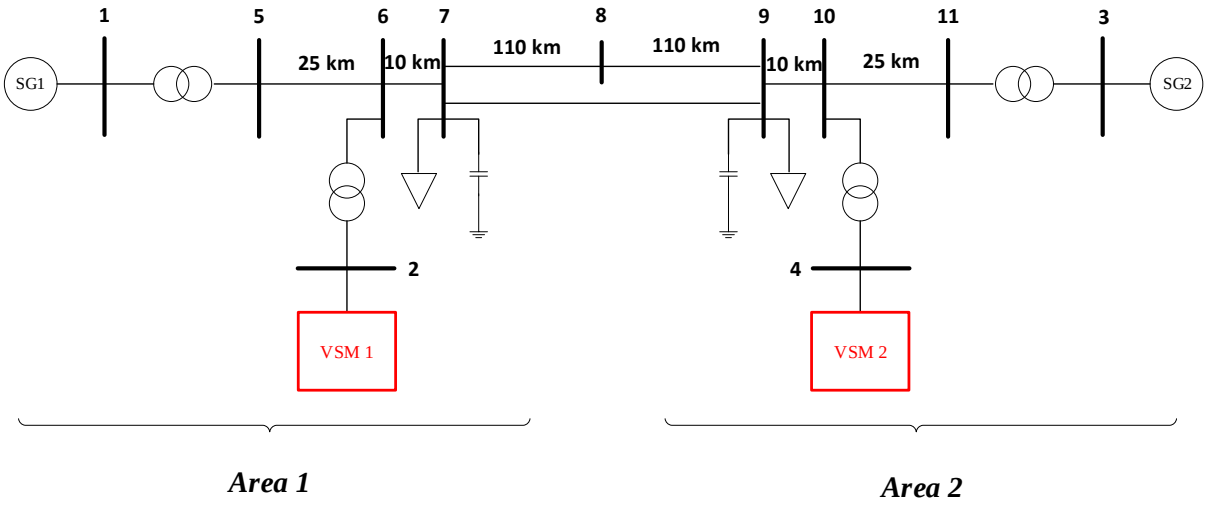

Figure 4-4 Single line diagram of modified two-area system.

system is demonstrated in Figure 4-4. The SGs in bus 2 and bus 4 are replaced with two VSMs respectively. The power balance of system is maintained by making power from VSMs to be equal to output power from original SGs. The PSSs of SG1 and SG2 are deactivated to facilitate a clear demonstration about the impacts of VSMs on LFOs. Most system parameters can be found in [159] and detailed parameters of VSM controller are listed in Table A-4 in the Appendix.

(1) Electro-Mechanical Stability Analysis

The modal analysis is first applied to two-area system to accurately obtain the characteristics of LFOs. The oscillatory patterns of LFO are shown in Table 4-1. It can be observed from Table 4-1 that there are three LFO modes of the modified two-area system. Theoretically, for traditional SGs, $n-1$ intrinsic LFO modes exist in system if there are *n* swing equations. In this case, two SGs and two VSMs are modelled in two-area system. Therefore, the inherent three LFO modes are caused by four rotor dynamic equations. It demonstrates that there are one inter-area mode and two local modes which is similar to that of original two-area benchmark system.

TABLE 4-1
EIGENVALUE ANALYSIS RESULTS OF REVISED TWO-AREA SYSTEM

No.	Frequency (Hz)	Damping ratio	Dominant states
1	1.167	0.101	$\omega_{SG2}, \theta_{SG2}; \omega_{VSM2}, \theta_{VSM2}$
2	1.137	0.116	$\omega_{SG1}, \theta_{SG1}; \omega_{VSM1}, \theta_{VSM1}$
3	0.588	0.056	$\omega_{SG1}, \theta_{SG1}; \omega_{SG2}, \theta_{SG2};$ $\omega_{VSM1}, \theta_{VSM1}; \omega_{VSM2}, \theta_{VSM2}$

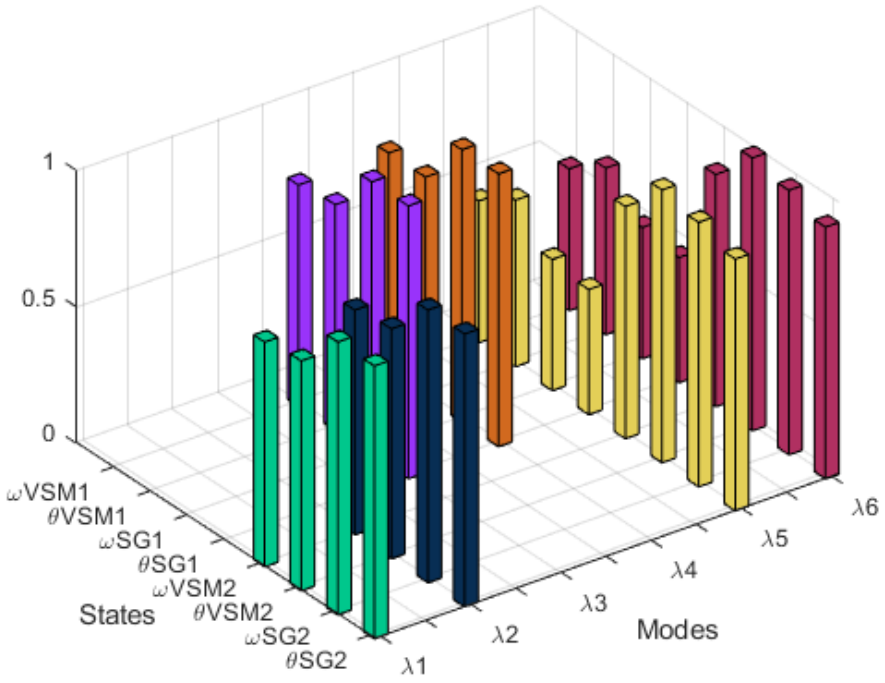

Figure 4-5 Normalised participation factor of low-frequency modes.

The normalised participation factor of three LFO modes is illustrated in Figure 4-5. The conjugate eigenvalues λ_1 and λ_2 are related to mode 1. The rotor states ($\theta_{SG2}, \omega_{SG2}, \theta_{VSM2}\ and\ \omega_{VSM2}$) with high participation factor values indicate that they have the most contribution to this local oscillation. The rotor states ($\theta_{SG1}, \omega_{SG1}, \theta_{VSM1}\ and\ \omega_{VSM1}$) of λ_3 and λ_4 in area 1 reveal they are dominant in mode 2. Similarly, the participation factor of λ_5 to λ_6 shows that virtual swing equation states ($\theta_{VSM}, \omega_{VSM}$) have a considerable interaction with SG rotor states (θ_{SG}, ω_{SG}).

The obtained mode shapes, which are based on right eigenvectors corresponding to rotor speeds, related to three LFO modes are presented in Figure 4-6. Figure 4-6 (a) demonstrates the mode shape of local mode 1 where SG2 oscillates against VSM2 in area 2. In addition, SG1 swings

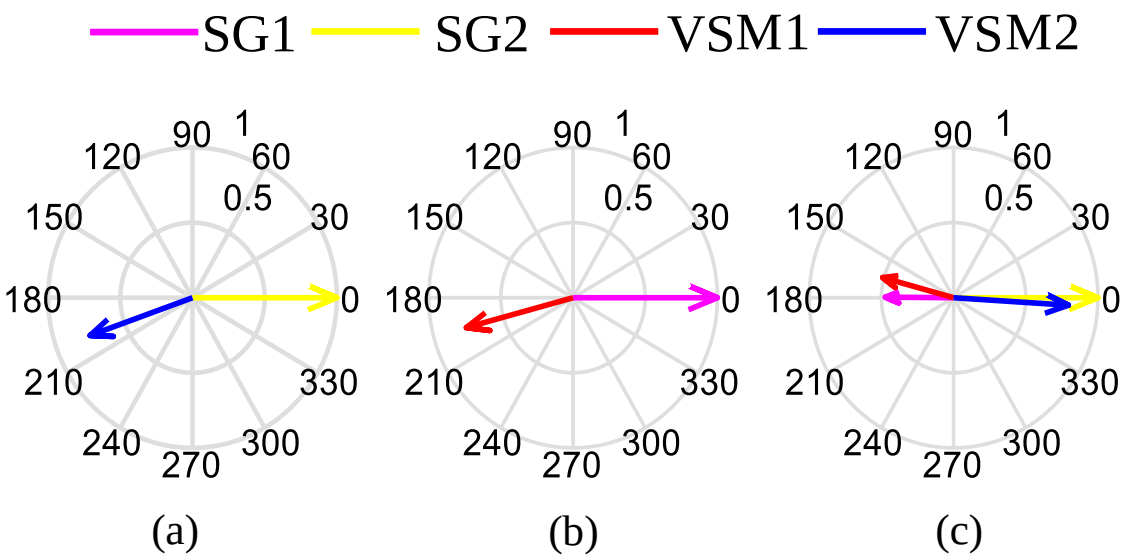

Figure 4-6 Mode shapes. (a) Mode 1; (b) Mode 2; (c) Mode 3.

against VSM1 in area 1 as shown in Figure 4-6 (b). For mode 3, it is obvious that the VSM and SG group in area 1 are oscillating against the other group in area 2.

For conventional SGs, homogenous generators in the same area are determined based on geographical locations and different areas are usually linked with weak tie-lines [159]. Based on the analytical results, it can be inferred that the integration of VSMs into power grid has similar effects on system LFO modes like SGs.

(2) Decentralised Sequential Supplementary Damping Controller for Multiple VSMs

The strong interactions between VSMs and SGs in the low-frequency range promotes the investigation of oscillation damping improvement. In order to improve system damping performance, the aforementioned coordinated decentralised sequential damping control is implemented for two-area system.

The feedback signals for damping control which are related to power oscillations are considered to be potential candidates. In this chapter, the electrical power from VSM is selected as feedback input signal for auxiliary damping controller. The supplementary stabilizing signal is added to the virtual excitation loop because additional regulation in active power loop may introduce mechanical vibrations and shorten the lifespan of mechanical structures if they are applied to wind system [168]. Since the feedback signal is sampled from local signal, the consideration of time compensation caused by communication delay is ignored in this chapter.

Before implementing Prony analysis, a step disturbance is injected to VSM1 to obtain the sampled data. A step change of V_n with 0.05 pu lasting 0.2s is applied to the Q-part of VSM1. The active power of VSM1, $P_{e,VSM1}$, is chosen as the output signal, which will then be sampled for Prony analysis. As can be observed in Figure 4-7, the approximately reconstructed signal by Prony method in red fits the actual signal well. The estimated LFO information is given in

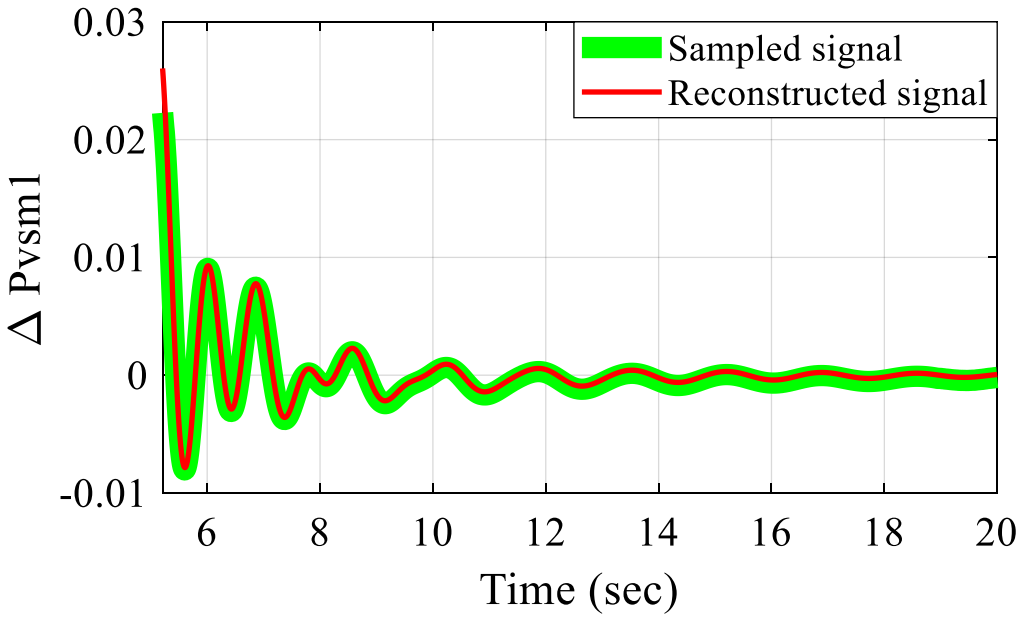

Figure 4-7 Reconstructed signal.

Table 4-2. The first estimated two modes imply that VSM1 has a high participation in these oscillations and this is consistent with the eigenvalue analysis results in Table 4-1. However, the mode with frequency 1.167 Hz is not identified by Prony method since VSM1 is not participated in it.

TABLE 4-2
IDENTIFIED REDUCED-ORDER SYSTEM TRANSFER FUNCTION

Mode	Frequency (Hz)	Damping ratio	Eigenvalue	Residue (R∠ϕ)
1	0.593	0.058	$-0.217 \pm \text{j}3.726$	$0.186\angle 2.95^{o}$
2	1.148	0.112	$-0.813 \pm j7.213$	$0.991\angle -24.03^{o}$
3	0	--	-0.00123	$-0.0133\angle 180^{o}$
4	0	--	-0.325	$-0.119\angle 180^{o}$
5	0	--	-0.974	$0.854\angle 0^{o}$
6	0	--	-1.551	$0.342\angle 180^{o}$

A reduced-order system transfer function (with V_n as input and $P_{e,VSM1}$ as output) can be developed based on the obtained information of eigenvalues and residues. The bode plot as depicted in Figure 4-8 shows that the reconstructed transfer function has a relatively good fitness of two-area system in the frequency range of interest.

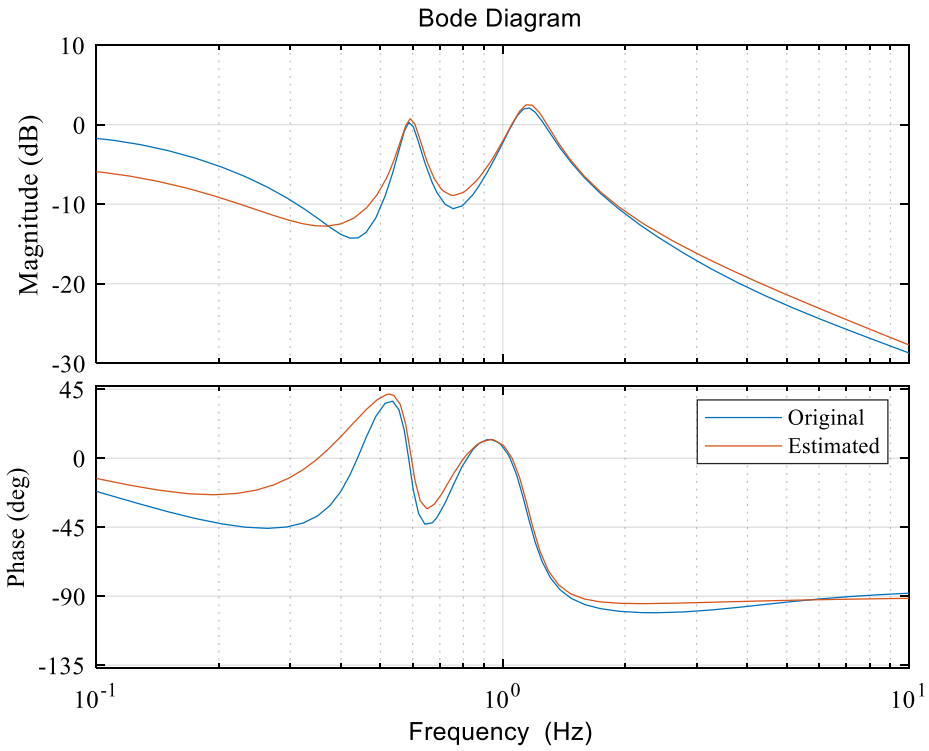

Figure 4-8 Bode plot.

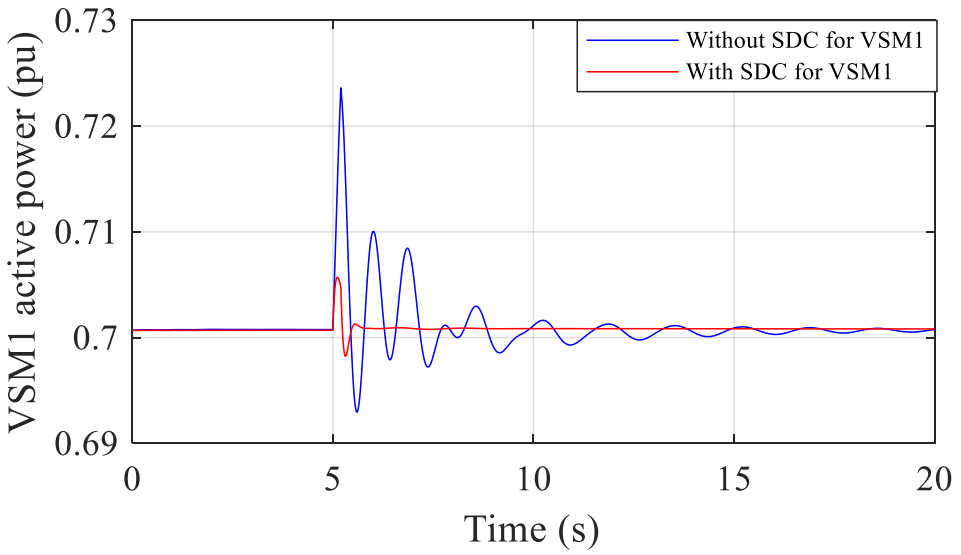

Figure 4-9 Dynamic response.

The parameters of lead-lag block can be calculated with the identified residue information in Table 4-2. Although mode 2 with large residue is chosen for calculation, the damping of other modes will be increased if possible. With identified transfer function, the gain K_{SDC} of SDC for VSM1 is determined using root-locus method. A step disturbance in V_n of VSM1 is applied to test the designed controller for VSM1. The simulation in Figure 4-9 shows that the oscillation with SDC is damped out quickly.

As there are two VSMs integrated into two-area system, the supplementary controller for each VSM should be designed in a coordinated manner if possible which aims to reduce the undesired interactions between auxiliary damping controllers. The decentralised sequential approach which has been presented in Section 4.4 is utilised to design multiple SDCs step by step, i.e., SDC1 for VSM1 and then SDC2 for VSM2. As the dynamics of SDC1 are already incorporated into Prony analysis before designing SDC2, the coordination of multiple SDCs is achieved. The controller parameters may be different with various design sequences while there is slight impact on overall system damping performance [144]. The

comparison of system damping with different design sequences is illustrated in Figure 4-10. (SDC1SDC2 represents designing VSM1 first and then VSM2, SDC2SDC1 represents the reversed sequence). It shows that the designed controller can enhance the damping of LFO modes and overall system damping is almost the same with different design sequences.

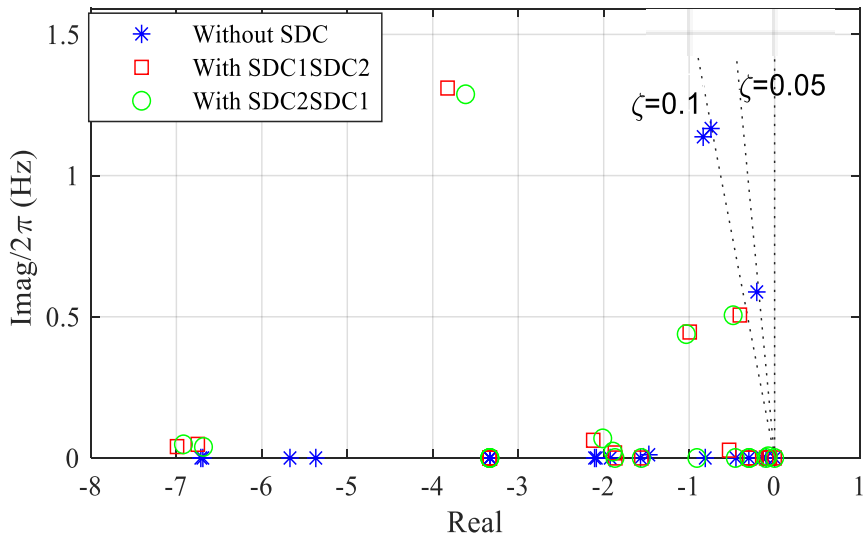

Figure 4-10 System damping comparison.

Considering the impacts of different virtual inertia and damping in the presence of designed controller, the eigenvalue locus of these two coefficients variation is demonstrated in Figure 4-11. It can be observed that three modes are shifted towards left within the varied range (5~15s). This indicates that the designed scheme may accommodate the application of high virtual inertia of VSM required by system. When virtual damping K_d increasing from $20pu$ to $50pu$, the two modes near imaginary axis are slightly affected. On the other hand, increasing K_d makes the mode with higher frequency to move towards left which means this mode becomes more stable. Therefore, it may be inferred that the robustness of designed controller can be guaranteed with a varied range of virtual inertia and damping coefficients.

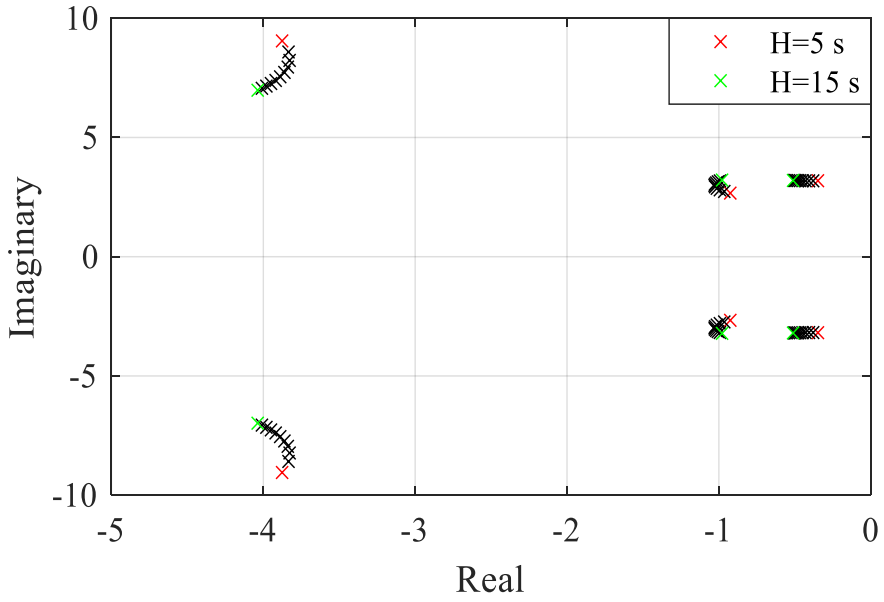

(a)

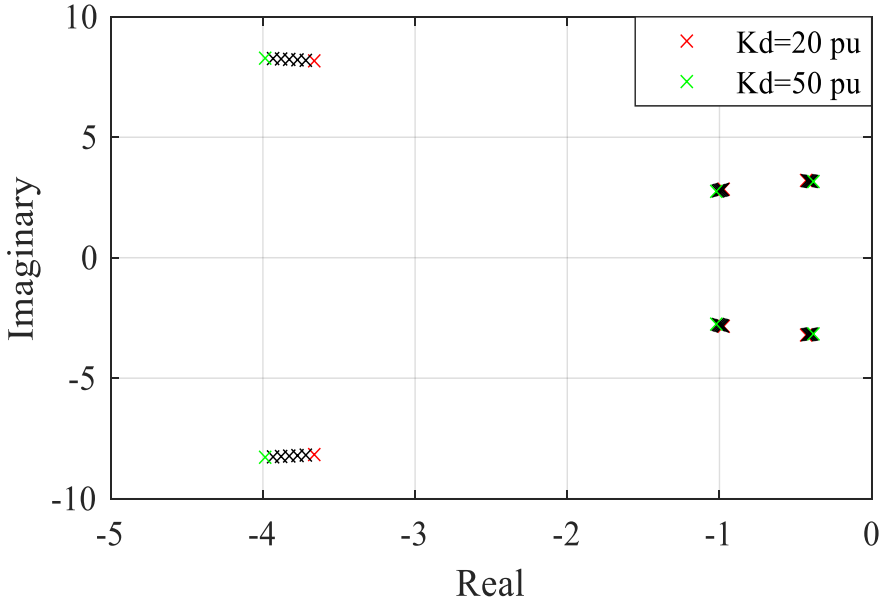

(b)

Figure 4-11 Impact of different virtual inertia and damping with designed controller. (a) H changing from 5s to 15s. (b) K_d changing from $20pu$ to $50pu$.

(3) Time-Domain Simulation

The effectiveness of designed coordinated damping controllers is examined based on time-domain simulations. Six cases with different system conditions are carried out on revised two-area system. The disturbances are organised as follows,

Case 1: The impact of small variations: A step disturbance of voltage lasting 0.2s with $0.05pu$ magnitude is applied to the excitation control of SG1.

Case 2: The impact of large disturbance. A three-phase-to-ground fault is excited on one of the transmission lines between two areas at 5s with a duration of 0.1s. And this disturbance is applied for Case 3, Case 5 and Case 6 as well.

Case 3: The impact of heavily loaded tie-line. A 300MW load in area 1 is transferred to area 2 which leads to the power flow through tie-line increasing from 413MW to 670MW.

Case 4: The impact of continuously changing load. A 15MW load is added to bus 7 at 2s, following by 25MW load increase at 10s, a decrease of 10MW load at 20s and a further 20 MW decrease at 30s.

Case 5: The impact of electrical distance of tie-line. The distance of tie-line between two areas is set as 180km, 220km and 260km respectively.

Case 6: The impact of penetration level of VSM. The SG1 in two-area system can be replaced with a new VSM to model a 3VSMs system. An all-VSMs system is developed if such replacement is also implemented for SG2. Therefore, the power from non-synchronous generators accounts for 50%, 75% and 100%.

The simulation results of Case 1 are illustrated in Figure 4-12. The system responses without the deigned scheme are plotted as well to show a clear comparison. It can be observed from Figure 4-12 that system damping is enhanced with the designed controller. The oscillation of tie-line power decays faster with the proposed coordinated controller. As shown in this figure, the active power oscillation of SG2 is also suppressed significantly. In addition, the observed oscillations in rotor speed and active power of VSM1 die down faster due to the improved damping from supplementary controller.

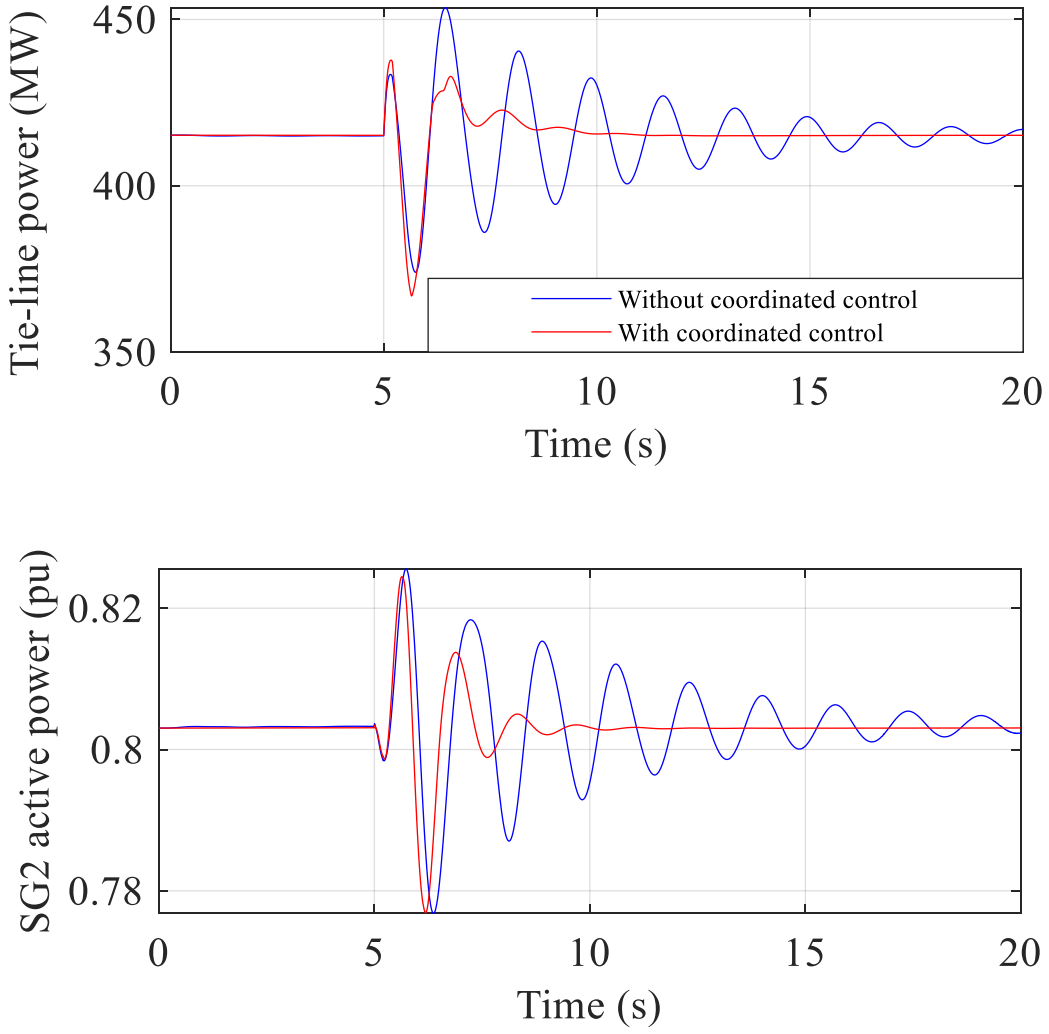

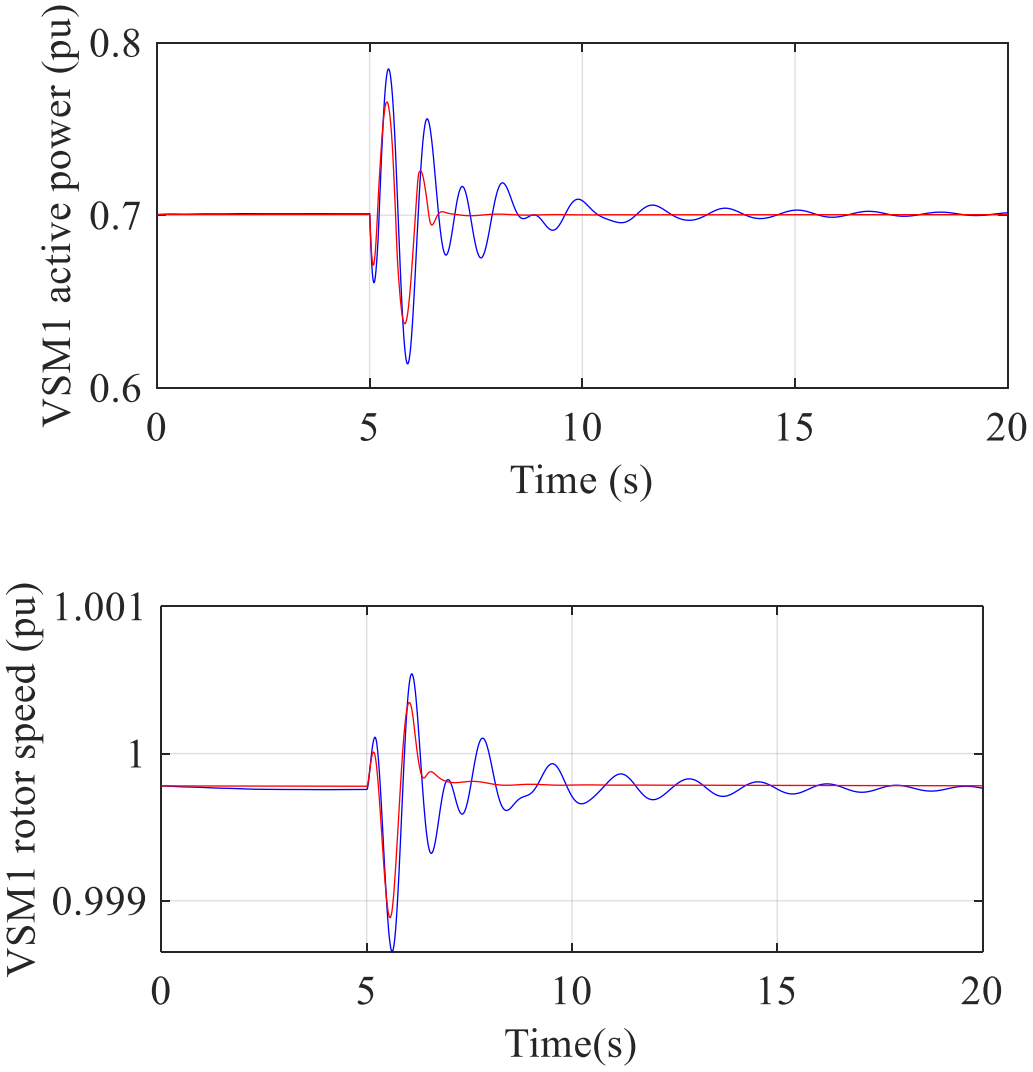

Figure 4-12 Two-area system responses under generator excitation disturbance.

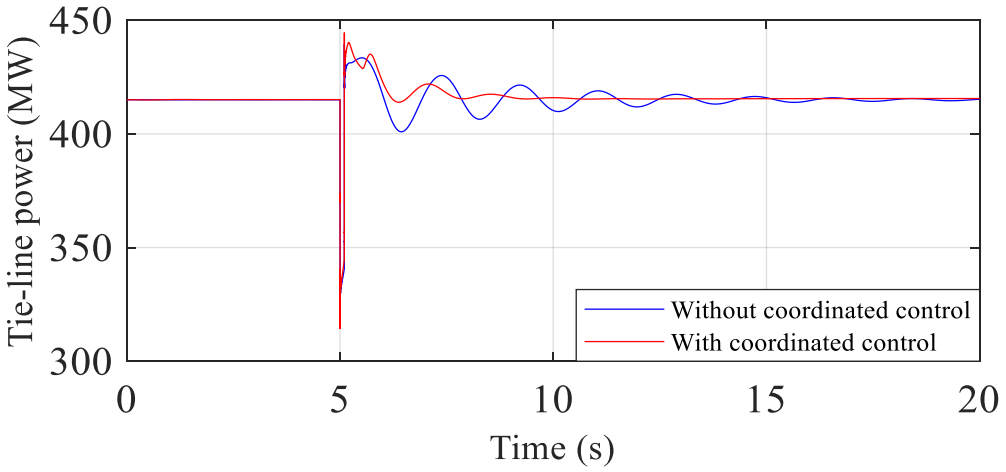

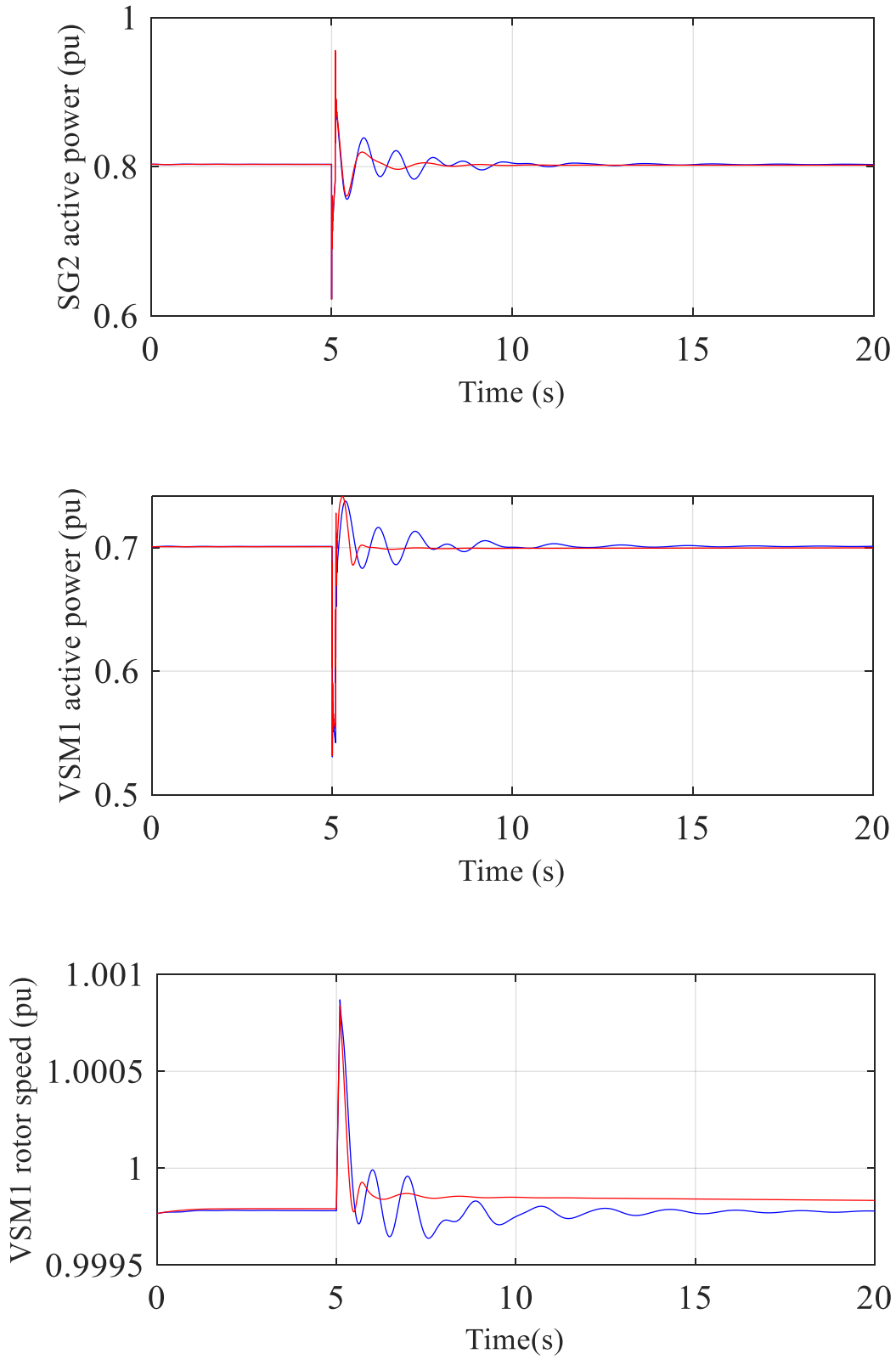

Figure 4-13 Two-area system responses under fault disturbance.

The simulation results of Case 2 which considers a serious contingency three-phase-to-ground fault are illustrated in Figure 4-13. The three-phase-to-ground fault is much severer than single-phase fault and it may lead to the trip of transmission lines. As shown in Figure 4-13, the oscillations suppression can be observed in the selected system signals. Therefore, the damping improvement from designed controllers under large disturbances can still be provided.

To observe the functionality of designed supplementary controllers under heavily loaded tie-line condition, the simulation results of Case 3 are presented in Figure 4-14. From this figure, it can be observed that the active power oscillations of four sources (SGs and VSMs) with designed scheme is suppressed quickly than that without designed control.

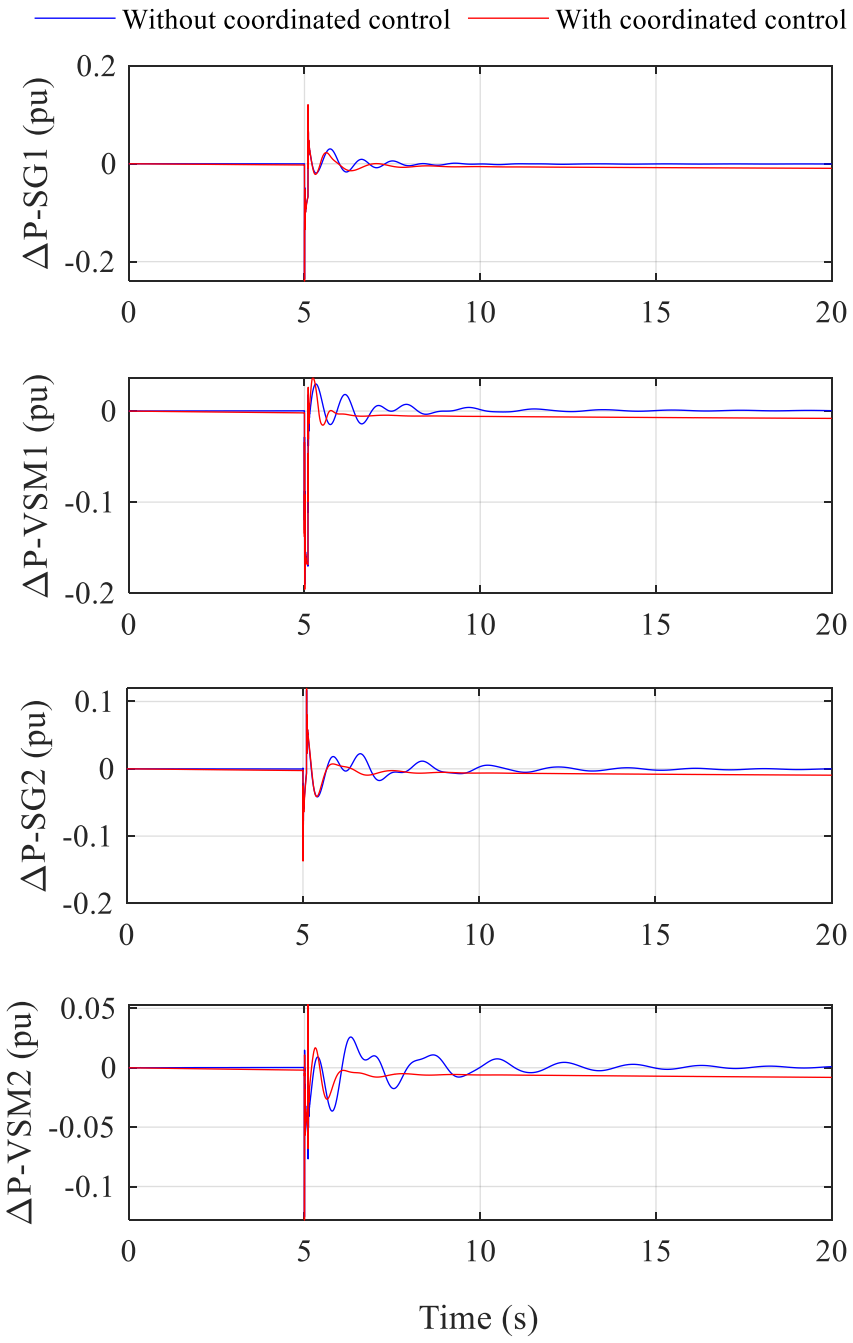

Figure 4-14 Two-area system simulation for heavily loaded tie-line.

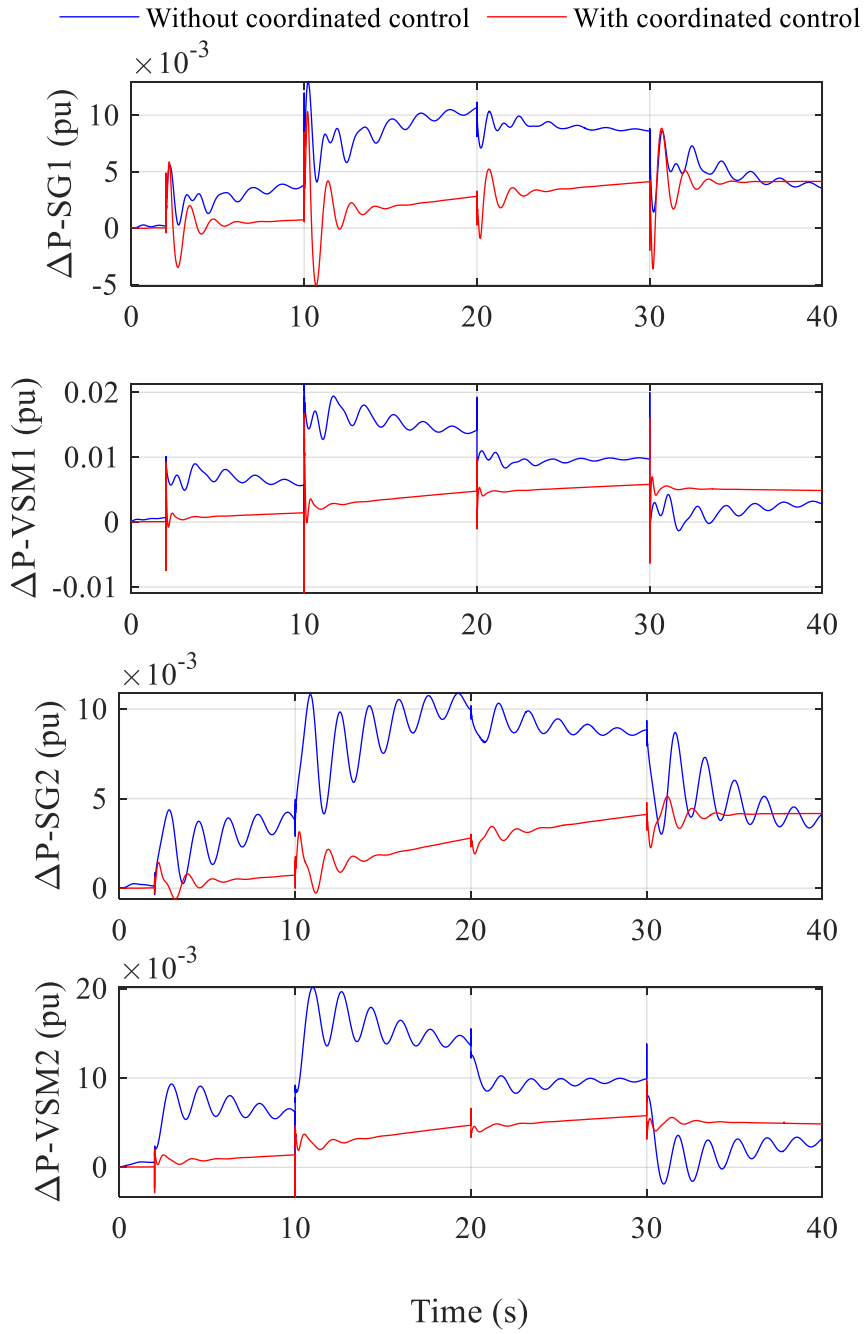

Figure 4-15 Two-area system simulation for continuously changing load.

The purpose of Case 4 is to test whether the damping contributions from coordinated controllers can be guaranteed for varying load conditions. As demonstrated in Figure 4-15, the

action power oscillations observed in SG and VSM are effectively suppressed with continuously changing load.

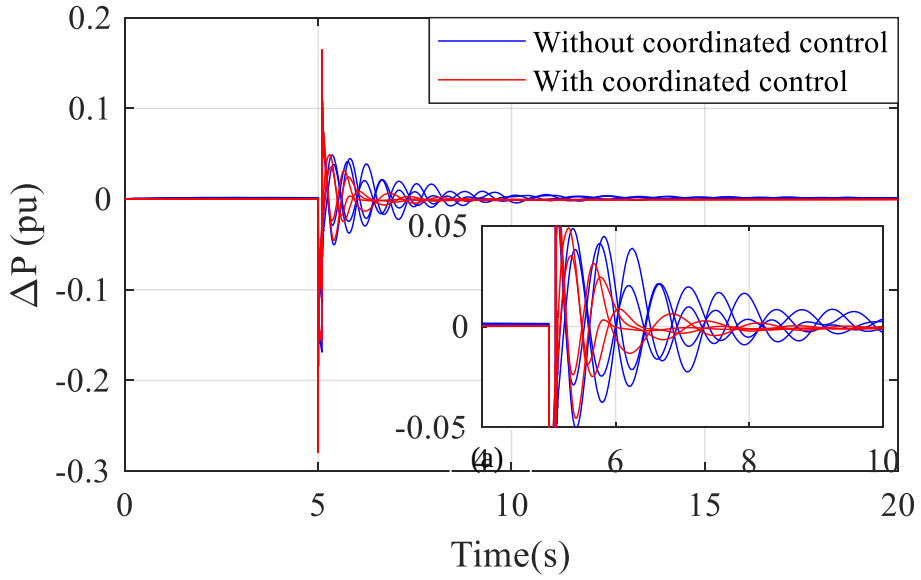

(a)

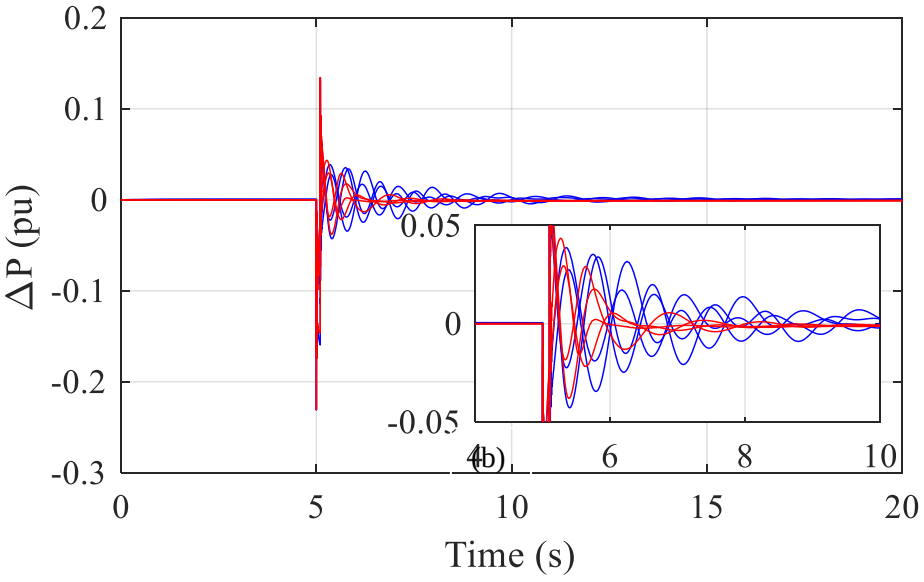

(b)

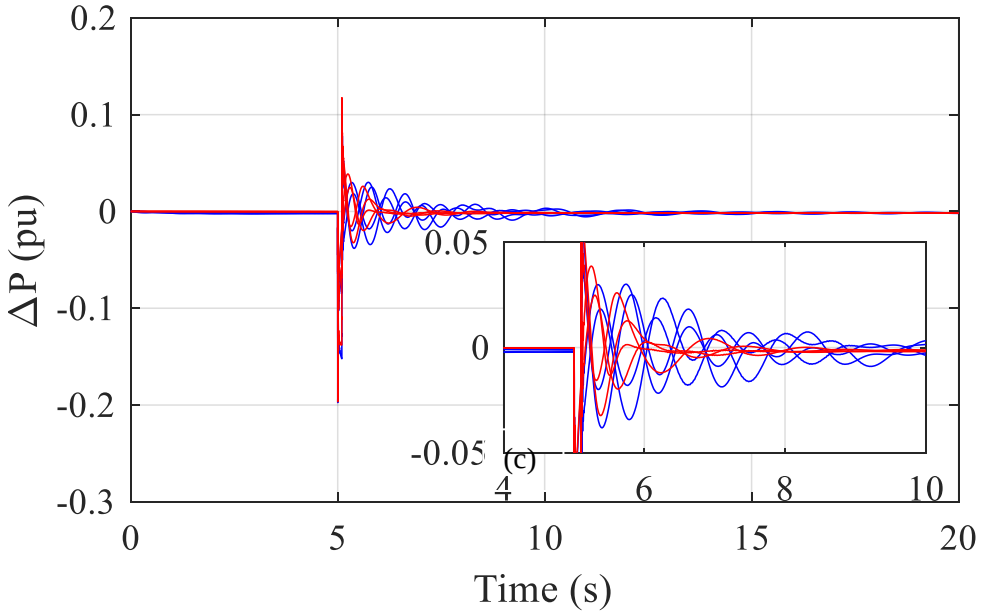

(c)

Figure 4-16 Two-area system simulation for different electrical distance. (a) 180km. (b) 220km. (c) 260km.

The test to show the functions of designed damping controllers for different length of tie-line is illustrated in Figure 4-16. The active power from all devices is plotted on the same figure. From Figure 4-16, the alleviation of active power oscillation indicates the designed scheme can provide additional damping to system. The improved damping is achieved for these three scenarios which consider the variations of tie-line length.

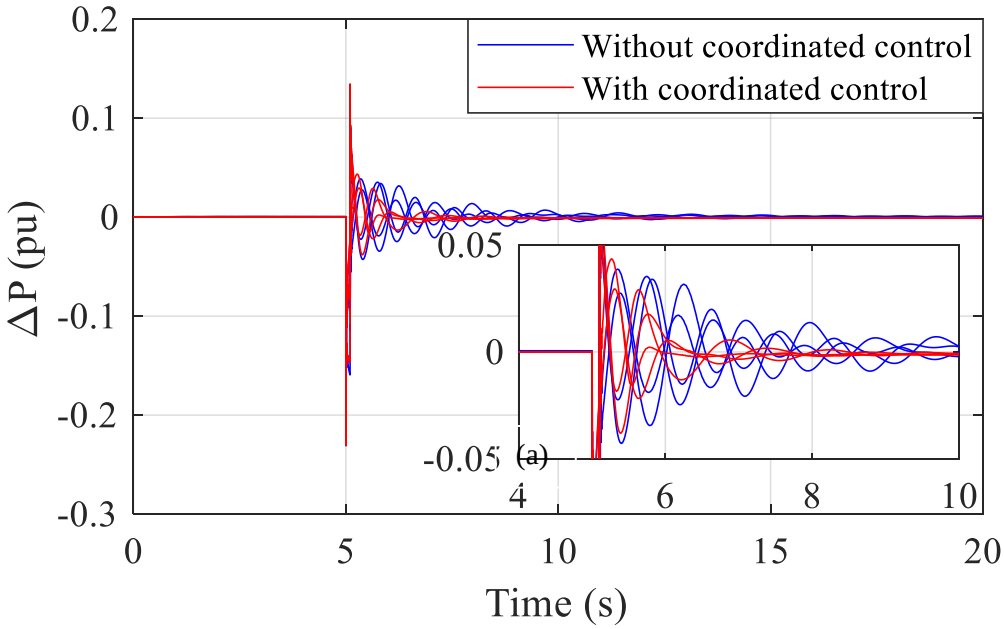
Without coordinated control
With coordinated control
ΔP (pu)
Time (s)
(a)

(a)

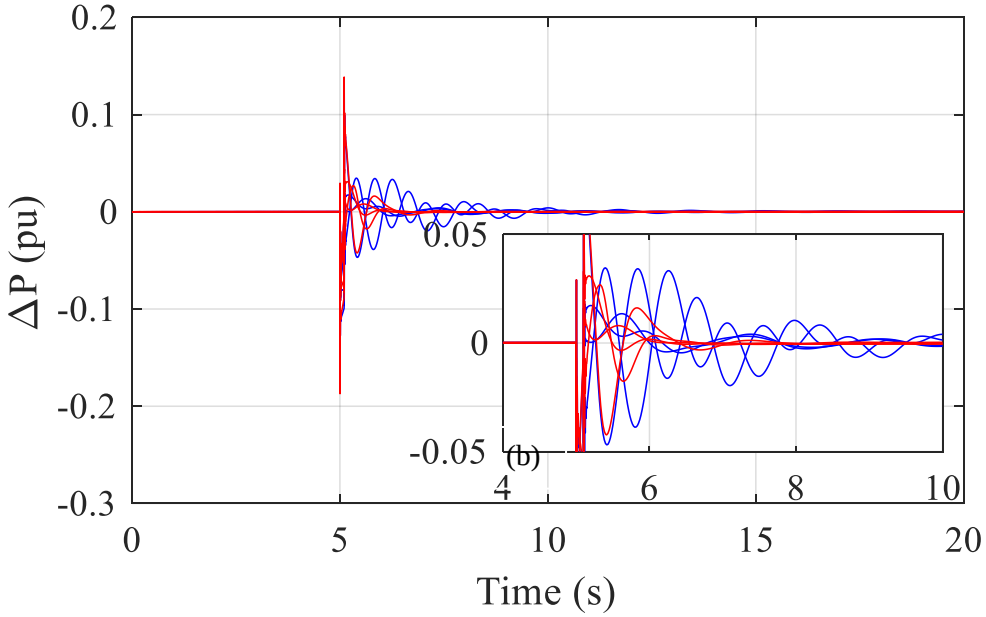
ΔP (pu)
Time (s)
(b)

(b)

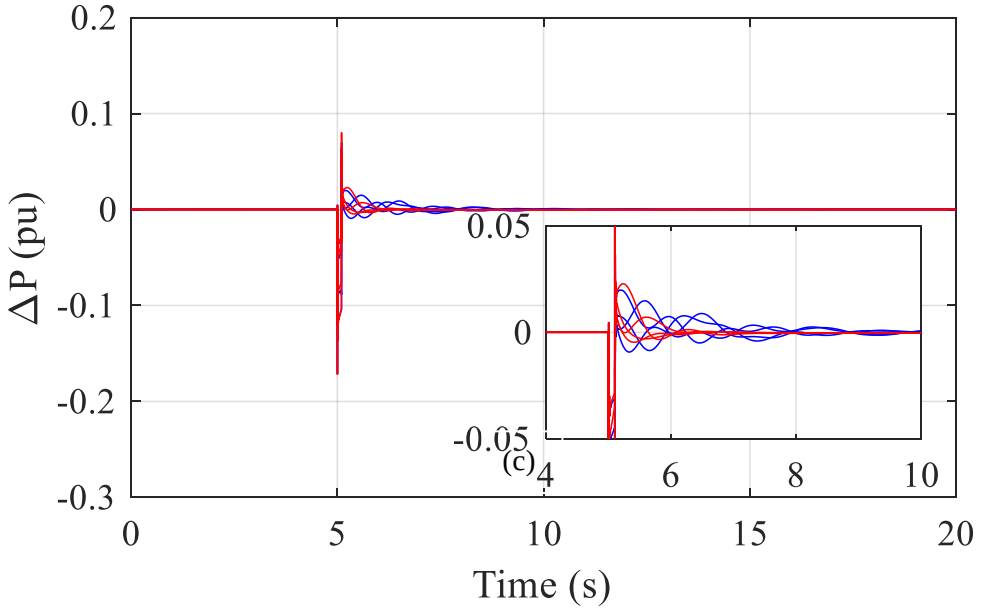

(c)

Figure 4-17 Two-area system simulation for different penetration level. (a) 50%. (b) 75%. (c) 100%.

Figure 4-17 demonstrates the simulation results of Case 6 considering different levels of non-synchronous generation. For those situations with different penetration level, it is noticeable that not only the active power of SG, but also the real power from VSM achieve better damping performance with coordinated control.

Based on the simulation results above, the satisfactory damping performance is guaranteed under various types of disturbances. Although the coordinated supplementary controllers are primarily designed on the basis of small signal analysis, the enhanced damping performance under large disturbances demonstrates that the designed controller can exhibit effectiveness and robustness against different system conditions.

4.5.2 Test Results of 39-Bus System

The feasibility and robustness of proposed method is further investigated in a more complex power system. A modified system based on New England 39-bus benchmark is developed as illustrated in Figure 4-18. In the modified system, three VSMs are installed at bus 31, bus 34 and bus 38 respectively. The power from original SG2, SG5 and SG9 are replaced with three VSMs. The PSSs are activated for the remaining SGs except SG1.The VSM controller parameters are the same as before and detailed system parameters of other components can be found in [169]. The supplementary controller is first designed for VSM2 and followed by VSM5 and VSM9. The effectiveness and robustness of designed controller are examined under various disturbances and time-domain simulation results are presented as below.

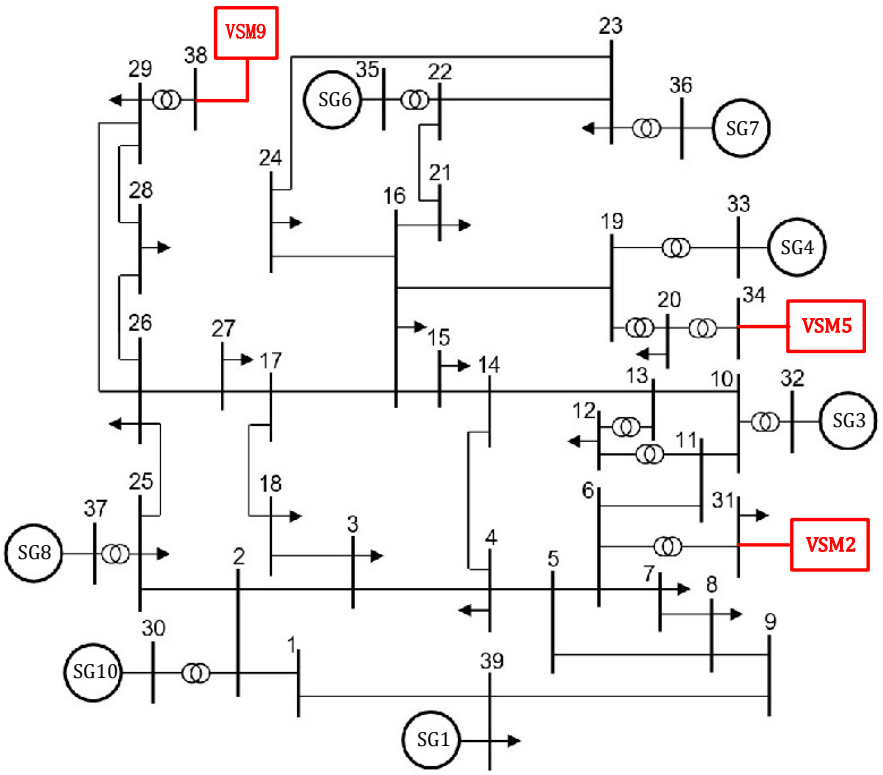

Figure 4-18 Modified New-England 39-bus system.

(1) Excitation Disturbance of Synchronous Generator

The excitation disturbance induced in this part is applying a step-up disturbance with 0.05pu amplitude to the excitation voltage reference of SG10 for 0.2s. The active power of SG1, the power flow on Line 15-16, the rotor speed and active power of VSM9 are selected signals to observe system responses. The simulation results are presented in Figure 4-19.

(2) Load Variation Disturbance

In this case, the variation of active power loads is applied to test system performance. An additional 200 MW load is added at Bus 16. The same signals as part (1) are shown in Figure 4-20 to observe the effects of designed controller.

(3) Three-Phase-to-Ground Fault Disturbance

A three-phase-to-ground fault is simulated for this case to model a severe disturbance. The fault with a duration of 0.1s is applied to bus 3 at 5s. The simulation results of the same selected signals in previous parts are demonstrated in Figure 4-21.

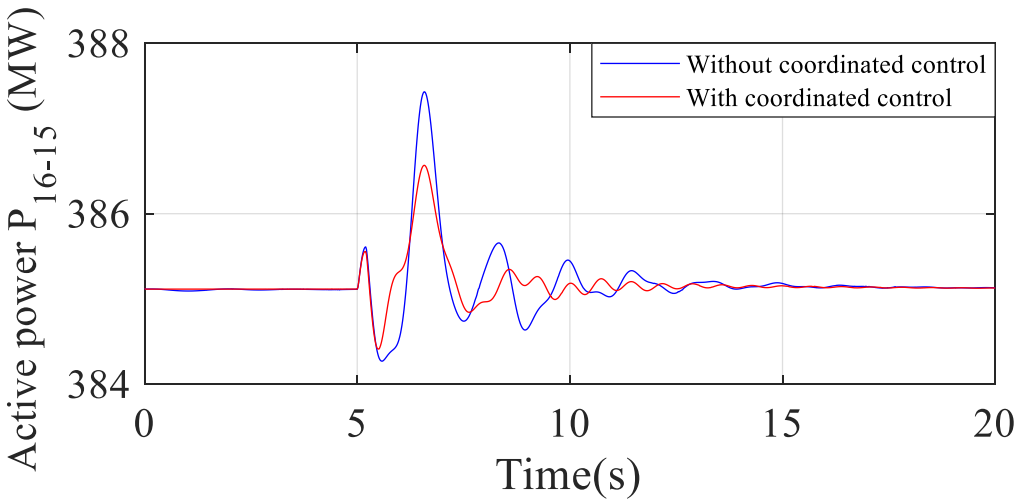

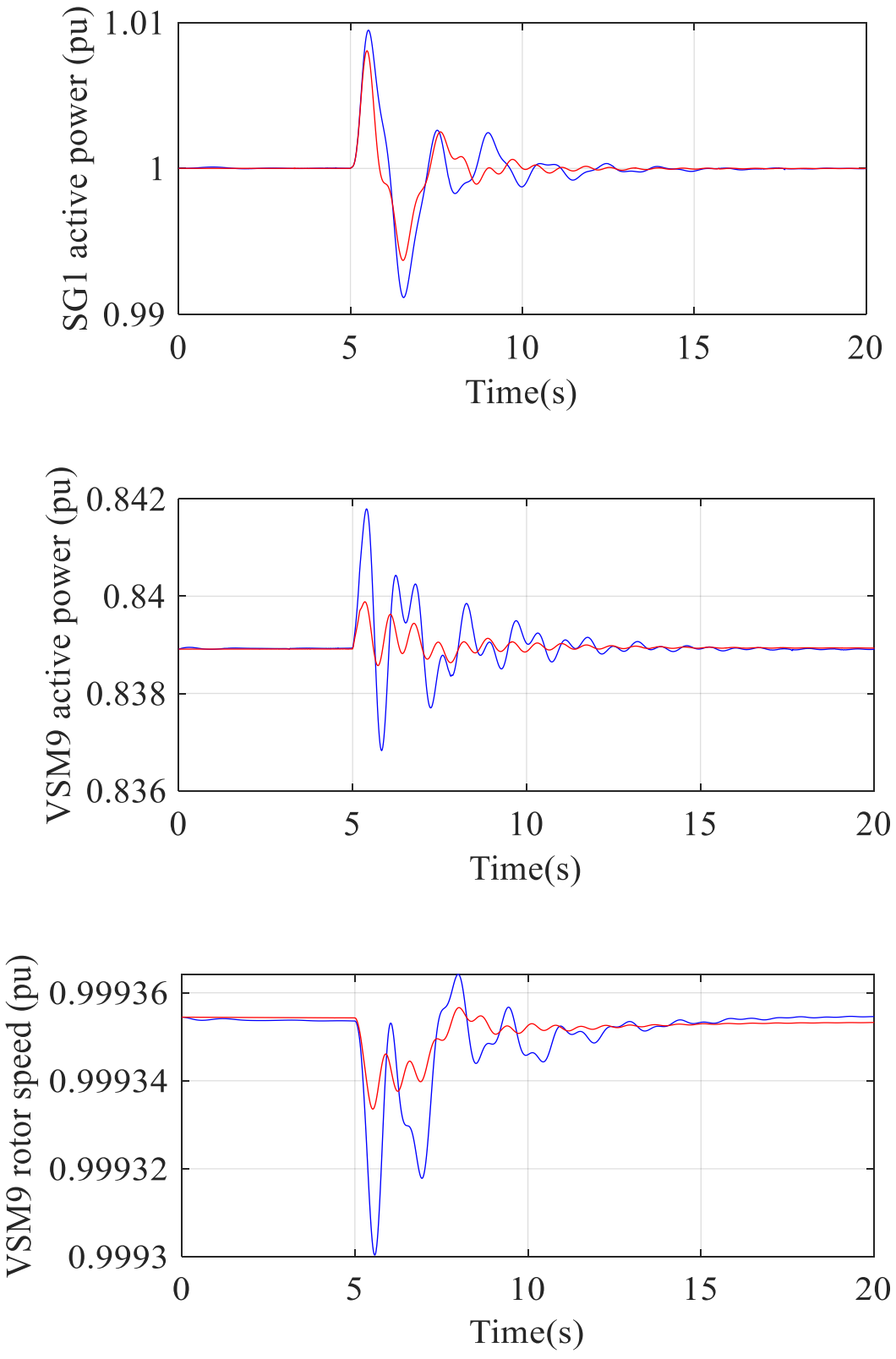

Figure 4-19 39-bus system responses under generator excitation disturbance.

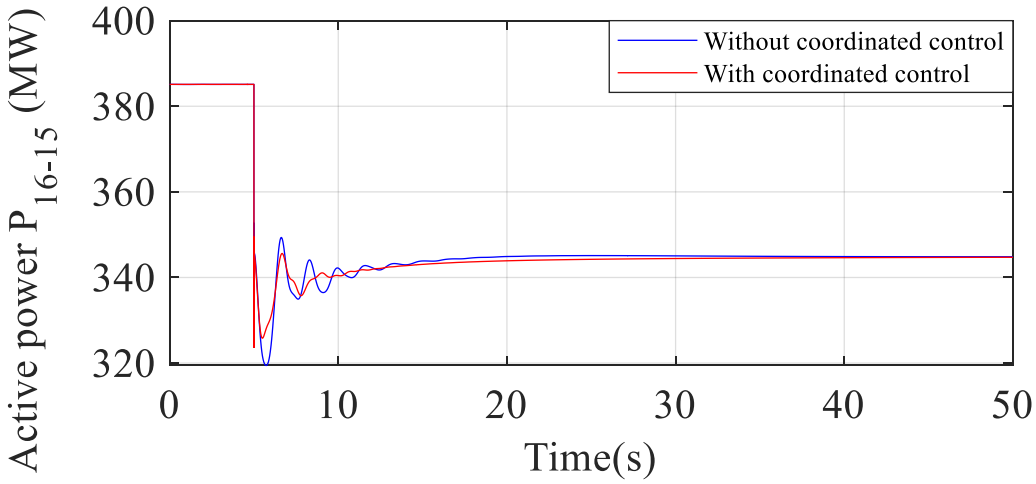
Without coordinated control
With coordinated control
Active power P 16-15 (MW)
400
380
360
340
320
0
10
20
30
40
50
Time(s)

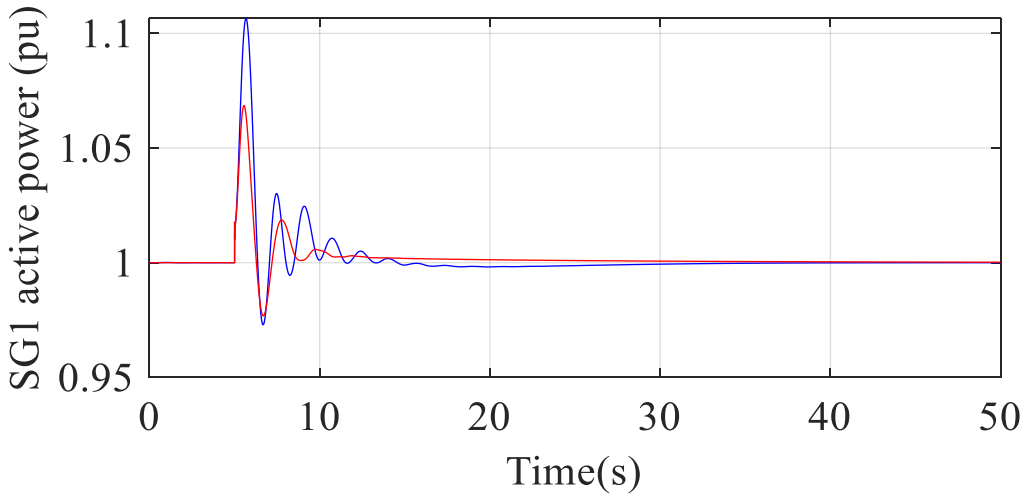
SG1 active power (pu)
1.1
1.05
1
0.95
0
10
20
30
40
50
Time(s)

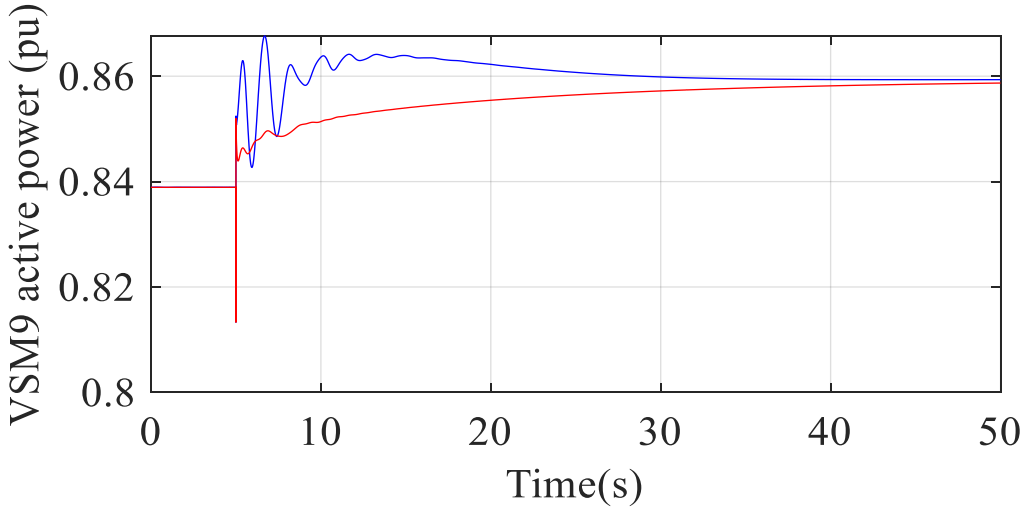
VSM9 active power (pu)
0.86
0.84
0.82
0.8
0
10
20
30
40
50
Time(s)

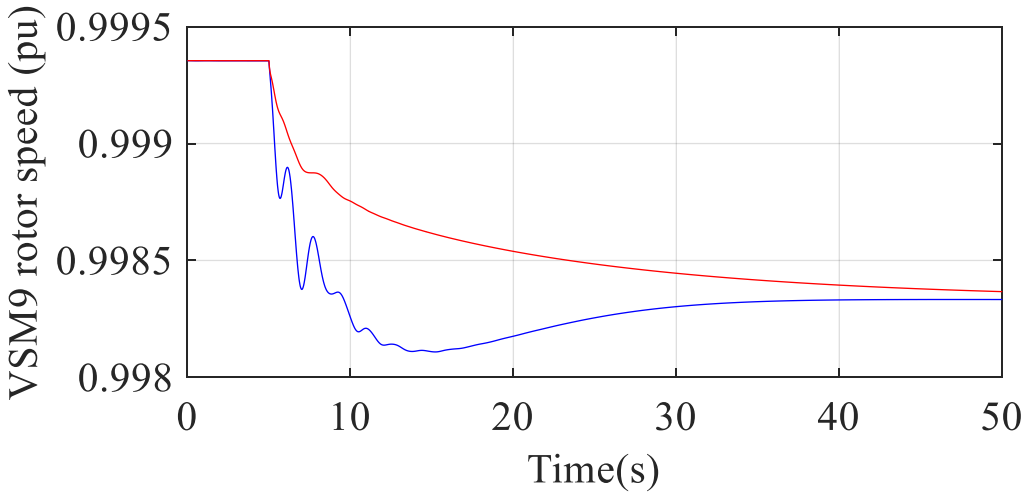

Figure 4-20 39-bus system responses under load disturbance.

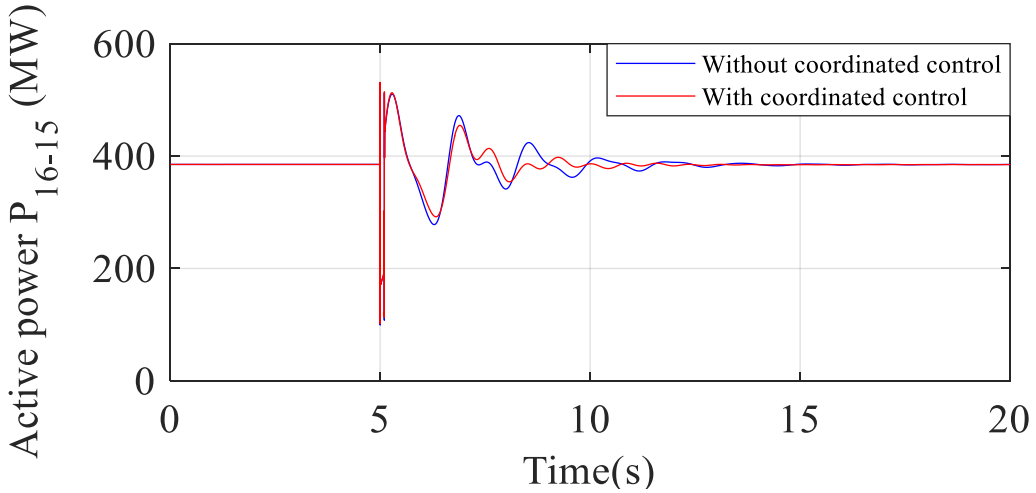

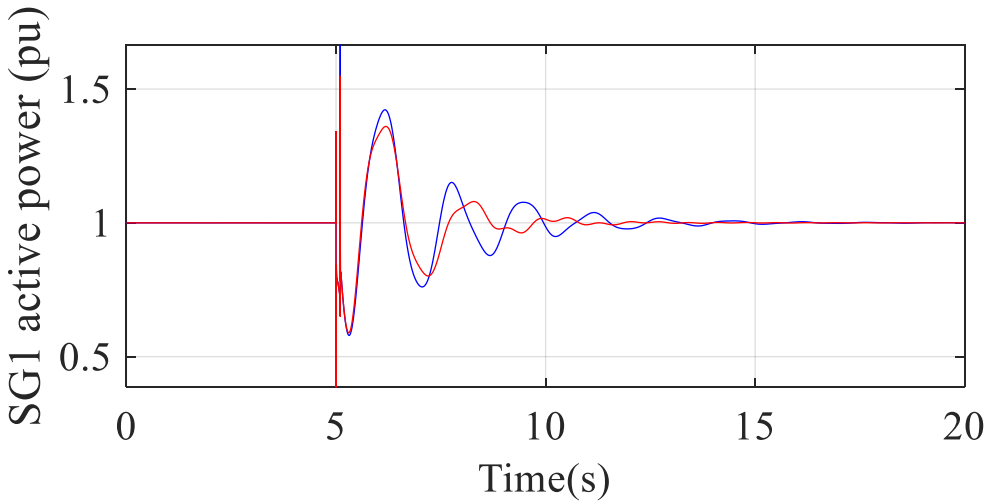

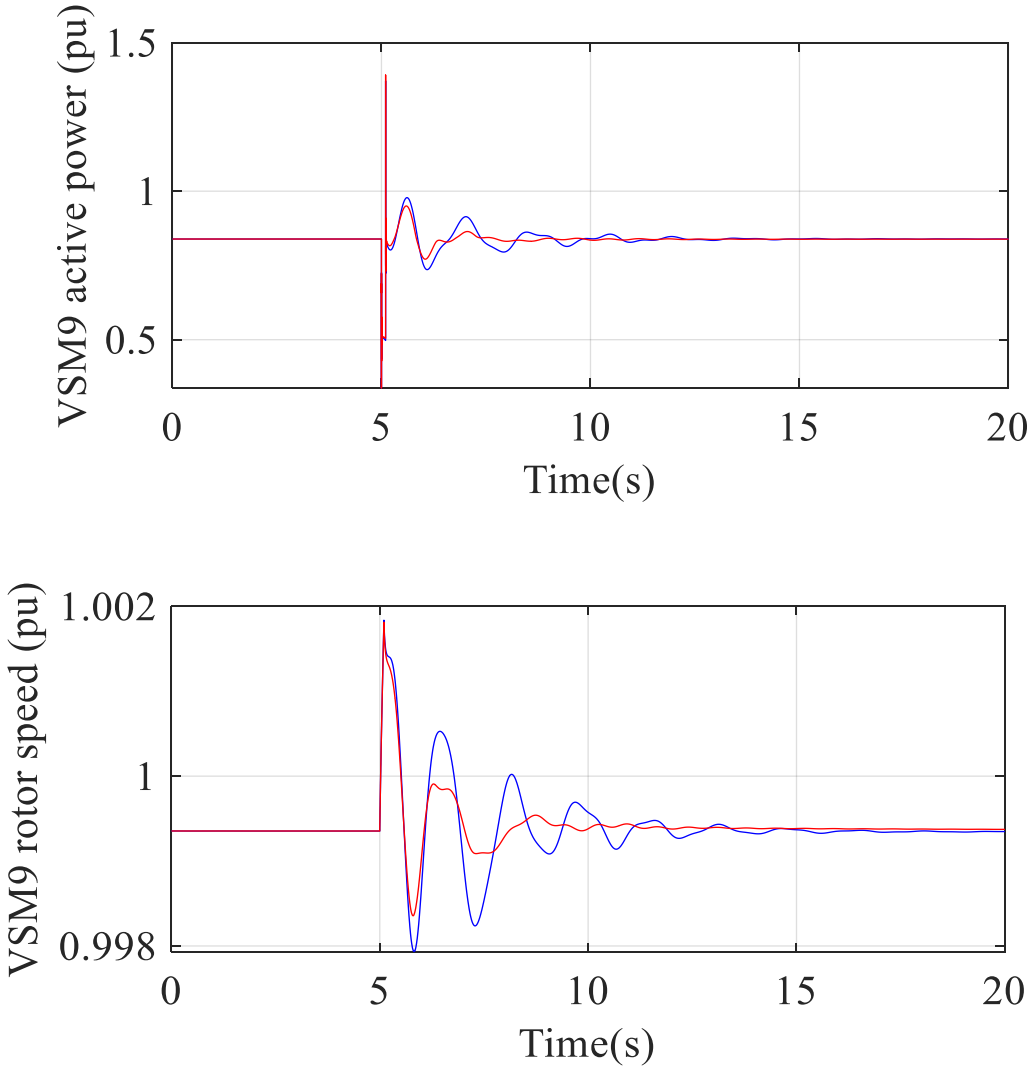

Figure 4-21 39-bus system responses under fault disturbance.

From the simulation results in Figure 4-19 to Figure 4-21, it can be observed that the oscillations in active power and rotor speed of VSM9 can be effectively suppressed with designed controller. Meanwhile, the oscillation magnitude of power flow on line 15-16 is alleviated as well. The power oscillation of SG1 also confirms the damping support from supplementary controller. The proposed scheme exhibits its robustness against alterations of disturbance type.

4.6 Summary

This chapter has discussed the impacts of multiple VSMs on power system LFOs. The scrutiny of system LFO modes via modal analysis reveals that VSMs are participating in LFO and have strong interactions with traditional SGs. Then a coordinated decentralised sequential approach is proposed for designing SDCs for multiple VSMs. The measurement-based Prony method facilitates modes identification for controller design and this feature makes it more flexible and applicable for practical power system. The robustness and effectiveness of designed controller is examined on modified two-area system and 39-bus system. The simulation results under various disturbances confirms the damping provision from coordinated supplementary controllers.

CHAPTER 5 ANALYSIS OF VIRTUAL SYNCHRONOUS MACHINE ON POWER SYSTEM FORCED OSCILLATION

5.1 Introduction

The forced oscillation has attracted increasing attention due to its serious resonance instability to power systems. In addition, the periodical fluctuation from renewables can also act as sources of forced oscillation. This chapter explores the impacts of VSM on power system forced oscillation. Section 5.2 analytically gives the detailed derivation of forced oscillation with VSM. Time-domain simulations and further discussions of test systems are presented in Section 5.3. Finally, major conclusions of this chapter are drawn in Section 5.4.

5.2 Mathematical Derivation of Forced Oscillation with VSM

In this section, the mathematical analysis to demonstrate the impacts of VSM on FO is explicitly presented.

5.2.1 VSM Control

The VSM control as depicted Figure 2-1 is implemented for mathematical analysis, detailed description has been given in previous chapters. The equation of VSM core block is rewritten as below for easy following:

$$\begin{cases} 2H\frac{d\omega_{vir}}{dt} = P_m - P_e - K_d(\omega_{vir} - \omega_n) \\ \frac{d\delta_{vir}}{dt} = \omega_b\omega_{vir} \end{cases} \tag{5-1}$$

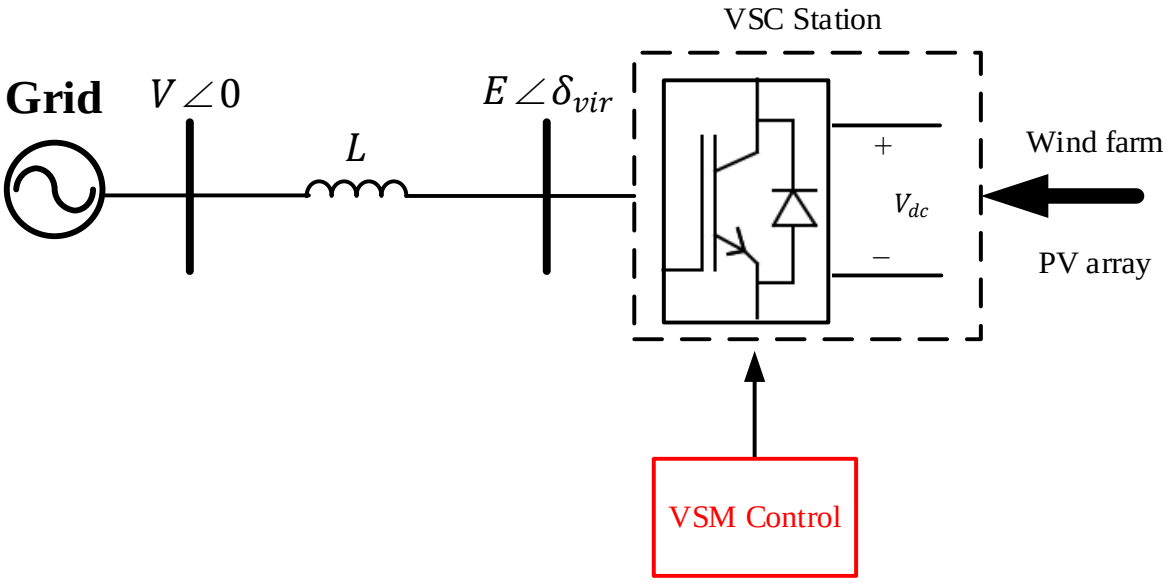

Figure 5-1 Single VSC connected to infinite bus.

The VSM inherits electro-mechanical power oscillation characteristics from SG. On the other hand, the increasing integration of renewables has become a potential forced oscillation source when suffering periodically disturbances [65, 68, 77, 79]. Therefore, there is a potential resonance risk when power electronic interfaced devices of renewables adopt VSM control.

5.2.2 Forced Oscillation of Infinite Bus System with VSM

The explanation of forced oscillation related to VSM control starts from a simple system as illustrated in Figure 5-1. The DC side power is assumed to be from PV plant or wind farm. By linearising swing equation (5-1),

$$\begin{cases} 2H\frac{d\Delta\omega_{vir}}{dt} = \Delta P_m - \Delta P_e - K_d(\Delta\omega_{vir} - \Delta\omega_n) \\ \frac{d\Delta\delta_{vir}}{dt} = \omega_b\Delta\omega_{vir} \end{cases} \tag{5-2}$$

If transmission line is primarily inductive, the following equation can be obtained after substituting ΔP_e into (5-2).

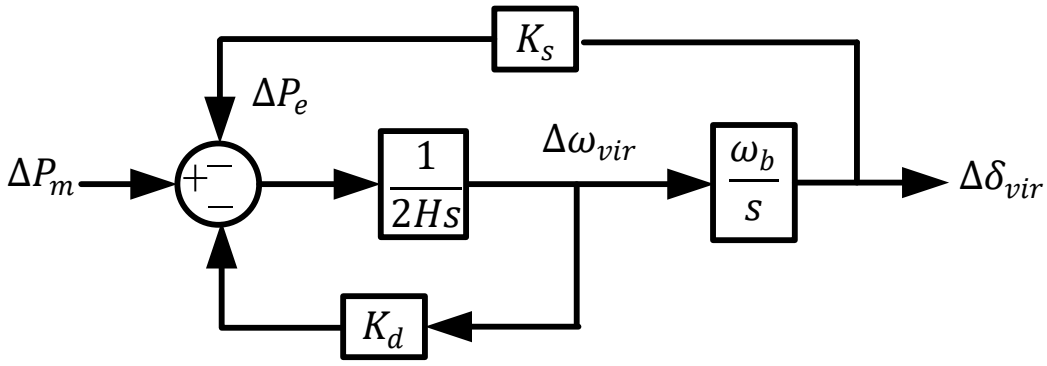

Figure 5-2 Block diagram of linearised virtual swing equation.

$$\frac{2H}{\omega_b}\frac{d^2\Delta\delta_{vir}}{dt^2}+\frac{K_d}{\omega_b}\frac{d\Delta\delta_{vir}}{dt}+K_s\Delta\delta_{vir}=\Delta P_m \tag{5-3}$$

where $K_s=\frac{VE}{X_L}\cos\delta_0$ and this is the virtual synchronous coefficient. The schematic diagram of small signal model is demonstrated in Figure 5-2.

In general, the variations of P_m is ignored and therefore it is treated as a constant. If a sustained disturbance exists in P_m, e.g., periodic wind speed fluctuation, then ΔP_m needs to be considered in the linearised equation. Assuming $\Delta P_m=d_1\sin\omega_l t+d_2\sin\omega_l t$, the solution of second-order non-homogeneous linear differential equation can be obtained as:

$$\begin{cases}\Delta\delta_{vir}(t)=\Delta\delta_1(t)+\Delta\delta_2(t)\\ \Delta\delta_1(t)=e^{-\frac{K_d}{4H}t}(C_1\cos\omega_d t+C_2\sin\omega_d t)\\ \qquad\qquad (K_d^2-8\omega_b K_s H<0)\\ \Delta\delta_2(t)=\frac{d_1\omega_b\left(K_s\omega_b-2H\omega_l^2\right)-d_2\omega_b K_d\omega_l}{\left(K_s\omega_b-2H\omega_l^2\right)^2+K_d^2\omega_l^2}\cos\omega_l t\\ \qquad\qquad +\frac{d_2\omega_b\left(K_s\omega_b-2H\omega_l^2\right)+d_1\omega_b K_d\omega_l}{\left(K_s\omega_b-2H\omega_l^2\right)^2+K_d^2\omega_l^2}\sin\omega_l t\end{cases} \tag{5-4}$$

where $\Delta\delta_1(t)$ and $\Delta\delta_2(t)$ are the ordinary solution and special solution. For ordinary solution $\Delta\delta_1(t)$, $\omega_d=\sqrt{\frac{\omega_b K_s}{2H}-\frac{K_d^2}{16H^2}}$ and constants C_1, C_2 are dependent on system initial conditions.

Generally, $\Delta\delta_1(t)$ will die out because of the damping term $e^{-\frac{K_d}{4H}t}$. Therefore, the special solution $\Delta\delta_2(t)$ becomes the focus.

If further assuming that $d_2 = 0$ (or $d_1 = 0$), then $\Delta\delta_2(t)$ can be developed as:

$$\begin{cases} \Delta\delta_2(t) = \frac{d_1\omega_b\left(K_s\omega_b - 2H\omega_l^2\right)}{\left(K_s\omega_b - 2H\omega_l^2\right)^2 + K_d^2\omega_l^2}\cos\omega_l t \\ \qquad\qquad + \frac{d_1\omega_b K_d\omega_l}{\left(K_s\omega_b - 2H\omega_l^2\right)^2 + K_d^2\omega_l^2}\sin\omega_l t \\ \qquad\qquad = \frac{d_1\omega_b}{\sqrt{\left(K_s\omega_b - 2H\omega_l^2\right)^2 + K_d^2\omega_l^2}}\sin(\omega_l t + \phi) \end{cases} \tag{5-5}$$

where $\phi = \arctan\frac{K_s\omega_b - 2H\omega_p^2}{K_d\omega_p}$. Therefore, the maximal oscillation magnitude is:

$$|\Delta\delta_2(t)|_{max} = \frac{d_1\omega_b}{K_d\sqrt{\frac{\omega_b K_s}{2H}}} \ (when\ \omega_l = \sqrt{\frac{K_s\omega_b}{2H}}) \tag{5-6}$$

It can be observed that the oscillation magnitude is affected by disturbance frequency (ω_l), virtual damping coefficient K_d and virtual inertia constant H. And their relationships can be clearly presented in Figure 5-3 and Figure 5-4. From Figure 5-3, it can be seen that the natural system frequency decreases with the increasing of virtual inertia constant H. However, larger H will amplify the maximal oscillation magnitude. Figure 5-4 demonstrates that the oscillation magnitude is suppressed with larger virtual damping coefficient K_d while its impact on system natural frequency is not obvious.

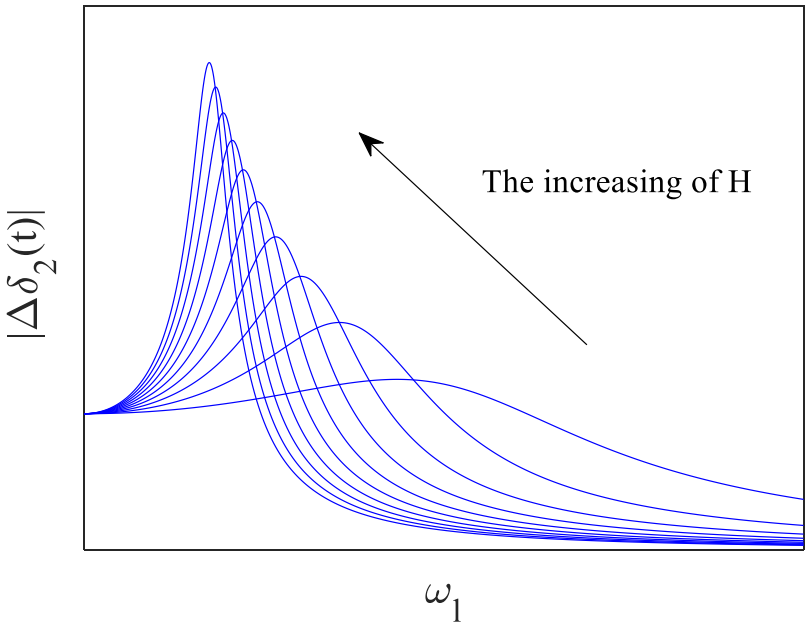

Figure 5-3 Forced oscillation magnitude curve - Mag vs. H.

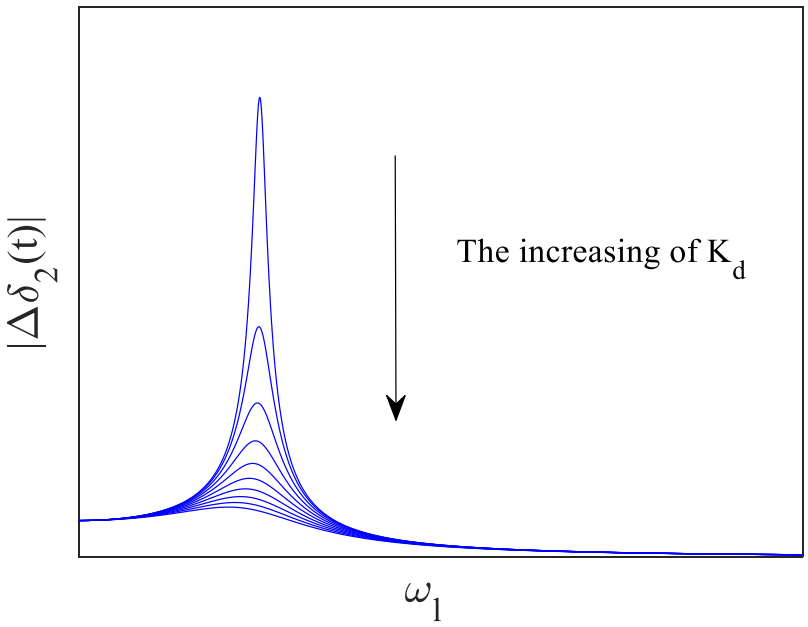

Figure 5-4 Forced oscillation magnitude curve - Mag vs. K_d.

5.2.3 Forced Oscillation of Multi-Machine System with VSM

For a multi-machine system with VSM, the small signal dynamics can be described as,

$$\frac{d\Delta \boldsymbol{x}(t)}{dt} = \boldsymbol{A}\Delta \boldsymbol{x}(t) + \boldsymbol{B}\Delta \boldsymbol{u}(t) \tag{5-7}$$

where $\boldsymbol{x}(\boldsymbol{t})$ and $\boldsymbol{u}(\boldsymbol{t})$ are the system state vector and external disturbances. If the system suffers disturbances with sinusoidal forms,

$$\begin{cases} \Delta \boldsymbol{u}(t) = [u_1(t) \quad u_2(t) \quad \dots \quad \dots \quad u_m(t)]^T \\ \qquad\quad = [d_1 sin(\omega_1 t) \quad d_2 sin(\omega_2 t) \quad \dots \quad \dots \quad d_m sin(\omega_m t)]^T \end{cases} \tag{5-8}$$

Then the solution of differential equations is [170],

$$\begin{cases} \Delta \boldsymbol{x}(t) = \Delta \boldsymbol{x_1}(t) + \Delta \boldsymbol{x_2}(t) \\ \qquad\quad = e^{\boldsymbol{A}t}\Delta \boldsymbol{x}(0) + \int_0^t e^{\boldsymbol{A}(t-\tau)}\boldsymbol{B}u(\tau)d\tau \end{cases} \tag{5-9}$$

It consists of two parts, the zero-state response (natural oscillation component) $\Delta \boldsymbol{x_1}(t)$ and zero-input response (forced oscillation component) $\Delta \boldsymbol{x_2}(t)$. The natural oscillation will damp out eventually and forced oscillation is the concern in this section.

The observed system forced oscillation can be further simplified in terms of system modes information [65],

$$\begin{cases} \Delta \boldsymbol{y}(\boldsymbol{t}) = \boldsymbol{C}\Delta \boldsymbol{x_2}(t) = \Delta \boldsymbol{y_1}(t) + \Delta \boldsymbol{y_2}(t) \\ \qquad\quad = \sum_{i=1}^{n}\sum_{r=1}^{q}\sum_{l=1}^{m}[Ze^{-\zeta_r \omega_{nr} t}\sin(\omega_{dr} t + \gamma_{ir} + \alpha_{rl} - \varphi) \\ \qquad\qquad\qquad -Z\beta \sin(\omega_l t + \gamma_{ir} + \alpha_{rl} - \varphi)] \end{cases} \tag{5-10}$$

$$\begin{cases} Z = \frac{2c_i|\phi_{ir}||\psi_{rl}|d_l\omega_l}{\sqrt{\left(\omega_{nr}^2 - \omega_l^2\right)^2 + 4\zeta_r^2\omega_{nr}^2\omega_l^2}} \\ \varphi = \tan^{-1}\left(\frac{\omega_{nr}^2 - \omega_l^2}{2\zeta_r\omega_{nr}^2}\right) \\ \beta = \sqrt{1 + \left(\frac{\omega_{nr}^2}{\omega_l^2} - 1\right)\cos^2(\gamma_{ir} + \alpha_{rl} - \varphi)} \end{cases} \tag{5-11}$$

where $\boldsymbol{C}$ is the output matrix, and system mode information is represented as:

$$\lambda_r = \sigma_r + j\omega_{dr} = -\zeta_r\omega_{nr} + j\sqrt{1-\zeta_r^2}\omega_{nr} \tag{5-12}$$

where λ_r, ζ_r and ω_{nr} are the rth mode, damping ratio and undamped frequency, ϕ_{ir} and ψ_{rl} are the right and left eigenvector related to rth mode. The first term in the observed forced oscillation is identical to natural oscillation which will die out gradually. $\Delta\boldsymbol{y_2}(t)$ is the main forced oscillation component. The defined maximal oscillation magnitude [65] can be obtained as:

$$Z_{max} = \frac{c_i|\phi_{ir}||\psi_{rl}|d_l}{\zeta_r\omega_{nr}} \ (\omega_l = \omega_{nr}) \tag{5-13}$$

Figure 5-5 shows that the resonance effect is serious especially when disturbance frequency is close to natural mode frequency. Increasing damping ratio or shifting system frequency away from disturbance frequency can suppress the forced oscillation magnitude.

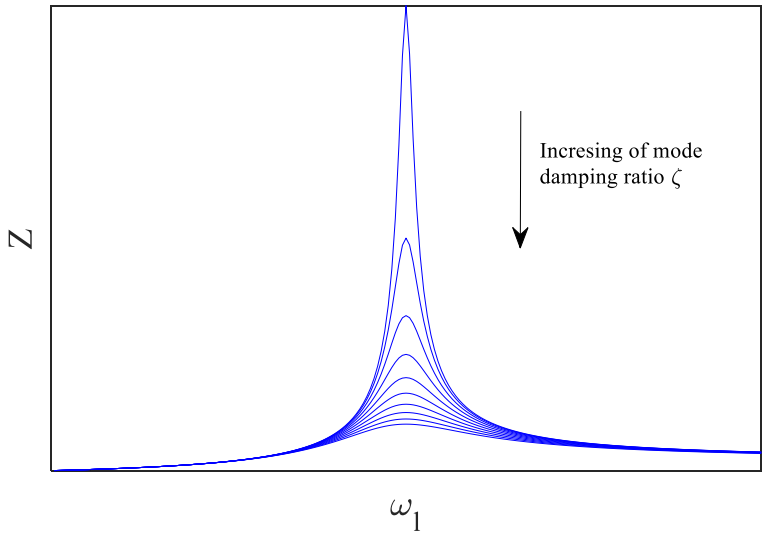

Figure 5-5 forced oscillation magnitude curve of multi-machine system.

5.3 Case Studies

Based on the aforementioned mathematical analysis, an infinite bus system and a modified two-area system is developed first. For infinite bus system, the impacts of VSM on forced oscillation characteristics are validated via time-domain simulations. Fast-Fourier-Transformation (FFT) analysis is carried out to confirm the forced oscillation component. For two-area system, dynamic simulations are carried out to verify the results of modal analysis and eigenvalue locus reveals how the parameters of VSM influence forced oscillation. Further simulation studies are conducted in a modified 39-bus system with 3 VSCs to compare the impacts of VSM and VCC on FO.

5.3.1 Single Converter Infinite Bus (SCIB) System

The system topology is illustrated in Figure 5-1 and VSM controller parameters are listed in Table 5-1. The frequency response of developed system ($\Delta\delta_{vir}$ is the output and ΔP_m is the input) is depicted in Figure 5-6. There is a peak for magnitude-frequency plot which demonstrates the system natural oscillation frequency is 11.8 rad/s. Therefore, the maximal forced oscillation magnitude caused by serious resonance is expected to be observed if the periodic disturbance frequency is close to system natural frequency.

TABLE 5-1
VSM CONTROLLER PARAMETERS

H	5 s	K	5 pu
K_d	50 pu	D_q	10 pu

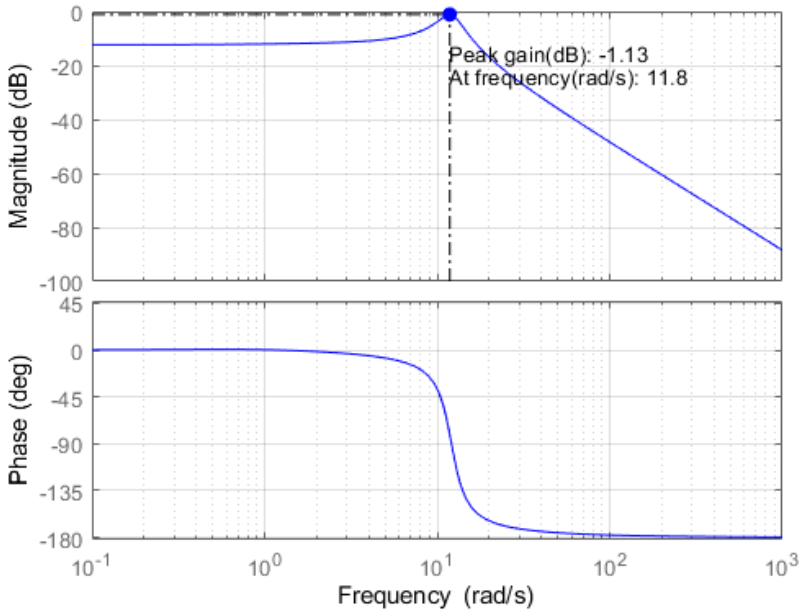

Figure 5-6 Frequency response of $\Delta\delta_{vir}/\Delta P_m$.

To verify the analysis, a sinusoidal disturbance $\Delta P_m = 0.05 \sin \omega_l t$ is applied at the DC side of VSC station. Three values of ω_l ($6.8\, rad/s$, $11.8\, rad/s$, $16.8\, rad/s$) are considered to examine the impacts of disturbance frequency. The simulations in Figure 5-7(a) shows that forced oscillation will be excited if there is a sustained disturbance. The smaller the difference between disturbance frequency and system natural frequency is, the larger the oscillation magnitude becomes. It can be observed that the forced oscillation magnitude is driven over three times larger than disturbance when disturbance frequency equals to the natural frequency. The FFT analysis result in Figure 5-7(b) confirms the forced oscillation component in active power. Therefore, the implementation of VSM introduces a potential risk of forced oscillation and such phenomenon should be concerned.

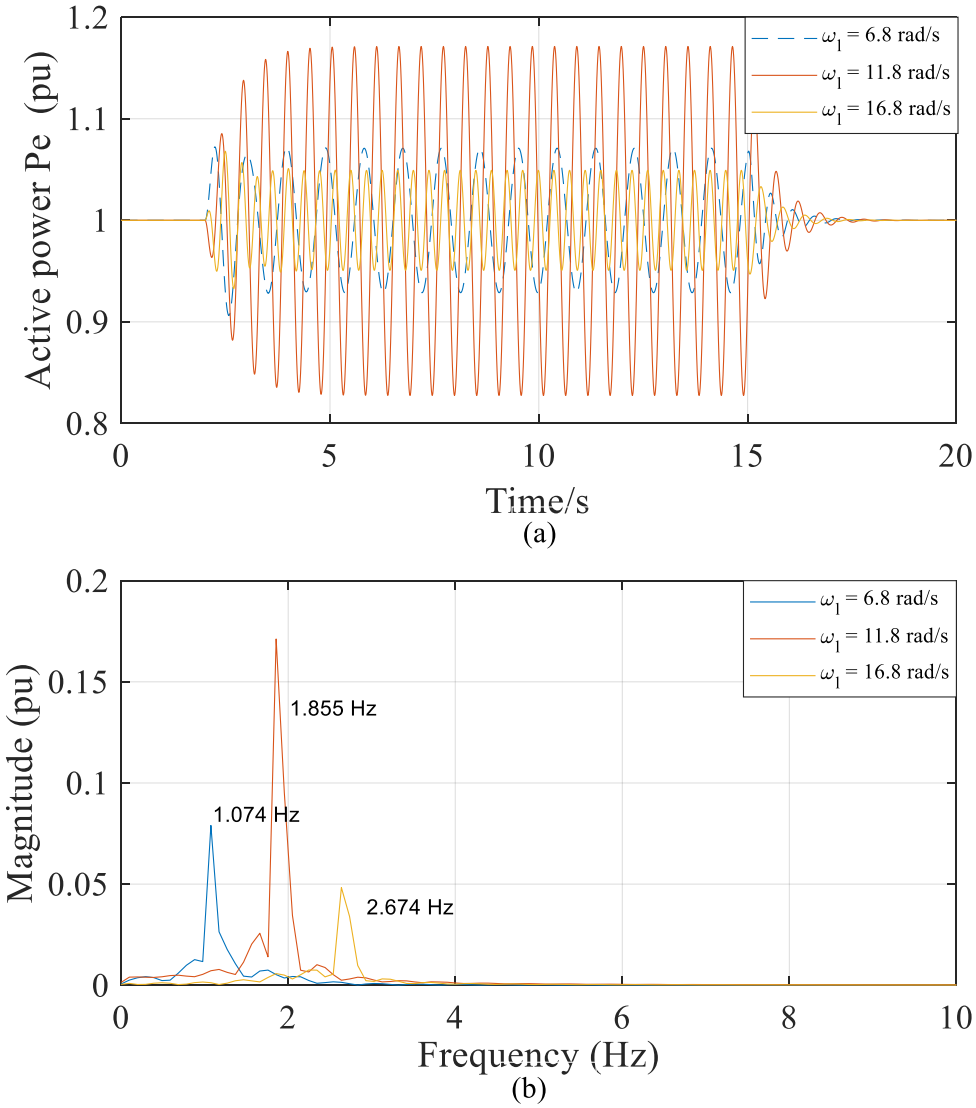

Figure 5-7 Electrical power oscillation. (a) Time-domain simulation. (b) FFT analysis.

In order to explore the impacts of virtual rotor control parameters on forced oscillation, the variations of virtual inertia constant H and virtual damping coefficient K_d are investigated. The changes on system natural frequency (ω_{nr}) caused by different H and K_d are presented in Table 5-2 and Table 5-3. The external sustained oscillation magnitude remains the same (0.05 pu) while disturbance frequency matches ω_{nr} to observe the maximal oscillation.

TABLE 5-2
SYSTEM NATURAL FREQUENCY WITH DIFFERENT H

No.	H (s)	$\omega_{nr}(rad/s)$
1	2.5	16.3
2	5.0	11.8
3	10	8.48

TABLE 5-3
SYSTEM NATURAL FREQUENCY WITH DIFFERENT K_d

No.	K_d (pu)	$\omega_{nr}(rad/s)$
1	25	11.8
2	50	11.8
3	100	11.8

Time-domain simulation results concerning the virtual parameters variation are illustrated in Figure 5-8 and Figure 5-9. From Figure 5-8 (a), it is obvious that system natural frequency is decreased because of the increasing virtual inertia constant. However, the maximal oscillation magnitude becomes larger with higher virtual inertia from VSM. The results are confirmed again by FFT analysis in Figure 5-8 (b). As shown in Figure 5-9, The system natural frequency ω_{nr}remains the same with different virtual damping coefficient. It can also be observed that a larger K_d is beneficial for reducing the magnitude of forced oscillation. Therefore, the higher inertia may exaggerate forced oscillation while larger damping can alleviate the oscillation.

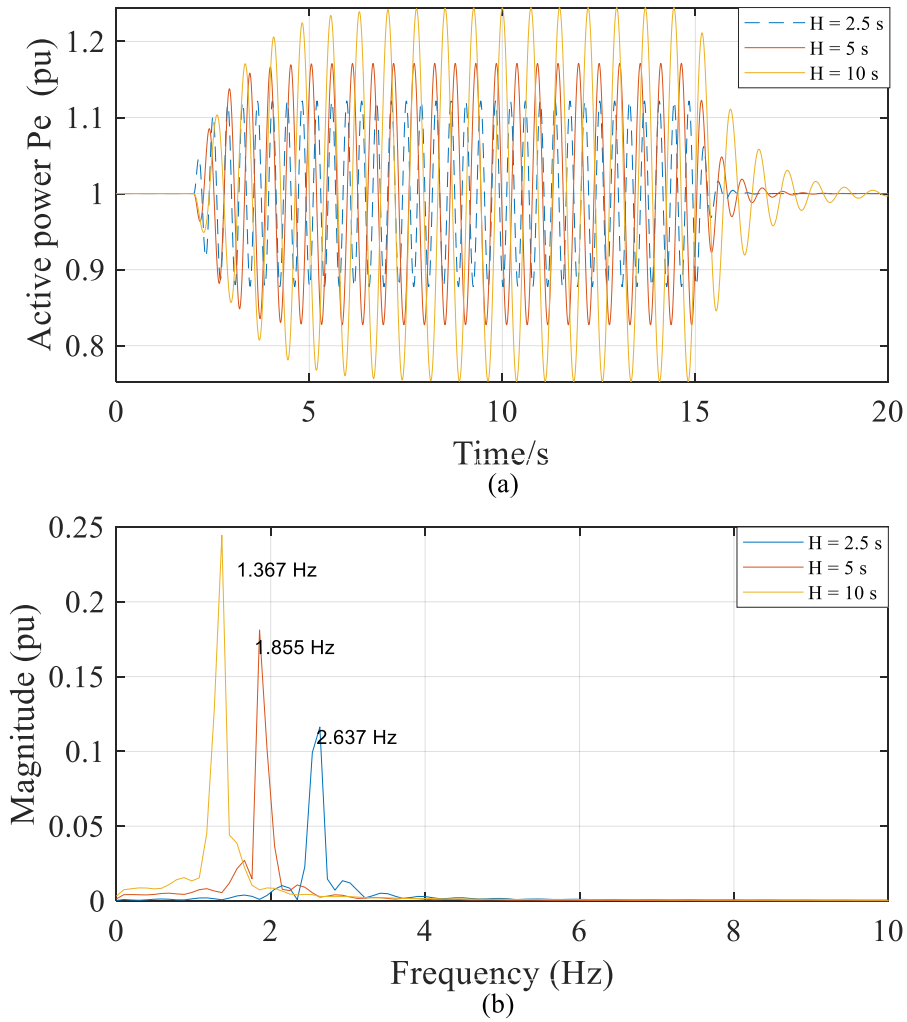

Figure 5-8 Electrical power oscillation. (a) time-domain simulation. (b) FFT analysis.

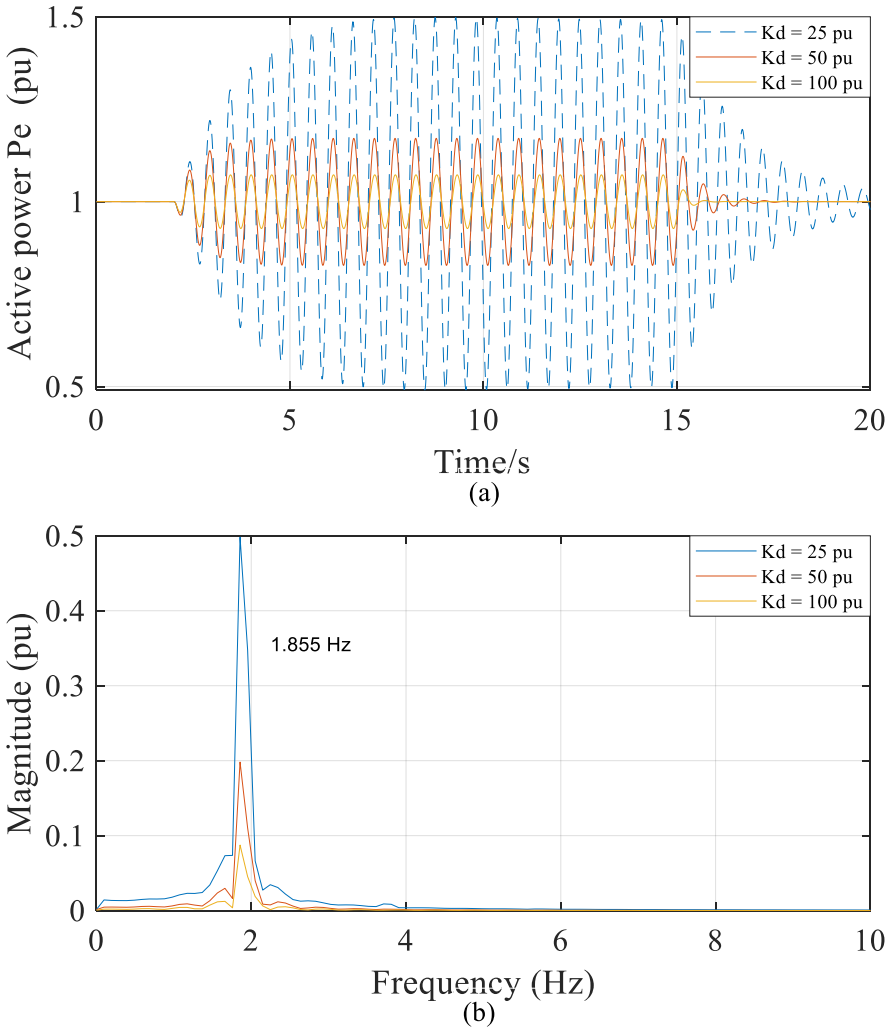

Figure 5-9 Electrical power oscillation. (a) time-domain simulation. (b) FFT analysis.

The virtual impedance is widely implemented for VSM controllers due to its contribution to system performance improvement and current limiting capability [85, 171]. The structure of VSM control with virtual impedance is the same with Chapter 3. The impact of virtual inductance on forced oscillation is illustrated in Figure 5-10. The frequency response of $\Delta P_m/\Delta P_e$ indicates that system natural frequency decreases with the increasing of virtual inductance. However,

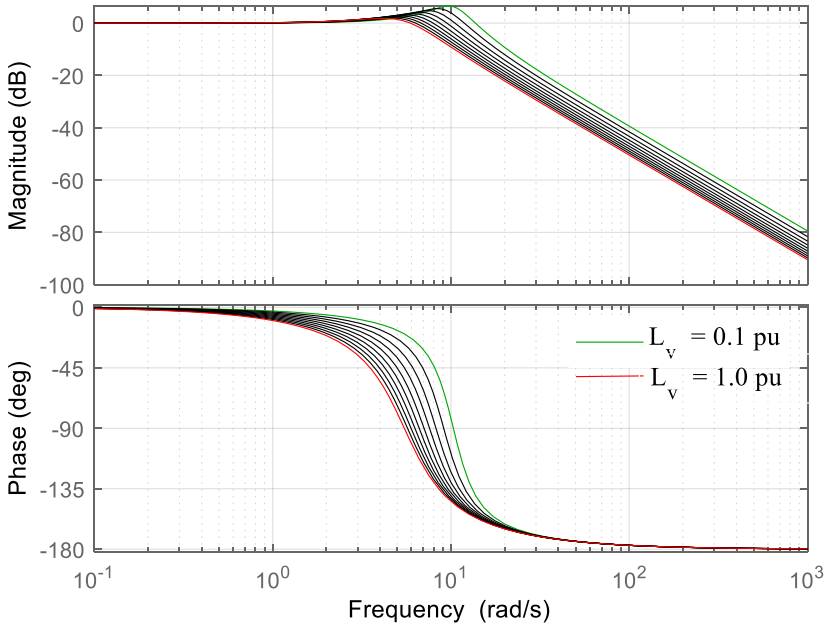

Figure 5-10 System frequency response of different L_v.

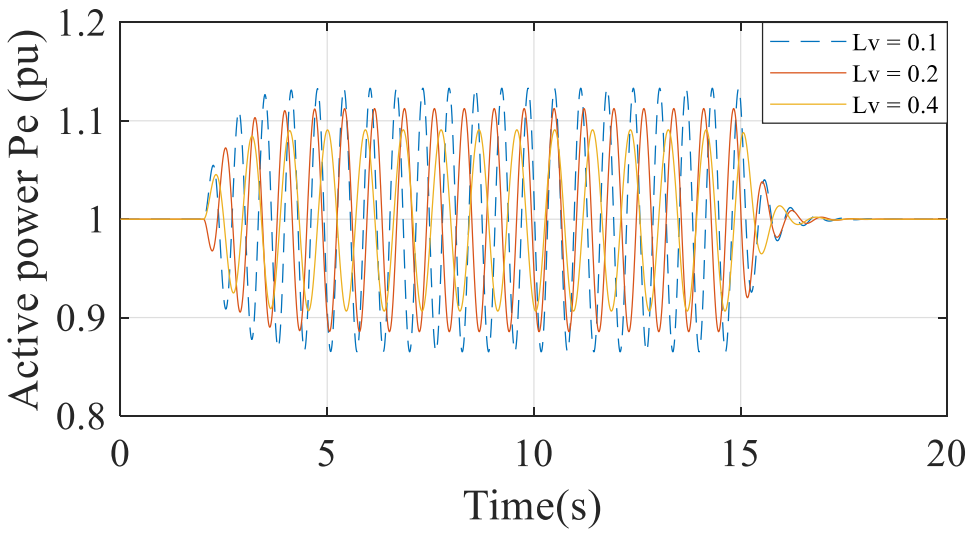

Figure 5-11 Electrical power oscillation of different L_v.

the peak is smaller with higher virtual inductance which means the oscillation magnitude becomes smaller as well. The simulation results in Figure 5-11 also confirm the effects of virtual impedance on system forced oscillation.

5.3.2 Two-Area System with VSM

A revised two-area system is first developed to investigate the impacts of VSM on multi-machine system. The system topology is shown in Figure 5-12 where a VSM controlled VSC station is connecting to Bus 4 to replace original SG4 with equivalent active power. The parameters of VSM controller with virtual impedance has been listed in Table A-4 and other system parameters can be found in [159]

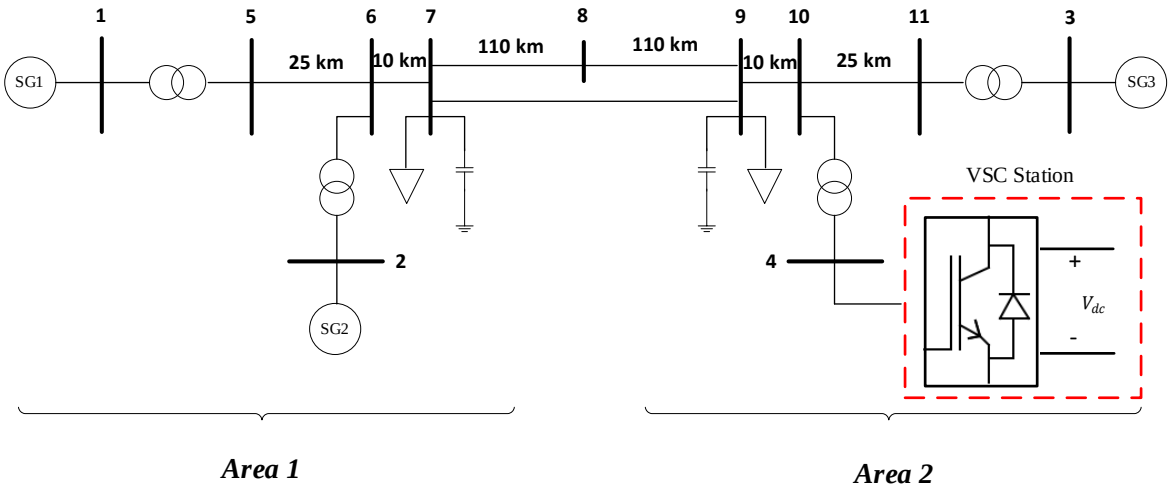

Figure 5-12 Topology of revised two-area system.

TABLE 5-4
EIGENVALUE ANALYSIS RESULTS OF REVISED TWO-AREA SYSTEM

No.	Frequency (Hz)	Damping ratio	Dominant states (PF)
1	1.076 (Local)	0.100	$\omega_{SG1}(0.821), \theta_{SG1}(0.820);$ $\omega_{SG2}(1.000), \theta_{SG2}(0.999)$
2	1.036(Local)	0.119	$\omega_{SG3}(1.000), \theta_{SG3}(0.995);$ $\omega_{VSM}(0.737), \theta_{VSM}(0.756)$
3	0.629 (Inter-area)	0.095	$\omega_{SG1}(0.785), \theta_{SG1}(0.749);$ $\omega_{SG2}(0.455), \theta_{SG2}(0.435);$ $\omega_{SG3}(0.768), \theta_{SG3}(0.732);$ $\omega_{VSM}(0.848), \theta_{VSM}(1.000)$

The modal analysis is applied to modified two-area system and the obtained system modes information is presented in Table 5-4. Similarly, three LFO modes including two local modes and one inter-area mode are identified. The participation factor indicates VSM is highly participating in mode 2 and mode 3. This is mainly because that VSM is mimicking the characteristics of SG, therefore it will participate in relevant LFO. These system natural modes lay the foundation for following forced oscillation analysis.

The VSM related modes (mode 2 and mode 3) are the focus of this chapter and they are selected to analyse the impacts of VSM on forced oscillation. If the disturbance from VSC with a frequency close to these two LFO modes, there will be a risk of exciting forced oscillation with large magnitude. For mode 2, the frequency of disturbance $\Delta P_m = 0.05\sin(2\pi f_l t)$ is set as $f_l = 1.036\ Hz$. The disturbance is located at SG side or VSM side respectively. The simulation results are depicted in Figure 5-13. It can be seen that the oscillation magnitude of VSM and

SG3 are larger than that of SG1 and SG2. The resonance effect amplifies the oscillation which brings high stress to system. This can be attributed to the high participation of VSM and SG3 in mode 2 while SG1 and SG2 are not involved.

In addition, the periodic disturbance with mode 3 frequency is also investigated. The disturbance amplitude remains the same while frequency is changed to 0.629 Hz. Since all devices are engaged in this inter-area mode, the disturbance source is considered to be

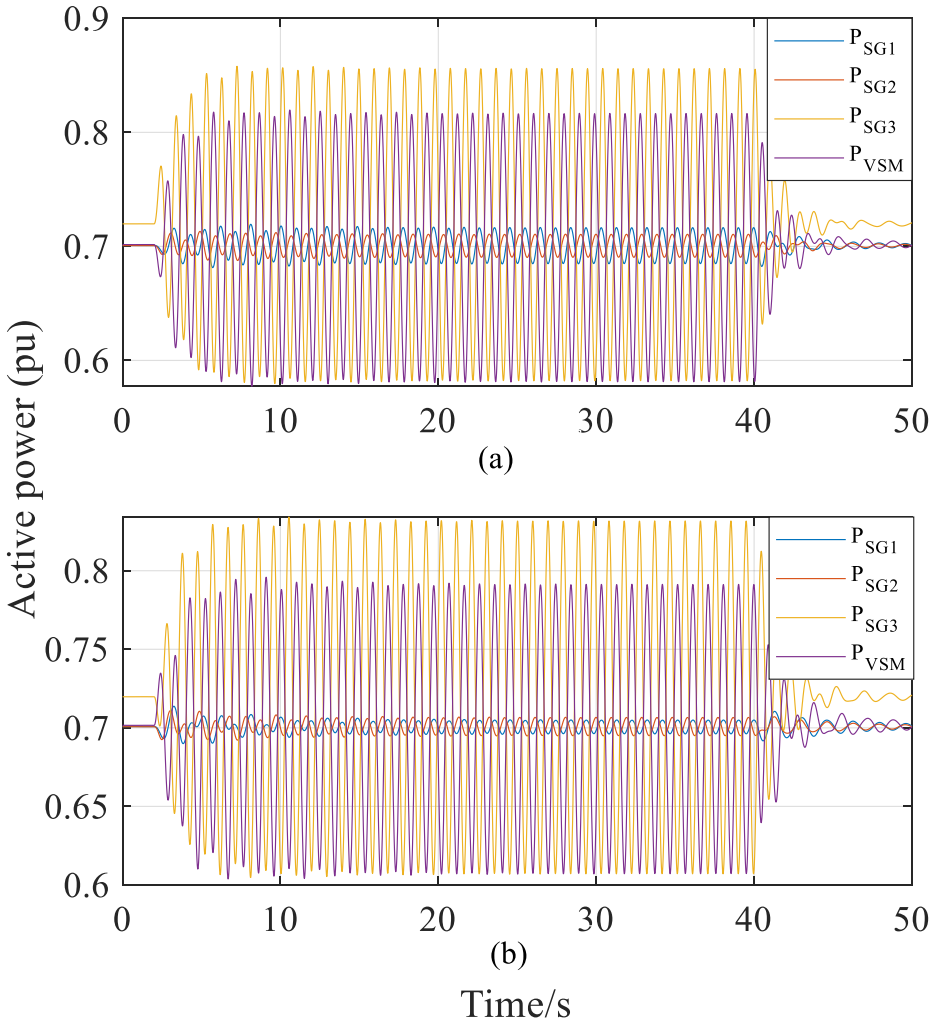

Figure 5-13 Electrical power oscillation of mode 2. (a) Disturbance at SG side. (b) Disturbance at VSM side

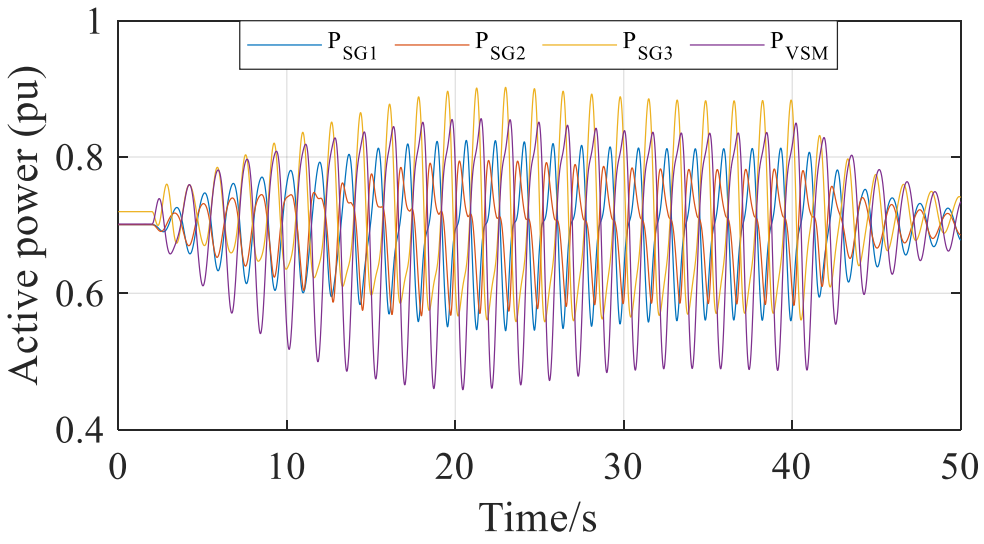

Figure 5-14 Electrical power oscillation of mode 3.

located at VSM side. The time-domain simulation results are presented in Figure 5-14. The serious forced oscillation in the active power of SGs and VSM where the magnitude of active power is amplified two or three times larger than forced oscillation source is observed. The oscillation magnitude of VSM is the highest and the oscillation in SG2 is the smallest. This is consistent with the participation factor results of mode 3 listed in Table 5-4. The higher participation factor implies a larger oscillation magnitude.

Multiple measures have been introduced to reduce the magnitude of forced power oscillation [65] which will lighten the stress of power system and afford more time to locate the source of forced oscillation. As VSM controller parameters can be flexibly adjusted, the eigenvalue locus of different controller parameters variation is demonstrated in Figure 5-15.

The eigenvalue locus of virtual inertia constant variation is given in Figure 5-15(a). It is obvious that mode 2 and mode 3 are affected by the variation of virtual inertia H while mode 1 exhibits no changes since VSM is not participated in this mode. With the increasing of virtual

inertia, the eigenvalues of mode 2 and mode 3 move towards RHP, indicating that larger virtual inertia constant will decrease the damping ratio of these two modes. At the meantime, the

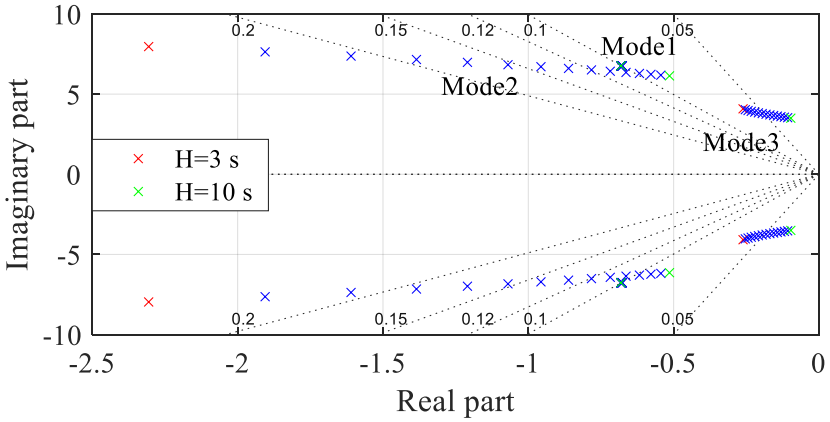

(a)

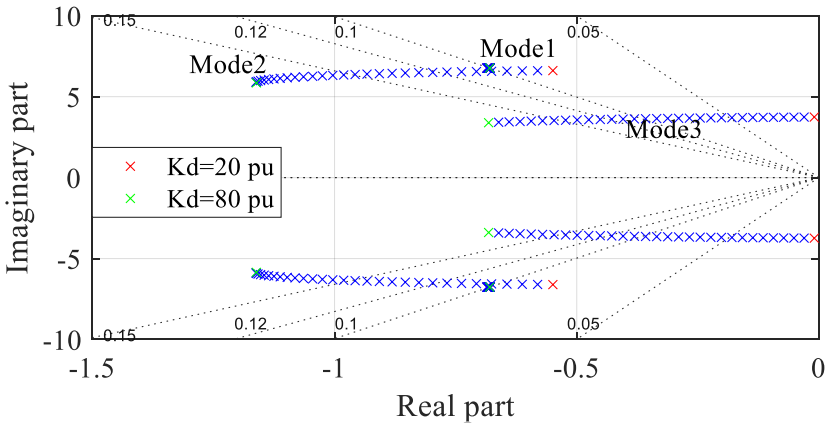

(b)

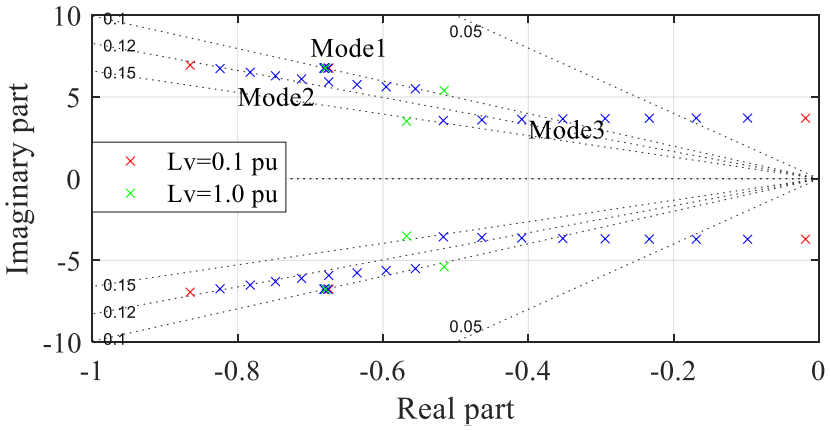

(c)

Figure 5-15 Eigenvalue locus under variation of VSM parameters. (a) Virtual inertia coefficient changing from 3s to 10s. (b) Virtual damping coefficient changing from $20pu$ to $80pu$. (c) Virtual inductance changing from $0.1pu$ to $1.0pu$.

modes frequency also experiences a decline. Besides, the damping ratio of mode 3 is the lowest and it is closer to imaginary axis. This represents mode 3 is the dominant one among three LFO modes.

The eigenvalue locus of virtual damping coefficient which changes from $20pu$ to $80pu$ is illustrated in Figure 5-15(b). Mode 2 and mode 3 are pushed towards LHP with the increasing of damping coefficient which means that the damping ratio of these two modes increases with larger K_d. Besides, the frequency of mode 3 almost remains the same and the frequency variation of mode 2 is also negligible. Similarly, the variation of virtual damping coefficient still has few effects on mode 1 due to the same reason.

Since virtual impedance is incorporated into VSM control, the eigenvalue locus of virtual inductance L_v is demonstrated in Figure 5-15(c). It illustrates that mode 2 and mode 3 are significantly affected by the variation of virtual inductance. The eigenvalues of mode 2 move towards right with the increasing of virtual inductance L_v while the movement of mode 3 is in an opposite direction. Therefore, the choice of L_v should be attentively considered. For this case, L_v can be introduced to increase the damping ratio of mode 3 since damping ratio of mode 2 is satisfactory and its damping is lightly affected within the varied range. Furthermore, the frequency of mode 2 decreases with larger L_v while frequency of mode 3 almost remains the same within the variation of L_v.

The forced oscillation simulation results of modified two-area system with varied virtual inertia constant are presented in Figure 5-16 and Figure 5-17. For mode 2, only SG3 and VSM are

involved in this oscillation and FO can be observed as shown in Figure 5-16. The damping ratio increases with the decreasing of virtual inertia H. Besides, the variation of H also changes natural mode frequency which means disturbance frequency is moved away from system frequency. Therefore, the oscillation magnitude becomes smaller under these combined effects.

As all devices participate in mode 3, the electrical power of SG1 and VSM are presented in Figure 5-17. Similarly, both damping ratio and frequency increases with smaller H. Therefore, smaller virtual inertia constant from VSM is helpful for oscillation suppression while this may be conflicted with the situation if high inertia is required.

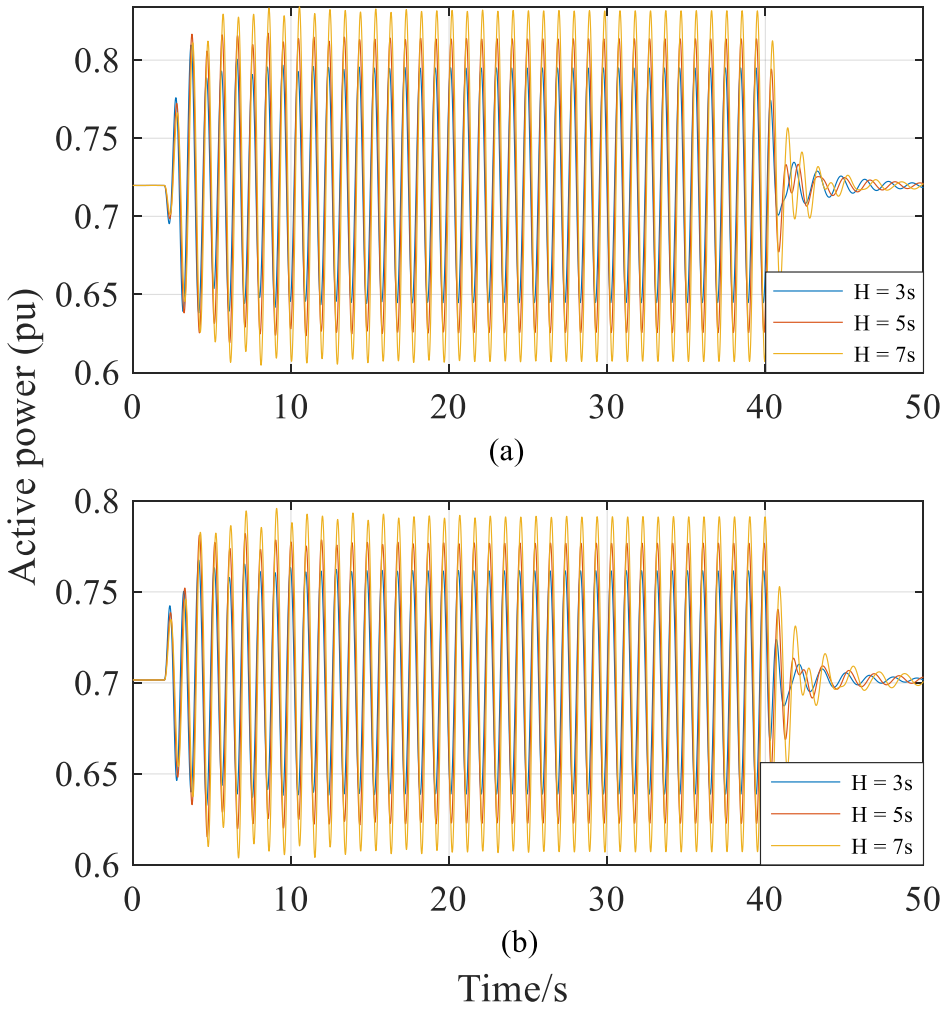

Figure 5-16 Electrical power oscillation of local mode ($f_l = f_{mode2}$). (a) Active power of SG3. (b) Active power of VSM.

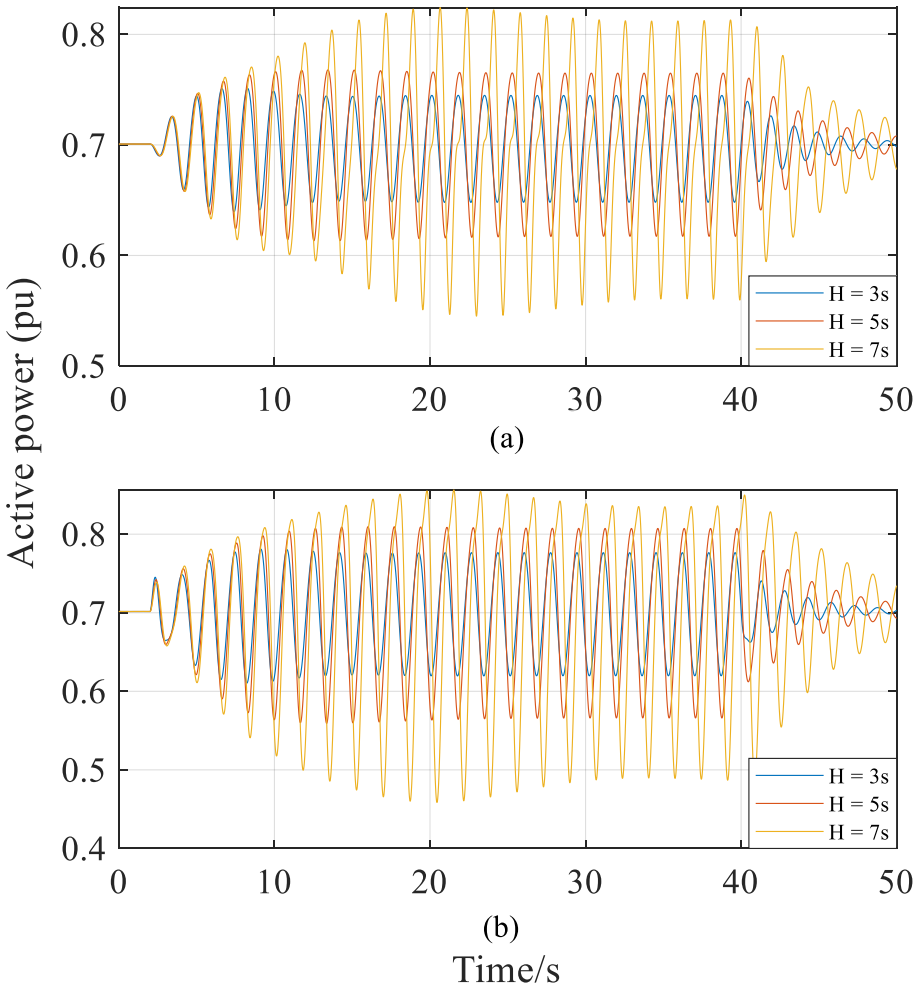

Figure 5-17 Electrical power oscillation of inter-area mode ($f_l = f_{mode3}$). (a) active power of SG1. (b) active power of VSM.

The simulation results concerning the impacts of virtual damping K_d are depicted in Figure 5-18 and Figure 5-19. It can be observed that larger K_d is conducive to alleviating forced oscillation magnitude. For both mode 2 and mode 3, the larger the virtual damping is, the smaller the oscillation magnitude is.

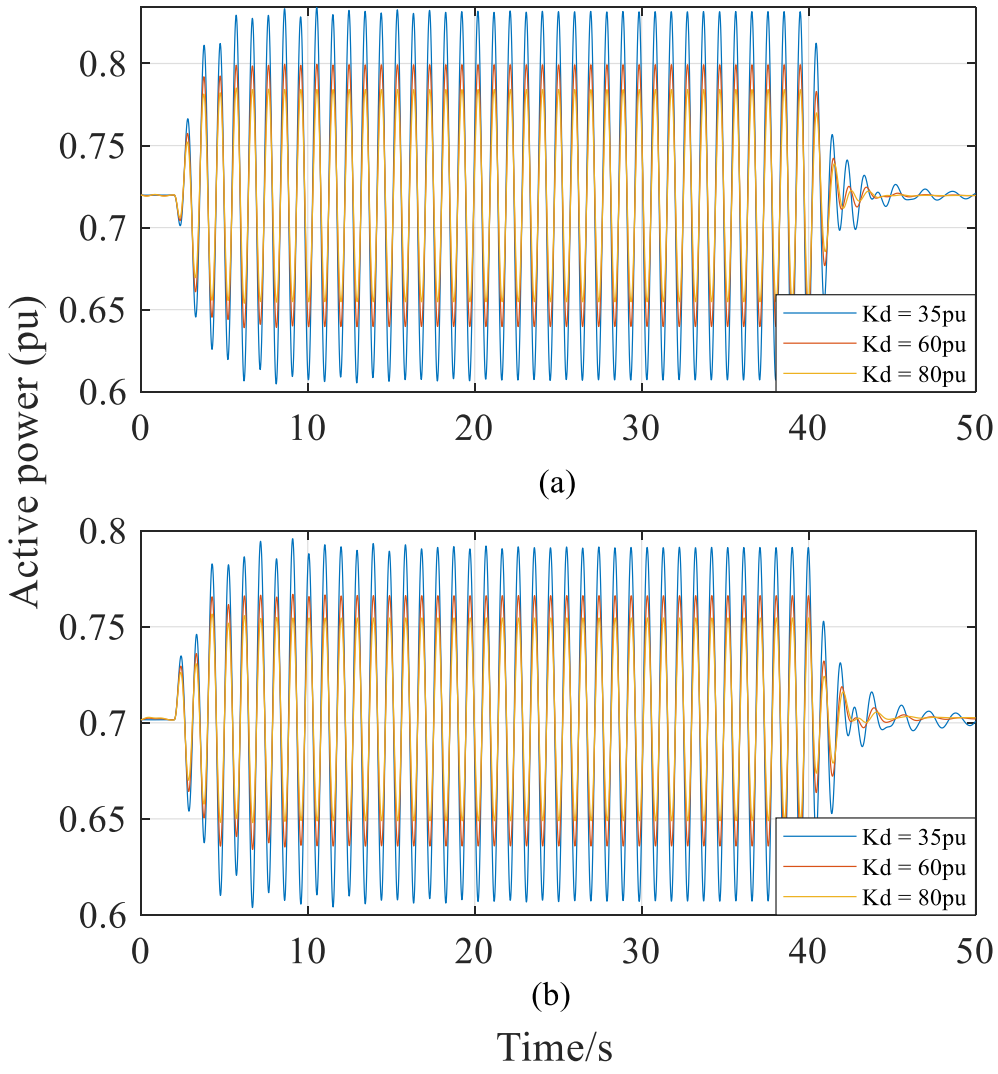

Figure 5-18 Electrical power oscillation of local mode ($f_l = f_{mode2}$). (a) active power of SG3. (b) active power of VSM.

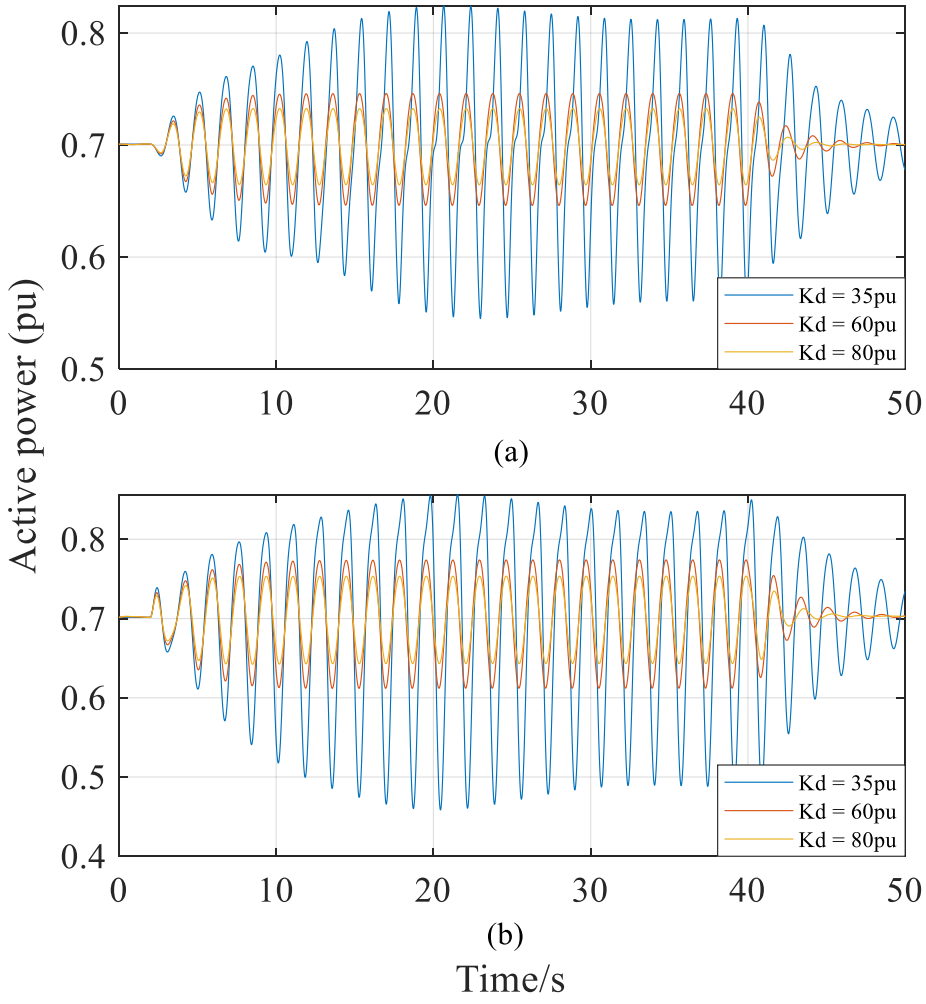

Figure 5-19 Electrical power oscillation of inter-area mode ($f_l = f_{mode3}$). (a) active power of SG1. (b) active power of VSM.

Figure 5-20 and Figure 5-21demonstrate the impacts of virtual inductance L_v on forced oscillation. For mode 2, although the damping ratio decreases with the increasing of L_v, the frequency of mode 2 changes as well which means the disturbance frequency is far away from natural frequency. As depicted in Figure 5-20, the magnitude of forced oscillation decreases with larger virtual inductance, indicating that separating the natural frequency and disturbance frequency is a more effective measure to reduce forced oscillation amplitude. However, the

virtual inductance L_v shows a different impact on mode 3. The damping ratio of mode 3 increased with higher L_v while the mode frequency almost remains the same. Consequently, the magnitude of forced oscillation is reduced.

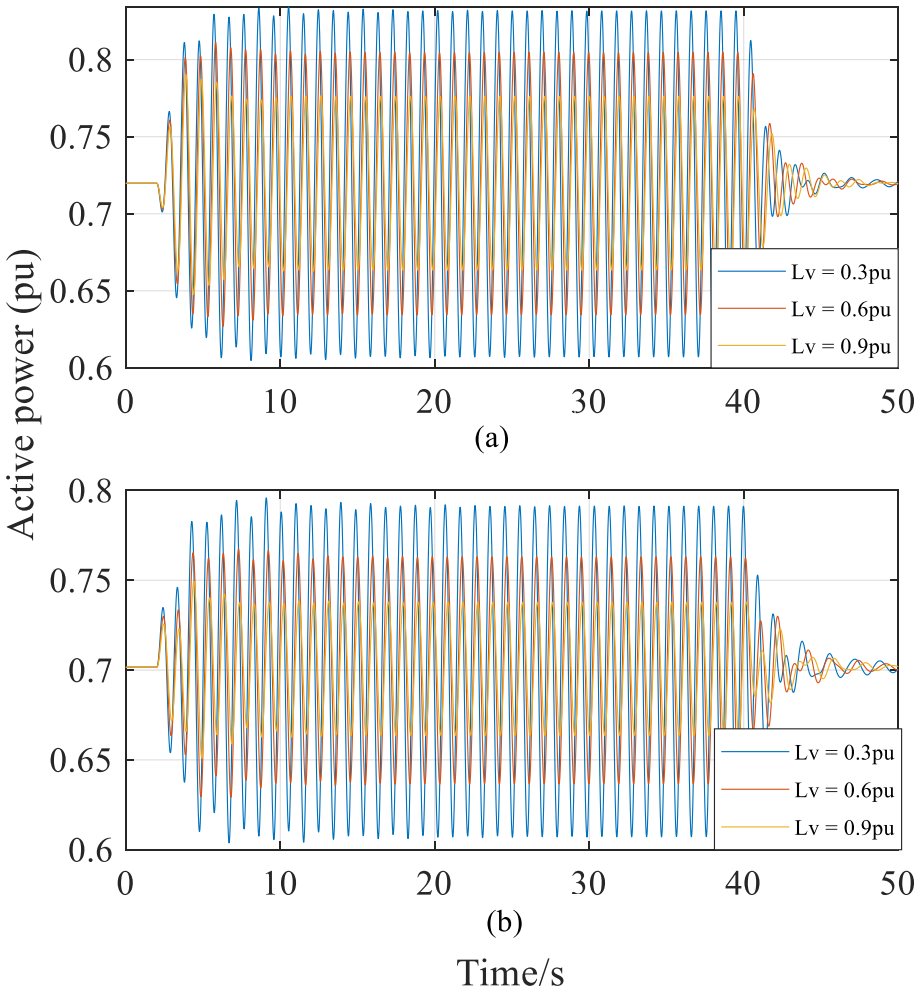

Figure 5-20 Electrical power oscillation of local mode ($f_l = f_{mode2}$). (a) active power of SG3. (b) active power of VSM.

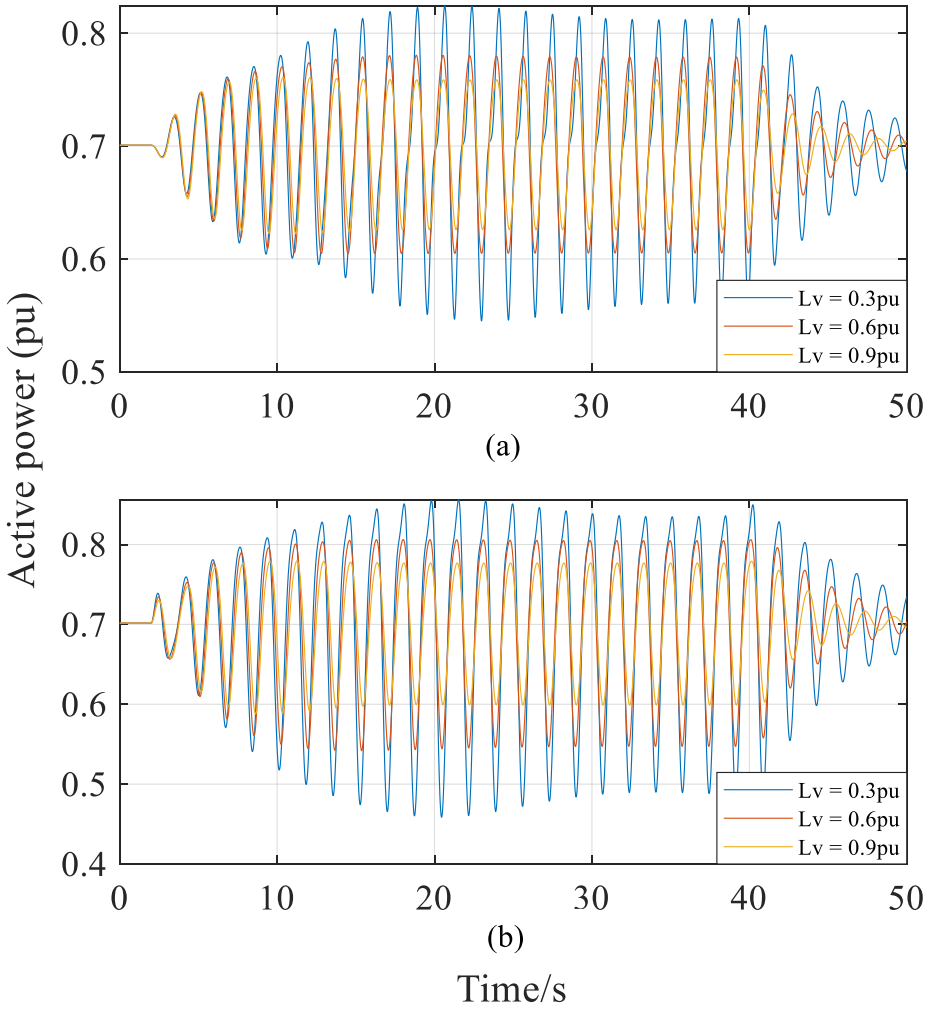

Figure 5-21 Electrical power oscillation of inter-area mode ($f_l = f_{mode3}$). (a) active power of SG1. (b) active power of VSM.

5.3.3 Comparison of VSC with VCC and VSM

The impacts of VSC with different control schemes on forced oscillation is examined in this section. the simulations of VSC station in Figure 5-12 with VCC (PV control) and VSM control are carried out (The PSSs of SG1 and SG3 are activated). The disturbance frequency is set to 0.65 Hz (inter-area mode) with 0.05pu magnitude.

Firstly, the disturbance source is located at SG1 side and simulations of converter active power are presented in Figure 5-22. It can be observed that the power oscillation magnitude of VSM controlled VSC is much larger than that of VSC with VCC. Therefore, the serious forced oscillation from SG may be propagated to the other areas of system through VSM controlled devices due to the interactions between VSM and SG (e.g., VSM controlled VSC-HVDC).

In addition, the same disturbance is relocated at converter side, and simulations of SG1 active power are depicted in Figure 5-23. It is obvious that the magnitude of forced oscillation is larger if converter is equipped with VSM control which will exaggerate the instability issue under this disturbance frequency.

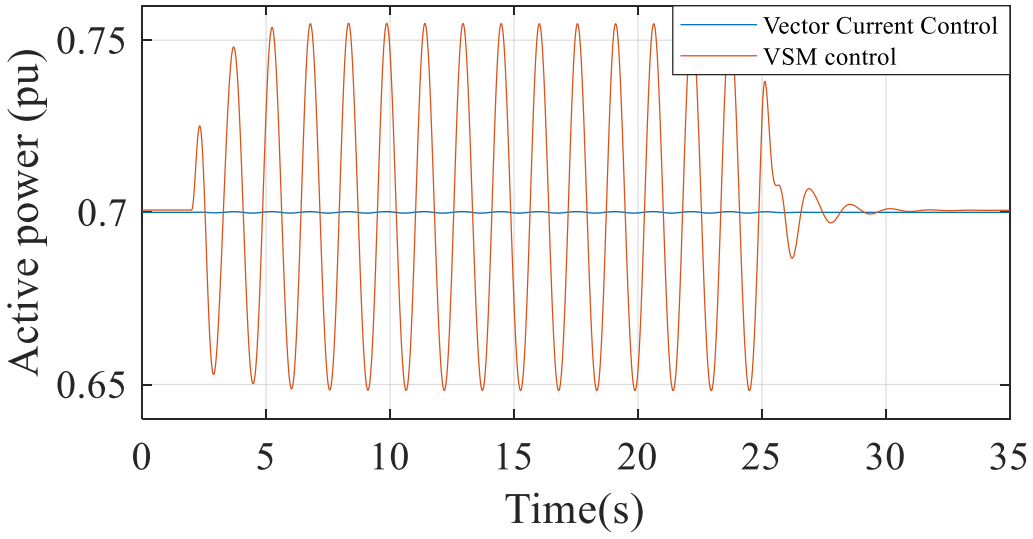

Figure 5-22 Electrical power oscillation of converter.

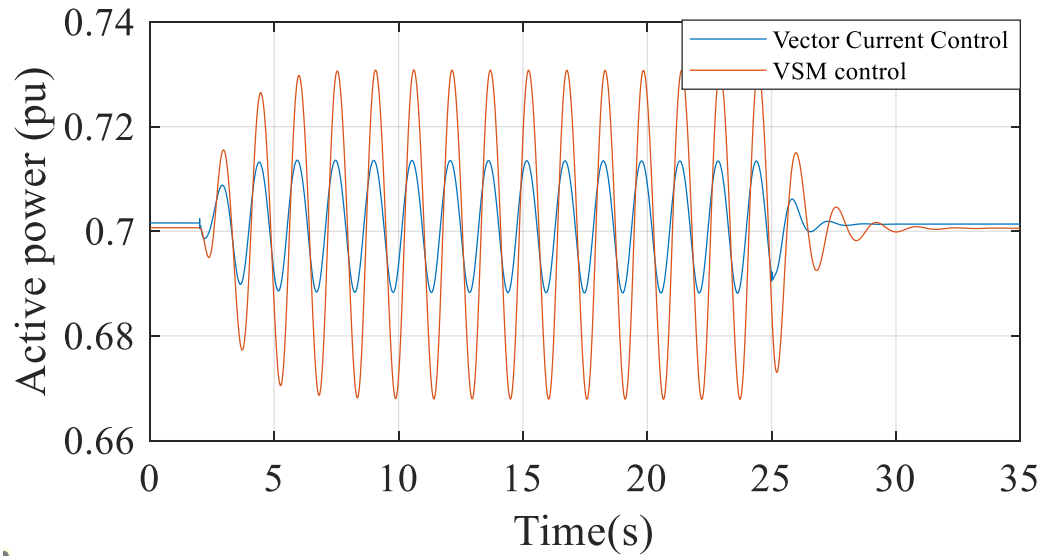

Figure 5-23 Electrical power oscillation of SG1.

A modified 39 bus system [169] is also modelled to investigate the impacts of VSM on forced oscillation. The system topology is demonstrated in Figure 5-24. Three VSC stations replace original SGs at bus 31, bus 36 and bus 37 with the same active power. The VSC adopts VSM and VCC respectively. The disturbance frequency is set according to the inter-area mode frequencies in VSM-controlled system ($f_1 = 0.633\,Hz$) and system with VCC ($f_2 = 0.916\,Hz$). The disturbance magnitude is still 0.05 pu and is located at SG1 side and VSC8 side. The simulation results are illustrated in Figure 5-25 and Figure 5-26.

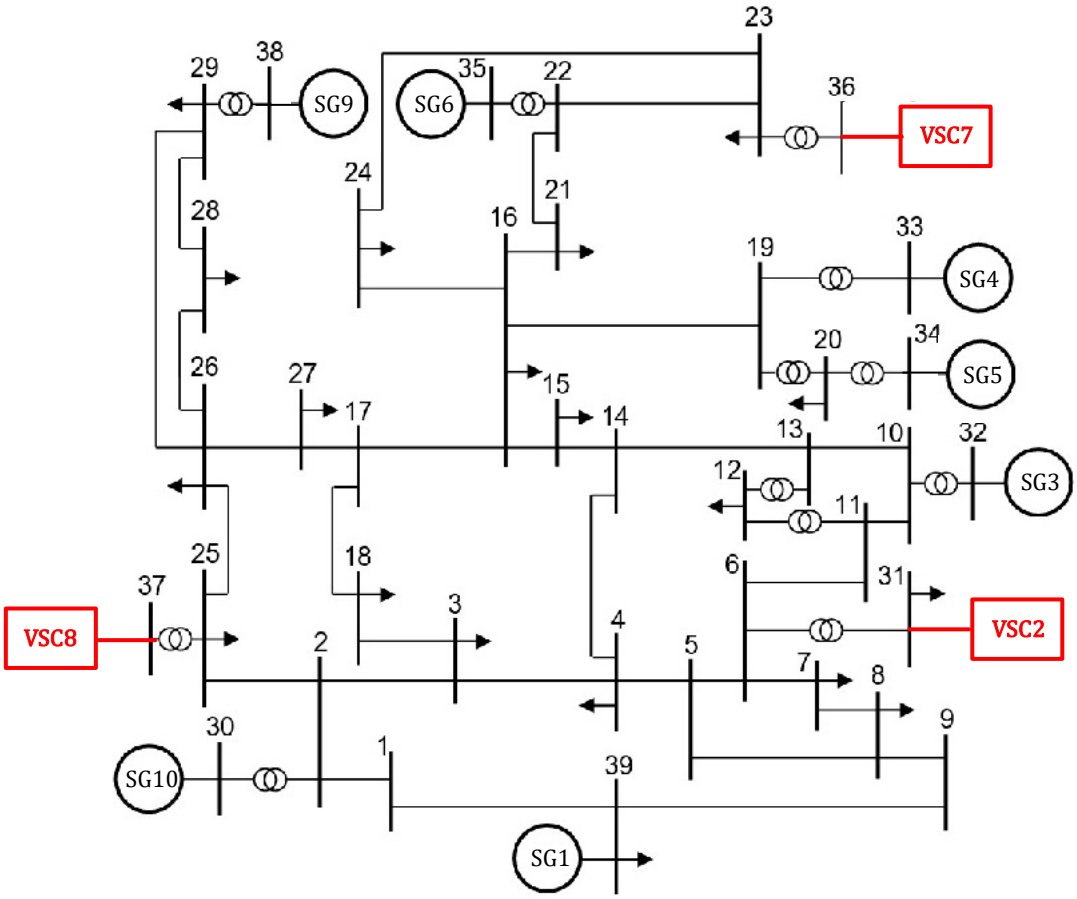

Figure 5-24 Topology of modified 39-bus system.

When disturbance frequency is set to 0.633 Hz, it can be observed from Figure 5-25 that the active power oscillation magnitudes of SG1 and VSC7 in VSM-controlled system are larger than that of system with VCC under both conditions where the forced oscillation source is at SG1 side and VSC7 side. The resonance effect exaggerates the oscillations as shown in Figure 5-25 (a), (c) and (d). Besides, the VSM-controlled VSC responds to the oscillations in low-frequency range and the active power oscillation magnitude is greater than vector-controlled system. Therefore, the forced oscillation is prone to being propagated to other devices through VSM-controlled units as described before.

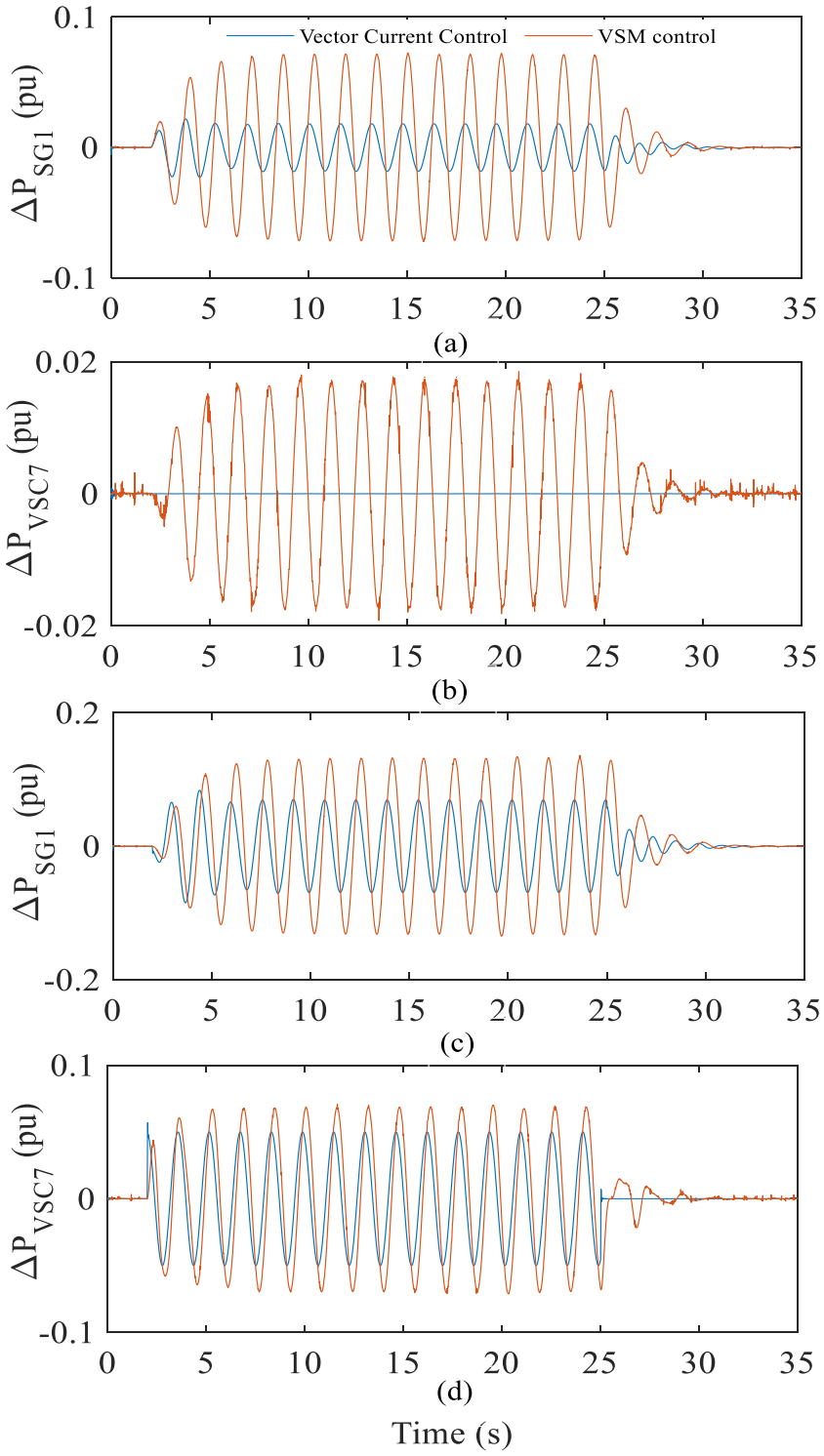

Figure 5-25 Electrical power oscillation ($f_l = 0.633\ Hz$). (a)(b) Disturbance at SG side. (c)(d) Disturbance at converter side.

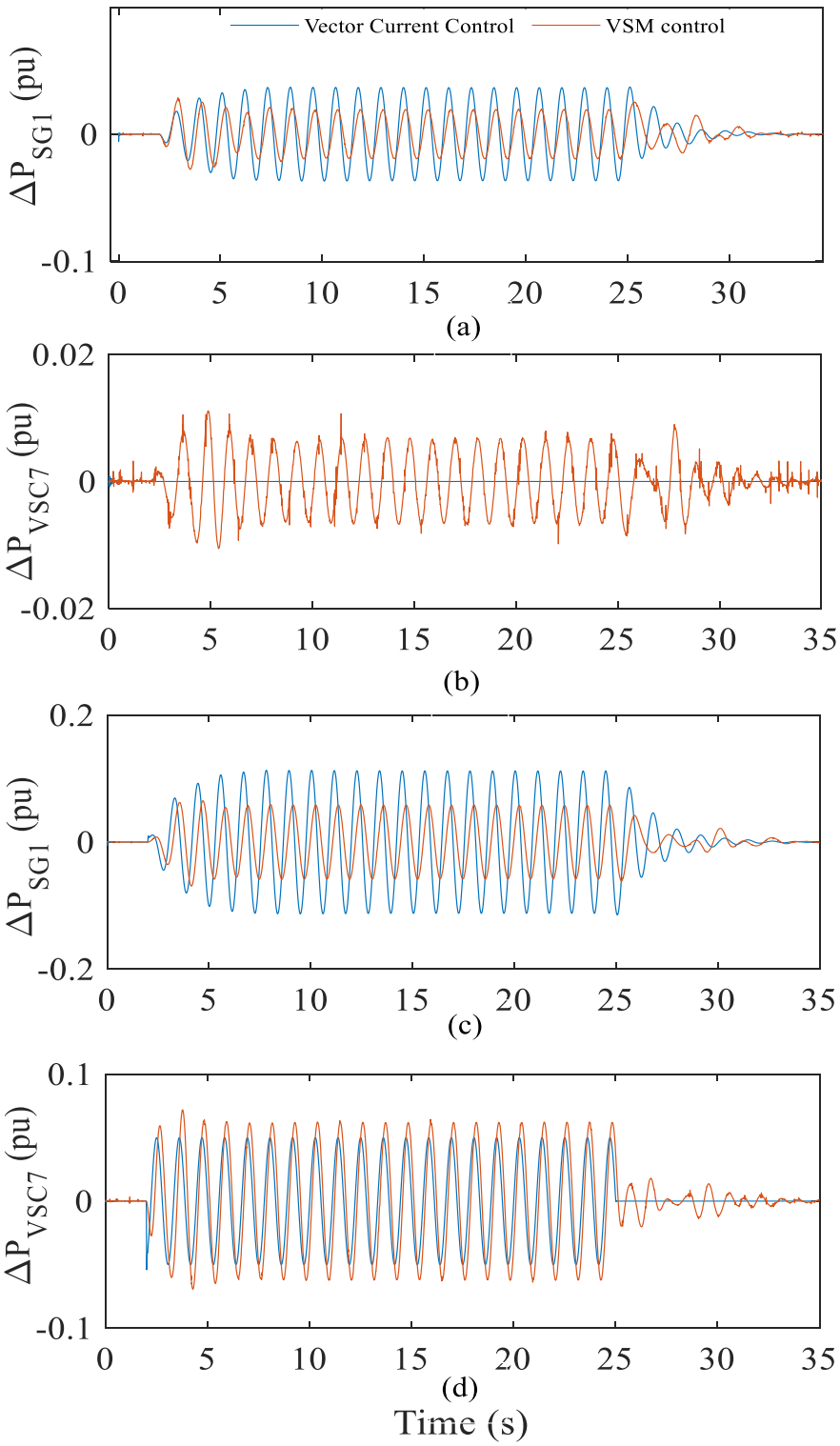

Figure 5-26 Electrical power oscillation ($f_l = 0.916\ Hz$). (a)(b) Disturbance at SG side. (c)(d) Disturbance at converter side.

If the disturbance frequency is changed to $0.916\ Hz$ which is closer to the inter-area mode frequency of system with VCC the active power oscillation magnitude of SG1 is smaller in VSM-controlled system in both cases and these simulation results are depicted in Figure 5-26 (a) and (c). However, the oscillation of active power inVSC7 is different from that of SG1. As observed in Figure 5-26 (b) and (d), the active power oscillation amplitude of VSM controlled system is still larger than the system with VCC due to the oscillation characteristics of VSM in low-frequency range.

Therefore, based on the simulation results in Figure 5-25 and Figure 5-26, it can be inferred that the oscillation magnitude is more amplified if the disturbance frequency is in the proximity of system LFO modes. For VSM-controlled converter, the instability of forced oscillation can be exaggerated due to inherited power oscillation characteristics from SG.

5.4 Summary

The impact of VSM control on power system forced oscillation have been analytically discussed in this chapter. It is demonstrated that VSM controlled converters may exaggerate forced oscillation due to the interaction between VSM and SG in the electro-mechanical range. The major findings are summarised as follows:

- For the SCIB system, it has been shown that virtual damping and virtual inertia affect the forced oscillation characteristics. The increasing of virtual inertia magnifies forced oscillation magnitude and reduces system natural frequency. Larger damping coefficient is helpful for reducing oscillation magnitude while it has little influence on system natural frequency. It has also been shown that larger virtual inductance leads to the decrease of system natural frequency and it can reduce oscillation amplitude.
- For a multi-machine system with VSM controlled devices, the adjustment of virtual controller parameters can affect the features of oscillation modes which VSM is participating in. Increasing mode damping or separating the frequency between disturbance and natural mode can reduce forced oscillation amplitude. And the latter seems to be a more effective measure.
- Comparing to the units with VCC, the forced oscillation from SG can more easily propagate to other areas through VSM controlled devices. Besides, VSM control is more likely to exaggerate the system instability of other areas

CHAPTER 6 CONCLUSIONS AND FUTURE WORK

6.1 Conclusions

Due to the increasing development of renewable energy and wide application of power converters, the power system is transforming into a power electronics dominated structure. However, growing concerns over low inertia issues promote the exploration of VSM control which aims to enhance system resilience to disturbances. This thesis focuses on investigating the impacts of VSM on power system from the perspectives of sub-synchronous stability, LFO and forced oscillation. The main research work can be summarised as following:

6.1.1 Sub-Synchronous Stability Analysis of PMSG-Based Wind Farm in Series Compensated Network

Considering the fact that wind energy is distantly located at remote areas, the series compensation technology is implemented in transmission network to shorten the electrical distance, and therefore increasing power transfer capability. However, the potential sub-synchronous instability is introduced at the mean time. The SSCI attracts increasing attention as this issue can endanger the safe operation of power system. Among these undesired interactions, PLL can adversely affect system stability in the sub-synchronous frequency range. Different from PLL-based VCC, the VSM can not only afford virtual inertia and damping provision, but also synchronise the power converters into AC grid without introducing PLL-related sub-synchronous issues. Chapter 3 mainly discusses the sub-synchronous stability of

PMSG-based wind farm with PLL-based control and PLL-less control. The main conclusions of this chapter are summarised as below:

- The detailed mathematical modelling of PMSG-based wind with VSM control and VCC in series-compensate network has been established. The modal analysis was conducted to identify the characteristics of SSO mode. A comprehensive information in terms of the mode frequency, damping ratio and dominant states of related modes were obtained to analyse the system sub-synchronous stability.
- Investigation of participation in SSO mode by vector current controlled wind turbine system and VSM controlled one were carried out to provide fundamental understanding of the control performance of these two different methods. For the studied systems, it was found that the SSO mode is affected significantly by PLL and series compensated transmission line if the wind farms adopt VCC. On the contrary, the VSM controlled wind farms are not actively engaged in the SSO. Therefore, the VSM control ensures the wind farms to accommodate higher compensation level and more wind renewables integrated to power system.
- Due to the inactive participation of VSM in SSO mode, the sub-synchronous stability can be guaranteed when considering virtual inertia and damping support. Currently, as most wind farms are employed with vector control, the system with hybrid control schemes where the VCC scheme and VSM control are implemented was investigated as well. From the studies, it was found that the SSO can be alleviated when a part of wind farm adopts VSM control.

6.1.2 Coordinated Damping Control Design for Power System with Multiple Virtual Synchronous Machines Based on Prony Method

The VSM control is originally proposed to address low inertia issues caused by the phase-out of SGs. As rotor dynamics is incorporated into VSM control, the power oscillation characteristics which are analogous to SGs are inevitably inherited as well. The LFO is one of the major concerns in large inter-connected power systems. This problem should be attentively considered when VSM is applied to large wind farms, PV plants or VSC HVDC because of the undesired interactions between VSM controllers and SGs. Therefore, Chapter 4 proposed a decentralised sequential control for coordinating the supplementary damping controllers of multiple VSMs. The main conclusions of this chapter are summarised as below:

- A comprehensive small signal analysis has been conducted to investigate the impacts of multiple VSMs on system LFO based on two-area system. It was revealed that VSMs are involved in LFO modes (both local and inter-area modes) due to the inherited oscillation characteristics. The virtual phase angle and angular frequency (θ_{vir} and ω_{vir}) participate in related modes significantly. Therefore, the VSMs can affect the system LFO modes similar to traditional SGs.
- Considering the infeasibility of obtaining system LFO modes characteristics with modal analysis, Prony analysis was applied for multiple VSMs supplementary damping controller design. It was used to extract low-frequency modes information with approximately linearizing the system model based on sampled data. Such measurement-based analysis provides more feasible and flexible design approach for SDC.

- A coordinated supplementary controller has been designed for the virtual exciter loop to provide additional damping to system. The decentralised sequential control technique was employed to coordinate the supplementary controller design for multiple VSMs. The effectiveness and robustness of designed controller were validated based on the simulation results in revised two-area and 39-bus system, it was demonstrated that the supplementary damping controllers are easy to implement and can suppress system LFOs effectively.

6.1.3 Analysis of Virtual Synchronous Machine Control on Power System Forced Oscillation

The forced oscillation has attracted increasing attention from researchers due to its serious resonance effect on power system. Such oscillation events have been recorded worldwide. Current research is mainly focused on forced oscillation source from SG. However, as mentioned above, the oscillatory characteristics of VSM makes this control scheme more likely to participate in LFO. The forced oscillation is prone to being excited when the frequency of sustained disturbance is in the proximity of system natural frequency. Therefore, Chapter 5 aims to investigate the impacts of VSM on power system forced oscillation. The main conclusions of this chapter are outlined as following:

- The mathematical analyses of an infinite bus with VSM and multi-machine system with VSM have been carried out. The linearized swing equation of infinite bus system revealed that the VSM control inherits the LFO characteristic from SG and therefore introduces a higher resonance possibility between disturbance and the inherited LFO mode. The state-space model of multi-machine system with VSM laid the foundation

for analysing the forced oscillation features. Besides, the simulations were conducted according to the specified systems above including a more complex 39-bus system to validate relevant analytical results.

- Based on aforementioned comprehensive modelling, the impacts of VSM controller parameters on the characteristics of forced oscillation are quantitively analysed. For infinite bus system, it was revealed that large virtual inertia, small virtual damping coefficient and large virtual impedance can contribute to reducing the forced oscillation magnitude. As for multi-machine system, it was found that increasing system damping ratio or shifting disturbance frequency from natural LFO frequency can reduce the magnitude of forced oscillation. And the latter seems to be a more effective measure.
- Based on the simulations of multi-machine system with VSM, it was shown that comparing to VCC, VSM control would be prone to contributing to the propagation of forced oscillation. If the frequency of disturbance is near the frequency of LFO modes, VSM may even exaggerate the instability.

6.2 Future Work

It is foreseen that more stringent regulations will be enforced by grid operators to integrate renewables into power systems. The VSM control which can provide ancillary service has been implemented in some research projects in both UK and China [172, 173], and the National Grid of UK recently specified some technical requirement for VSM operation [174]. There are still many issues related to VSM need to be further investigated. The following is a list of possible future research:

- The research in this thesis is mainly based on AC network. However, the DC grid has shown its advantages of cost-efficiency and power regulation for renewables integration. Therefore, it is worthwhile to investigate the impacts of VSM on Multi-Terminal DC System (MTDC) in terms of LFO and forced oscillation.
- The current research mainly focuses on VSM control from the source side. However, the VSM control has also been widely implemented for transmission systems and load systems. The characteristics and operation mechanism of an all-VSM based system including the source, transmission and load should be further investigated.
- For a power electronic dominated system, the black-start capability from VSC like traditional SGs is also a concern. As VSM emulates the characteristic of SG to stabilise voltage and frequency, the rapid and reliable system restoration from blackouts by VSM should be explored.

REFERENCES

[1] A. Guterres, *Carbon Neutrality by 2050: the World's Most Urgent Mission*, Dec. 2020. Accessed on: May 8, 2021. [Online]. Available: https://www.un.org/sg/en/content/sg/articles/2020-12-11/carbon-neutrality-2050-theworld%E2%80%99s-most-urgent-mission

[2] H. Ritchie and M. Roser, *Fossil fuel consumption*, Accessed on: May 9, 2021. [Online]. Available: https://ourworldindata.org/fossil-fuels

[3] International Energy Agency (IEA), *Global Energy Review 2020*, Accessed on: May 9, 2021. [Online]. Available: https://www.iea.org/reports/global-energy-review-2020

[4] S. Chu, Y. Cui, and N. Liu, "The path towards sustainable energy," *Nature Materials*, vol. 16, no. 1, pp. 16-22, 2017.

[5] M. Crippa *et al*, *Fossil CO2 emissions of all world countries - 2020 Report*, Accessed on: May 9, 2021. [Online]. Available: https://edgar.jrc.ec.europa.eu/

[6] "*UK enshrines new target in law to slash emissions by 78% by 2035"*, Apr. 20, 2021. Accessed on: Aug. 9, 2021. [Online]. Available: https://www.gov.uk/government/news/uk-enshrines-new-target-in-law-to-slash-emissions-by-78-by-2035

[7] Office for National Statistics, *Net zero and the different official measures of the UK's greenhouse gas emissions*, Jul. 24, 2019. Accessed on: Aug. 9, 2021. [Online]. Available: https://www.ons.gov.uk/economy/environmentalaccounts/articles/netzeroandthedifferentofficialmeasuresoftheuksgreenhousegasemissions/2019-07-24

[8] International Renewable Energy Agency (IRENA), *Renewable Capacity Statistics 2020*, Mar. 2020. [Online]. Available: https://www.irena.org/publications/2020/Mar/Renewable-Capacity-Statistics-2020

[9] Office for National Statistics, *Wind energy in the UK: June 2021*, Jun. 14, 2021. Accessed on: Aug. 9, 2021. [Online]. Available: https://www.ons.gov.uk/economy/environmentalaccounts/articles/windenergyintheuk/june2021

[10] J. Ostergaard *et al.*, "Energy Security Through Demand-Side Flexibility: The Case of Denmark," *IEEE Power Energy Mag.*, vol. 19, no. 2, pp. 46-55, 2021.

[11] BloombergNEF, *New Energy Outlook 2020*. [Online]. Available: https://about.bnef.com/new-energy-outlook/

[12] I. Erlich, F. Shewarega, C. Feltes, F. W. Koch, and J. Fortmann, "Offshore Wind Power Generation Technologies," *Proc. IEEE*, vol. 101, no. 4, pp. 891-905, 2013.

[13] M. Liserre, R. Cárdenas, M. Molinas, and J. Rodriguez, "Overview of Multi-MW Wind Turbines and Wind Parks," *IEEE Trans. Ind. Electron.*, vol. 58, no. 4, pp. 1081-1095, 2011.

[14] B. Kroposki *et al.*, "Achieving a 100% Renewable Grid: Operating Electric Power Systems with Extremely High Levels of Variable Renewable Energy," *IEEE Power Energy Mag.*, vol. 15, no. 2, pp. 61-73, 2017.

[15] B. Gustavsen and O. Mo, "Variable Transmission Voltage for Loss Minimization in Long Offshore Wind Farm AC Export Cables," *IEEE Trans. Power Del.*, vol. 32, no. 3, pp. 1422-1431, 2017.

[16] M. A. Ebrahim, M. N. Ahmed, H. S. Ramadan, M. Becherif, and J. Zhao, "Optimal metaheuristic-based sliding mode control of VSC-HVDC transmission systems," *Mathematics and Computers in Simulation*, vol. 179, pp. 178-193, 2021.

[17] J. Hu, *Experience of HVDC projects Role of Cigre B4 on Energy Decarbonization*. [Online]. Available: https://energia.gob.cl/sites/default/files/mini-sitio/04_cigre_joanne_hu.pdf

[18] A. Korompili, Q. Wu, and H. Zhao, "Review of VSC HVDC connection for offshore wind power integration," *Renew. Sustain. Energy Rev.*, vol. 59, pp. 1405-1414, 2016.

[19] Y. Li, H. Liu, X. Fan, and X. Tian, "Engineering practices for the integration of large-scale renewable energy VSC-HVDC systems," *Global Energy Interconnection*, vol. 3, no. 2, pp. 149-157, 2020.

[20] J. Khazaei, P. Idowu, A. Asrari, A. B. Shafaye, and L. Piyasinghe, "Review of HVDC control in weak AC grids," *Electr. Power Syst. Res.*, vol. 162, pp. 194-206, 2018.

[21] M. Darabian, A. Jalilvand, A. Ashouri, and A. Bagheri, "Stability improvement of large-scale power systems in the presence of wind farms by employing HVDC and STATCOM based on a non-linear controller," *Int. J. of Elect. Power Energy Syst.*, vol. 120, p. 106021, 2020.

[22] J. M. Maza-Ortega, E. Acha, S. García, and A. Gómez-Expósito, "Overview of power electronics technology and applications in power generation transmission and distribution," *J. Mod. Power Syst. Clean Energy*, vol. 5, no. 4, pp. 499-514, 2017.

[23] M. Wang *et al.*, "Review and outlook of HVDC grids as backbone of the transmission system," *CSEE J. Power Energy Syst.*, pp. 1-12, 2020.

[24] I. Jahn, G. Chaffey, N. Svensson, and S. Norrga, "A holistic method for optimal design of HVDC grid protection," *Electr. Power Syst. Res.*, vol. 196, p. 107234, 2021/07/01/ 2021.

[25] Q. Zhong, "Virtual Synchronous Machines: A unified interface for grid integration," *IEEE Power Electron. Mag.*, vol. 3, no. 4, pp. 18-27, 2016.

[26] International Renewable Energy Agency (IRENA), *Rise of Renewables in Cities*, Oct., 2020. [Online]. Available: https://www.irena.org/publications/2020/Oct/Rise-of-renewables-in-cities

[27] International Energy Agency (IEA), *Global EV Outlook 2020*, Jun., 2020. [Online]. Available: https://www.iea.org/reports/global-ev-outlook-2020

[28] BloombergNEF, *Electric Vehicle Outlook 2020*, [Online]. Available: https://about.bnef.com/electric-vehicle-outlook/

[29] J. Li, Y. Lei, Q. Huang, Z. Qin, and B. Chen, "Feature Analysis of Generalized Load Patterns Considering Active Load Response to Real-Time Pricing," *IEEE Access*, vol. 7, pp. 119443-119453, 2019.

[30] "IEEE Guide for Planning DC Links Terminating at AC Locations Having Low Short-Circuit Capacities," *IEEE Std 1204-1997*, pp. 1-216, 1997.

[31] H. Gu, R. Yan, and T. K. Saha, "Minimum Synchronous Inertia Requirement of Renewable Power Systems," *IEEE Trans. Power Syst.*, vol. 33, no. 2, pp. 1533-1543, 2018.

[32] W. Winter, K. Elkington, G. Bareux, and J. Kostevc, "Pushing the Limits: Europe's New Grid: Innovative Tools to Combat Transmission Bottlenecks and Reduced Inertia," *IEEE Power Energy Mag.*, vol. 13, no. 1, pp. 60-74, 2015.

[33] H. Gu, R. Yan, and T. Saha, "Review of system strength and inertia requirements for the national electricity market of Australia," *CSEE J. Power Energy Syst.*, vol. 5, no. 3, pp. 295-305, 2019.

[34] J. Fang, H. Li, Y. Tang, and F. Blaabjerg, "On the Inertia of Future More-Electronics Power Systems," *IEEE J. Emerg. Sel. Topics Power Electron.*, vol. 7, no. 4, pp. 2130-2146, 2019.

[35] G. Magdy, H. Ali, and D. Xu, "Effective control of smart hybrid power systems: Cooperation of robust LFC and virtual inertia control system," *CSEE J. Power Energy Syst.*, pp. 1-11, 2021.

[36] M. Zarifakis, W. T. Coffey, Y. P. Kalmykov, S. V. Titov, D. J. Byrne, and S. J. Carrig, "Active Damping of Power Oscillations Following Frequency Changes in Low Inertia Power Systems," *IEEE Trans. Power Syst.*, vol. 34, no. 6, pp. 4984-4992, 2019.

[37] Y. Bian, H. Wyman-Pain, F. Li, R. Bhakar, S. Mishra, and N. P. Padhy, "Demand Side Contributions for System Inertia in the GB Power System," *IEEE Trans. Power Syst.*, vol. 33, no. 4, pp. 3521-3530, 2018.

[38] P. Du and W. Li, "Frequency Response Impact of Integration of HVDC Into a Low-Inertia AC Power Grid," *IEEE Trans. Power Syst.*, vol. 36, no. 1, pp. 613-622, 2021.

[39] Q. Zhong and G. Weiss, "Synchronverters: Inverters That Mimic Synchronous Generators," *IEEE Trans. Ind. Electron.*, vol. 58, no. 4, pp. 1259-1267, 2011.

[40] S. D'Arco, J. A. Suul, and O. B. Fosso, "A Virtual Synchronous Machine implementation for distributed control of power converters in SmartGrids," *Electr. Power Syst. Res.*, vol. 122, pp. 180-197, 2015.

[41] Q. Zhong, "Power-Electronics-Enabled Autonomous Power Systems: Architecture and Technical Routes," *IEEE Trans. on Ind. Electron.*, vol. 64, no. 7, pp. 5907-5918, 2017.

[42] International Renewable Energy Agency (IRENA), *Renewable Capacity Statistics 2021*, Mar., 2021. [Online]. Available: https://www.irena.org/publications/2021/March/Renewable-Capacity-Statistics-2021

[43] J. Sun *et al.*, "Renewable energy transmission by HVDC across the continent: system challenges and opportunities," *CSEE J. Power Energy Syst.*, vol. 3, no. 4, pp. 353-364, 2017.

[44] Y. Song, "Balance the wind power generation and transmission—case study in China,", *Wind Energy*, vol. 19, no. 9, pp. 1749-1756, 2016.

[45] R. Ferdinand, M. Cupelli, and A. Monti, "Multipoint Synchronized Recordings in Offshore Wind Farms With Continuous Measurement Power Quality Meters," *IEEE Trans. Instrum. Meas.*, vol. 67, no. 12, pp. 2785-2795, 2018.

[46] L. Zhang, H. Nee, and L. Harnefors, "Analysis of Stability Limitations of a VSC-HVDC Link Using Power-Synchronization Control," *IEEE Trans. Power Syst.*, vol. 26, no. 3, pp. 1326-1337, 2011.

[47] M. Sahni *et al.*, "Sub-synchronous interaction in Wind Power Plants- part II: An ercot case study," in *Proc. IEEE Power Energy Soc. Gen.Meeting*, 2012, pp. 1-9.

[48] L. Wang, X. Xie, Q. Jiang, H. Liu, Y. Li, and H. Liu, "Investigation of SSR in Practical DFIG-Based Wind Farms Connected to a Series-Compensated Power System," *IEEE Trans. Power Syst.*, vol. 30, no. 5, pp. 2772-2779, 2015.

[49] W. Du, X. Wang, and H. Wang, "Sub-synchronous interactions caused by the PLL in the grid-connected PMSG for the wind power generation," *Int. J. Electr. Power Energy Syst.*, vol. 98, pp. 331-341, 2018.

[50] S. Zhao, N. Wang, R. Li, B. Gao, B. Shao, and S. Song, "Sub-synchronous control interaction between direct-drive PMSG-based wind farms and compensated grids," *Int. J. Electr. Power Energy Syst.*, vol. 109, pp. 609-617, 2019.

[51] Y. Xu, M. Zhang, L. Fan, and Z. Miao, "Small-Signal Stability Analysis of Type-4 Wind in Series-Compensated Networks," *IEEE Trans. Energy Convers.*, vol. 35, no. 1, pp. 529-538, 2020.

[52] M. Beza and M. Bongiorno, "On the Risk for Subsynchronous Control Interaction in Type 4 Based Wind Farms," *IEEE Trans. Sustain. Energy*, vol. 10, no. 3, pp. 1410-1418, 2019.

[53] X. Wang, M. G. Taul, H. Wu, Y. Liao, F. Blaabjerg, and L. Harnefors, "Grid-Synchronization Stability of Converter-Based Resources—An Overview," *IEEE Open J. Ind. Appl.*, vol. 1, pp. 115-134, 2020.

[54] H. Liu *et al.*, "Subsynchronous Interaction Between Direct-Drive PMSG Based Wind Farms and Weak AC Networks," *IEEE Trans. Power Syst.*, vol. 32, no. 6, pp. 4708-4720, 2017.

[55] S. Li, T. A. Haskew, R. P. Swatloski, and W. Gathings, "Optimal and Direct-Current Vector Control of Direct-Driven PMSG Wind Turbines," *IEEE Trans. Power Electron.*, vol. 27, no. 5, pp. 2325-2337, 2012.

[56] V. Yaramasu, B. Wu, P. C. Sen, S. Kouro, and M. Narimani, "High-power wind energy conversion systems: State-of-the-art and emerging technologies," *Proc. IEEE*, vol. 103, no. 5, pp. 740-788, 2015.

[57] T. Xue, J. Lyu, H. Wang, and X. Cai, "A Complete Impedance Model of a PMSG-Based Wind Energy Conversion System and Its Effect on the Stability Analysis of MMC-HVDC Connected Offshore Wind Farms," *IEEE Trans. Energy Convers.*, pp. 1-1, 2021.

[58] W. Yao, L. Jiang, J. Wen, Q. H. Wu, and S. Cheng, "Wide-Area Damping Controller of FACTS Devices for Inter-Area Oscillations Considering Communication Time Delays," *IEEE Trans. Power Syst.*, vol. 29, no. 1, pp. 318-329, 2014.

[59] X. Sui, Y. Tang, H. He, and J. Wen, "Energy-Storage-Based Low-Frequency Oscillation Damping Control Using Particle Swarm Optimization and Heuristic Dynamic Programming," *IEEE Trans. Power Syst.*, vol. 29, no. 5, pp. 2539-2548, 2014.

[60] Y. Shu, X. Zhou, and W. Li, "Analysis of low frequency oscillation and source location in power systems," *CSEE J. Power Energy Syst.*, vol. 4, no. 1, pp. 58-66, 2018.

[61] X. Zhang, C. Lu, S. Liu, and X. Wang, "A review on wide-area damping control to restrain inter-area low frequency oscillation for large-scale power systems with increasing renewable generation," *Renew. Sustain. Energy Rev.*, vol. 57, pp. 45-58, 2016.

[62] S. Eftekharnejad, V. Vittal, G. T. Heydt, B. Keel, and J. Loehr, "Small Signal Stability Assessment of Power Systems With Increased Penetration of Photovoltaic Generation: A Case Study," *IEEE Trans. Sustain. Energy*, vol. 4, no. 4, pp. 960-967, 2013.

[63] M. Garmroodi, D. J. Hill, G. Verbič, and J. Ma, "Impact of Tie-Line Power on Inter-Area Modes With Increased Penetration of Wind Power," *IEEE Trans. Power Syst.*, vol. 31, no. 4, pp. 3051-3059, 2016.

[64] J. Ma, P. Zhang, H. Fu, B. Bo, and Z. Dong, "Application of Phasor Measurement Unit on Locating Disturbance Source for Low-Frequency Oscillation," *IEEE Trans. Smart Grid*, vol. 1, no. 3, pp. 340-346, 2010.

[65] H. Ye, Y. Liu, P. Zhang, and Z. Du, "Analysis and Detection of Forced Oscillation in Power System," *IEEE Trans. Power Syst.*, vol. 32, no. 2, pp. 1149-1160, 2017.

[66] L. Zhu *et al.*, "A Comprehensive Method to Mitigate Forced Oscillations in Large Interconnected Power Grids," *IEEE Access*, vol. 9, pp. 22503-22515, 2021.

[67] P. Jiang, Z. Fan, S. Feng, X. Wu, H. Cai, and Z. Xie, "Mitigation of power system forced oscillations based on unified power flow controller," *J. Mod. Power Syst. Clean Energy,* vol. 7, no. 1, pp. 99-112, 2019.

[68] S. Feng, X. Wu, P. Jiang, L. Xie, and J. Lei, "Mitigation of Power System Forced Oscillations: An E-STATCOM Approach," *IEEE Access,* vol. 6, pp. 31599-31608, 2018.

[69] J. Follum, J. W. Pierre, and R. Martin, "Simultaneous Estimation of Electromechanical Modes and Forced Oscillations," *IEEE Trans. Power Syst.,* vol. 32, no. 5, pp. 3958-3967, 2017.

[70] Y. Liu, P. Ju, J. Chen, Y. Zhang, and Y. Yu, "Contrastive analysis of general and special forced oscillations of power systems," *CSEE J. Power Energy Syst.,* vol. 1, no. 1, pp. 61-68, 2015.

[71] S. A. N. Sarmadi and V. Venkatasubramanian, "Inter-Area Resonance in Power Systems From Forced Oscillations," *IEEE Trans. Power Syst.,* vol. 31, no. 1, pp. 378-386, 2016.

[72] M. A. Magdy and F. Coowar, "Frequency domain analysis of power system forced oscillations," *IEE Proc. Gener., Transm. Distrib.,* vol. 137, no. 4, pp. 261-268, Jul. 1990.

[73] S. A. N. Sarmadi, V. Venkatasubramanian, and A. Salazar, "Analysis of November 29, 2005 Western American Oscillation Event," *IEEE Trans. Power Syst.,* vol. 31, no. 6, pp. 5210-5211, 2016.

[74] J. G. Slootweg and W. L. Kling, "The impact of large scale wind power generation on power system oscillations," *Electr. Power Syst. Res.,* vol. 67, no. 1, pp. 9-20, 2003.

[75] D. S. L. Dolan and P. W. Lehn, "Simulation model of wind turbine 3p torque oscillations due to wind shear and tower shadow," *IEEE Trans. Energy Convers.,* vol. 21, no. 3, pp. 717-724, 2006.

[76] F. M. Hughes, O. Anaya-Lara, G. Ramtharan, N. Jenkins, and G. Strbac, "Influence of Tower Shadow and Wind Turbulence on the Performance of Power System Stabilizers for DFIG-Based Wind Farms," *IEEE Trans. Energy Convers.,* vol. 23, no. 2, pp. 519-528, 2008.

[77] C. Su, W. Hu, Z. Chen, and Y. Hu, "Mitigation of power system oscillation caused by wind power fluctuation," *IET Renew. Power Gener.,* vol. 7, no. 6, pp. 639-651, Nov. 2013.

[78] T. J. Larsen and T. D. Hanson, "A method to avoid negative damped low frequent tower vibrations for a floating, pitch controlled wind turbine," *J. Phys: Conf. Ser.,* Jul. 2007, vol. 75, no. 1, p. 012073.

[79] T. Surinkaew, K. Emami, R. Shah, S. Islam, and N. Mithulananthan, "Forced Oscillation in Power System with Renewable Generations," *Int. Conf. Smart PowerInternet Energy Syst.,* 2020, pp. 287-292: IEEE.

[80] M. Chen, D. Zhou, and F. Blaabjerg, "Modelling, Implementation, and Assessment of Virtual Synchronous Generator in Power Systems," *J. Mod. Power Syst. Clean Energy,* vol. 8, no. 3, pp. 399-411, 2020.

[81] J. Liu, Y. Miura, H. Bevrani, and T. Ise, "Enhanced Virtual Synchronous Generator Control for Parallel Inverters in Microgrids," *IEEE Trans. Smart Grid,* vol. 8, no. 5, pp. 2268-2277, 2017.

[82] S. Wang, J. Hu, and X. Yuan, "Virtual Synchronous Control for Grid-Connected DFIG-Based Wind Turbines," *IEEE J. Emerg. Sel. Topics Power Electron.,* vol. 3, no. 4, pp. 932-944, 2015.

[83] W. Yan, L. Cheng, S. Yan, W. Gao, and D. W. Gao, "Enabling and Evaluation of Inertial Control for PMSG-WTG Using Synchronverter With Multiple Virtual Rotating Masses in Microgrid," *IEEE Trans. Sustain. Energy,* vol. 11, no. 2, pp. 1078-1088, 2020.

[84] J. Fang, Y. Tang, H. Li, and X. Li, "A Battery/Ultracapacitor Hybrid Energy Storage System for Implementing the Power Management of Virtual Synchronous Generators," *IEEE Trans. Power Electron.,* vol. 33, no. 4, pp. 2820-2824, 2018.

[85] L. Huang *et al.*, "A Virtual Synchronous Control for Voltage-Source Converters Utilizing Dynamics of DC-Link Capacitor to Realize Self-Synchronization," *IEEE J. Emerg. Sel. Topics Power Electron.,* vol. 5, no. 4, pp. 1565-1577, 2017.

[86] J. Chen, M. Liu, F. Milano, and T. O'Donnell, "100% Converter-Interfaced generation using virtual synchronous generator control: A case study based on the irish system," *Electr. Power Syst. Res.,* vol. 187, p. 106475, 2020.

[87] Q. Xu, T. Dragicevic, L. Xie, and F. Blaabjerg, "Artificial Intelligence-Based Control Design for Reliable Virtual Synchronous Generators," *IEEE Trans. Power Electron.,* vol. 36, no. 8, pp. 9453-9464, 2021.

[88] L. Huang, H. Xin, and Z. Wang, "Damping low-frequency oscillations through VSC-HVDC stations operated as virtual synchronous machines," *IEEE Trans. Power Electron.,* vol. 34, no. 6, pp. 5803-5818, 2018.

[89] L. Huang, H. Xin, H. Yuan, G. Wang, and P. Ju, "Damping Effect of Virtual Synchronous Machines Provided by a Dynamical Virtual Impedance," *IEEE Trans. Energy Convers.,* vol. 36, no. 1, pp. 570-573, 2021.

[90] D. Pan, X. Wang, F. Liu, and R. Shi, "Transient Stability of Voltage-Source Converters With Grid-Forming Control: A Design-Oriented Study," *IEEE J. Emerg. Sel. Topics Power Electron.,* vol. 8, no. 2, pp. 1019-1033, 2020.

[91] A. Rodríguez-Cabero, J. Roldán-Pérez, and M. Prodanovic, "Virtual Impedance Design Considerations for Virtual Synchronous Machines in Weak Grids," *IEEE J. Emerg. Sel. Topics Power Electron.,* vol. 8, no. 2, pp. 1477-1489, 2020.

[92] X. Wang, Y. W. Li, F. Blaabjerg, and P. C. Loh, "Virtual-Impedance-Based Control for Voltage-Source and Current-Source Converters," *IEEE Trans. Power Electron.,* vol. 30, no. 12, pp. 7019-7037, 2015.

[93] W. Zhang, A. M. Cantarellas, J. Rocabert, A. Luna, and P. Rodriguez, "Synchronous Power Controller With Flexible Droop Characteristics for Renewable Power Generation Systems," *IEEE Trans. Sustain. Energy*, vol. 7, no. 4, pp. 1572-1582, 2016.

[94] Q. Zhong, P. Nguyen, Z. Ma, and W. Sheng, "Self-Synchronized Synchronverters: Inverters Without a Dedicated Synchronization Unit," *IEEE Trans. Power Electron.*, vol. 29, no. 2, pp. 617-630, 2014.

[95] W. Wu *et al.*, "Sequence impedance modeling and stability comparative analysis of voltage-controlled VSGs and current-controlled VSGs," *IEEE Trans. Ind. Electron.*, vol. 66, no. 8, pp. 6460-6472, 2018.

[96] Y. Cao *et al.*, "A virtual synchronous generator control strategy for VSC-MTDC systems," *IEEE Trans. Energy Convers.*, vol. 33, no. 2, pp. 750-761, 2017.

[97] A. Asrari, M. Mustafa, M. Ansari, and J. Khazaei, "Impedance analysis of virtual synchronous generator-based vector controlled converters for weak AC grid integration," *IEEE Trans. Sustain. Energy*, vol. 10, no. 3, pp. 1481-1490, 2019.

[98] S. Yazdani, M. Ferdowsi, M. Davari, and P. Shamsi, "Advanced Current-Limiting and Power-Sharing Control in a PV-Based Grid-Forming Inverter Under Unbalanced Grid Conditions," *IEEE J. Emerg. Sel. Topics Power Electron.*, vol. 8, no. 2, pp. 1084-1096, 2020.

[99] M. Guan, W. Pan, J. Zhang, Q. Hao, J. Cheng, and X. Zheng, "Synchronous Generator Emulation Control Strategy for Voltage Source Converter (VSC) Stations," *IEEE Trans. Power Syst.*, vol. 30, no. 6, pp. 3093-3101, 2015.

[100] R. Wang, L. Chen, T. Zheng, and S. Mei, "VSG-based adaptive droop control for frequency and active power regulation in the MTDC system," *CSEE J.Power Energy Syst.*, vol. 3, no. 3, pp. 260-268, 2017.

[101] M. Al-Tameemi, J. Liu, H. Bevrani, and T. Ise, "A Dual VSG-Based M3C Control Scheme for Frequency Regulation Support of a Remote AC Grid Via Low-Frequency AC Transmission System," *IEEE Access*, vol. 8, pp. 66085-66094, 2020.

[102] J. A. Suul, S. D. Arco, and G. Guidi, "Virtual Synchronous Machine-Based Control of a Single-Phase Bi-Directional Battery Charger for Providing Vehicle-to-Grid Services," *IEEE Trans. Ind. Appl.*, vol. 52, no. 4, pp. 3234-3244, 2016.

[103] D. Liu, Q. Zhong, Y. Wang, and G. Liu, "Modeling and control of a V2G charging station based on synchronverter technology," *CSEE J. Power Energy Syst.*, vol. 4, no. 3, pp. 326-338, 2018.

[104] H. Jafari, M. Moghaddami, T. O. Olowu, A. Sarwat, and M. Mahmoudi, "Virtual Inertia-Based Multi-Power Level Controller for Inductive Electric Vehicle Charging Systems," *IEEE J. Emerg. Sel. Topics Power Electron.*, pp. 1-1, 2020.

[105] L. Yuan, K. Meng, J. Huang, and Z. Y. Dong, "Investigating subsynchronous oscillations caused by interactions between PMSG-based wind farms and weak AC systems," *Int. J. Electr. Power Energy Syst.*, vol. 115, p. 105477, 2020.

[106] V. B. Virulkar and G. V. Gotmare, "Sub-synchronous resonance in series compensated wind farm: A review," *Renew. Sustain. Energy Rev.*, vol. 55, pp. 1010-1029, 2016.

[107] R. N. Damas, Y. Son, M. Yoon, S. Y. Kim, and S. Choi, "Subsynchronous Oscillation and Advanced Analysis: A Review," *IEEE Access*, vol. 8, pp. 224020-224032, 2020.

[108] R. K. Varma and A. Moharana, "SSR in Double-Cage Induction Generator-Based Wind Farm Connected to Series-Compensated Transmission Line," *IEEE Trans. Power Syst.*, vol. 28, no. 3, pp. 2573-2583, 2013.

[109] H. T. Ma, P. B. Brogan, K. H. Jensen, and R. J. Nelson, "Sub-Synchronous Control Interaction studies between full-converter wind turbines and series-compensated AC transmission lines," *IEEE Power Energy Soc. Gen. Meeting*, 2012, pp. 1-5.

[110] L. Zhang, L. Harnefors, and H. Nee, "Power-Synchronization Control of Grid-Connected Voltage-Source Converters," *IEEE Trans. Power Syst.*, vol. 25, no. 2, pp. 809-820, 2010.

[111] S. Sang, C. Zhang, X. Cai, M. Molinas, J. Zhang, and F. Rao, "Control of a Type-IV Wind Turbine With the Capability of Robust Grid-Synchronization and Inertial Response for Weak Grid Stable Operation," *IEEE Access*, vol. 7, pp. 58553-58569, 2019.

[112] D. Yang and X. Wang, "Unified Modular State-Space Modeling of Grid-Connected Voltage-Source Converters," *IEEE Trans. Power Electron.*, vol. 35, no. 9, pp. 9700-9715, 2020.

[113] O. Mo, S. D. Arco, and J. A. Suul, "Evaluation of Virtual Synchronous Machines With Dynamic or Quasi-Stationary Machine Models," *IEEE Trans. Ind. Electron.*, vol. 64, no. 7, pp. 5952-5962, 2017.

[114] J. Z. Zhou, H. Ding, S. Fan, Y. Zhang, and A. M. Gole, "Impact of Short-Circuit Ratio and Phase-Locked-Loop Parameters on the Small-Signal Behavior of a VSC-HVDC Converter," *IEEE Trans. Power Del.*, vol. 29, no. 5, pp. 2287-2296, 2014.

[115] L. Fan, R. Kavasseri, Z. L. Miao, and C. Zhu, "Modeling of DFIG-Based Wind Farms for SSR Analysis," *IEEE Trans. Power Del.*, vol. 25, no. 4, pp. 2073-2082, 2010.

[116] L. Fan and Z. Miao, "Nyquist-Stability-Criterion-Based SSR Explanation for Type-3 Wind Generators," *IEEE Trans. Energy Convers.*, vol. 27, no. 3, pp. 807-809, 2012.

[117] Y. Liao and X. Wang, "Impedance-Based Stability Analysis for Interconnected Converter Systems With Open-Loop RHP Poles," *IEEE Trans. Power Electron.*, vol. 35, no. 4, pp. 4388-4397, 2020.

[118] L. Harnefors, X. Wang, A. G. Yepes, and F. Blaabjerg, "Passivity-Based Stability Assessment of Grid-Connected VSCs—An Overview," *IEEE J. Emerg. Sel. Topics Power Electron.*, vol. 4, no. 1, pp. 116-125, 2016.

[119] D. Dong, B. Wen, D. Boroyevich, P. Mattavelli, and Y. Xue, "Analysis of Phase-Locked Loop Low-Frequency Stability in Three-Phase Grid-Connected Power Converters Considering Impedance Interactions," *IEEE Trans. Ind. Electron.*, vol. 62, no. 1, pp. 310-321, 2015.

[120] I. M. Canay, "A Novel Approach to the Torsional Interaction and Electrical Damping of the Synchronous Machine Part I: Theory," *IEEE Trans. Power Appa. Syst.*, vol. PAS-101, no. 10, pp. 3630-3638, 1982.

[121] Y. Huang, X. Yuan, J. Hu, P. Zhou, and D. Wang, "DC-Bus Voltage Control Stability Affected by AC-Bus Voltage Control in VSCs Connected to Weak AC Grids," *IEEE J. Emerg. Sel. Topics Power Electron.*, vol. 4, no. 2, pp. 445-458, 2016.

[122] Y. Li, H. Liu, M. Yin, and W. Song, "SSR Analysis of DFIG-based Series-compensated System Based on Complex Torque Analysis Method," *Int. Conf. Power Syst. Tech.*, 2018, pp. 1903-1908.

[123] X. Dong, J. Hou, Z. Wang, J. Pi, X. Tian, and Y. Jin, "Study on the subsynchronous resonance mechanism of DFIG based on the analysis of stator and rotor torques," *Int. Conf. Electric. Dist.*, 2016, pp. 1-6.

[124] K. Shi, W. Song, H. Ge, P. Xu, Y. Yang, and F. Blaabjerg, "Transient Analysis of Microgrids with Parallel Synchronous Generators and Virtual Synchronous Generators," *IEEE Trans. Energy Convers.*, 2019.

[125] T. Shintai, Y. Miura, and T. Ise, "Oscillation damping of a distributed generator using a virtual synchronous generator," *IEEE Trans. Power Del.*, vol. 29, no. 2, pp. 668-676, 2014.

[126] Y. Hirase, K. Sugimoto, K. Sakimoto, and T. Ise, "Analysis of resonance in microgrids and effects of system frequency stabilization using a virtual synchronous generator," *IEEE J. Emerg. Sel. Topics Power Electron.*, vol. 4, no. 4, pp. 1287-1298, 2016.

[127] J. Liu, Y. Miura, and T. Ise, "Fixed-parameter damping methods of virtual synchronous generator control using state feedback," *IEEE Access*, vol. 7, pp. 99177-99190, 2019.

[128] W. Wang, L. Jiang, Y. Cao, and Y. Li, "A Parameter Alternating VSG Controller of VSC-MTDC Systems for Low Frequency Oscillation Damping," *IEEE Trans. Power Syst.*, vol. 35, no. 6, pp. 4609-4621, 2020.

[129] F. Wilches-Bernal, R. H. Byrne, and J. Lian, "Damping of Inter-Area Oscillations via Modulation of Aggregated Loads," *IEEE Trans. Power Syst.*, vol. 35, no. 3, pp. 2024-2036, 2020.

[130] M. Baruwa and M. Fazeli, "Impact of Virtual Synchronous Machines on Low-Frequency Oscillations in Power Systems," *IEEE Trans. Power Syst.*, vol. 36, no. 3, pp. 1934-1946, 2021.

[131] J. Alipoor, Y. Miura, and T. Ise, "Power system stabilization using virtual synchronous generator with alternating moment of inertia," *IEEE J. Emerg. Sel. Topics Power Electron.,* vol. 3, no. 2, pp. 451-458, 2014.

[132] B. Gao, C. Xia, N. Chen, K. M. Cheema, L. Yang, and C. Li, "Virtual synchronous generator based auxiliary damping control design for the power system with renewable generation," *Energies,* vol. 10, no. 8, p. 1146, 2017.

[133] M. Ebrahimi, S. A. Khajehoddin, and M. Karimi-Ghartemani, "An Improved Damping Method for Virtual Synchronous Machines," *IEEE Trans. Sustain. Energy,* vol. 10, no. 3, pp. 1491-1500, 2019.

[134] Z. Shuai, W. Huang, Z. J. Shen, A. Luo, and Z. Tian, "Active Power Oscillation and Suppression Techniques between Two Parallel Synchronverters during Load Fluctuations," *IEEE Trans. Power Electron.,* 2019.

[135] J. M. Mauricio and A. E. Leon, "Improving Small-Signal Stability of Power Systems With Significant Converter-Interfaced Generation," *IEEE Trans. Power Syst.,* vol. 35, no. 4, pp. 2904-2914, 2020.

[136] M. Chen, D. Zhou, and F. Blaabjerg, "Active Power Oscillation Damping Based on Acceleration Control in Paralleled Virtual Synchronous Generators System," *IEEE Trans. Power Electron.,* vol. 36, no. 8, pp. 9501-9510, 2021.

[137] H. Ye, W. Pei, L. Kong, and T. An, "Low-Order Response Modeling for Wind Farm-MTDC Participating in Primary Frequency Controls," *IEEE Trans. Power Syst.,* vol. 34, no. 2, pp. 942-952, 2019.

[138] Y. Wang, J. Meng, X. Zhang, and L. Xu, "Control of PMSG-Based Wind Turbines for System Inertial Response and Power Oscillation Damping," *IEEE Trans. Sustain. Energy,* vol. 6, no. 2, pp. 565-574, 2015.

[139] L. Fan, H. Yin, and Z. Miao, "On Active/Reactive Power Modulation of DFIG-Based Wind Generation for Interarea Oscillation Damping," *IEEE Trans. Energy Convers.,* vol. 26, no. 2, pp. 513-521, 2011.

[140] C. Zhang, D. Ke, Y. Sun, C. Y. Chung, J. Xu, and F. Shen, "Coordinated Supplementary Damping Control of DFIG and PSS to Suppress Inter-Area Oscillations With Optimally Controlled Plant Dynamics," *IEEE Trans. Sustain. Energy,* vol. 9, no. 2, pp. 780-791, 2018.

[141] M. Edrah, K. L. Lo, and O. Anaya-Lara, "Impacts of High Penetration of DFIG Wind Turbines on Rotor Angle Stability of Power Systems," *IEEE Trans. Sustain. Energy,* vol. 6, no. 3, pp. 759-766, 2015.

[142] H. Huang and C. Y. Chung, "Coordinated Damping Control Design for DFIG-Based Wind Generation Considering Power Output Variation," *IEEE Trans. Power Syst.,* vol. 27, no. 4, pp. 1916-1925, 2012.

[143] T. Surinkaew and I. Ngamroo, "Coordinated Robust Control of DFIG Wind Turbine and PSS for Stabilization of Power Oscillations Considering System Uncertainties," *IEEE Trans. Sustain. Energy*, vol. 5, no. 3, pp. 823-833, 2014.

[144] J. Deng, C. Li, and X.-P. Zhang, "Coordinated design of multiple robust FACTS damping controllers: A BMI-based sequential approach with multi-model systems," *IEEE Trans. Power Syst.*, vol. 30, no. 6, pp. 3150-3159, 2015.

[145] M. Mao, C. Qian, and Y. Ding, "Decentralized coordination power control for islanding microgrid based on PV/BES-VSG," *CPSS Trans. Power Electron. Appl.*, vol. 3, no. 1, pp. 14-24, 2018.

[146] S. Adhikari, Q. Xu, Y. Tang, P. Wang, and X. Li, "Decentralized control of two DC microgrids interconnected with tie-line," *J. Mod. Power Syst. Clean Energy*, vol. 5, no. 4, pp. 599-608, 2017.

[147] J. Turunen *et al.*, "Comparison of Three Electromechanical Oscillation Damping Estimation Methods," *IEEE Trans. Power Syst.*, vol. 26, no. 4, pp. 2398-2407, 2011.

[148] Y. Hua and T. K. Sarkar, "Matrix pencil method for estimating parameters of exponentially damped/undamped sinusoids in noise," *IEEE Trans. Acoust., Speech, Signal Process.*, vol. 38, no. 5, pp. 814-824, 1990.

[149] D. Trudnowski, J. Smith, T. Short, and D. Pierre, "An application of Prony methods in PSS design for multimachine systems," *IEEE Trans. Power Syst.*, vol. 6, no. 1, pp. 118-126, 1991.

[150] A. R. Borden and B. C. Lesieutre, "Variable Projection Method for Power System Modal Identification," *IEEE Trans. Power Syst.*, vol. 29, no. 6, pp. 2613-2620, 2014.

[151] X. Xu, W. Ju, B. Wang, and K. Sun, "Real-Time Damping Estimation on Nonlinear Electromechanical Oscillation," *IEEE Trans. Power Syst.*, vol. 36, no. 4, pp. 3142-3152, 2021.

[152] M. Ghorbaniparvar, "Survey on forced oscillations in power system," *J. Mod. Power Syst. Clean Energy*, vol. 5, no. 5, pp. 671-682, 2017.

[153] S. Chevalier, P. Vorobev, and K. Turitsyn, "A Bayesian Approach to Forced Oscillation Source Location Given Uncertain Generator Parameters," *IEEE Trans. Power Syst.*, vol. 34, no. 2, pp. 1641-1649, 2019.

[154] B. Wang and K. Sun, "Location methods of oscillation sources in power systems: a survey," *J. Mod. Power Syst. Clean Energy*, vol. 5, no. 2, pp. 151-159, 2017.

[155] J. Tan, X. Wang, T. Wang, and Y. Zhang, "Alleviation of oscillations power of wind farm using flywheel energy storage," in *Proc. IEEE PES Gen. Meeting Conf. Expo.*, Jul. 2014, pp. 1-5.

[156] Y. Xu, W. Bai, S. Zhao, J. Zhang, and Y. Zhao, "Mitigation of forced oscillations using VSC-HVDC supplementary damping control," *Electr. Power Syst. Res.*, vol. 184, p. 106333, 2020.

[157] Y. Xia, K. H. Ahmed, and B. W. Williams, "Wind Turbine Power Coefficient Analysis of a New Maximum Power Point Tracking Technique," *IEEE Trans. Ind. Electron.*, vol. 60, no. 3, pp. 1122-1132, 2013.

[158] H. Huang, C. Mao, J. Lu, and D. Wang, "Small-signal modelling and analysis of wind turbine with direct drive permanent magnet synchronous generator connected to power grid," *IET Renewable Power Gener.* vol. 6, no. 1, pp. 48-58, 2012.

[159] P. Kundur, N. J. Balu, and M. G. Lauby, *Power system stability and control*. McGraw-hill New York, 1994.

[160] H. Geng, G. Yang, D. Xu, and B. Wu, "Unified Power Control for PMSG-Based WECS Operating Under Different Grid Conditions," *IEEE Trans. Energy Convers.*, vol. 26, no. 3, pp. 822-830, 2011.

[161] A. D. Hansen and G. Michalke, "Multi-pole permanent magnet synchronous generator wind turbines' grid support capability in uninterrupted operation during grid faults," *IET Renewable Power Gener.*, vol. 3, no. 3, pp. 333-348, 2008.

[162] Q.-C. Zhong, Z. Ma, W.-L. Ming, and G. C. Konstantopoulos, "Grid-friendly wind power systems based on the synchronverter technology," *Energy Convers. Manage.*, vol. 89, pp. 719-726, 2015.

[163] J. Yao, X. Wang, J. Li, R. Liu, and H. Zhang, "Sub-Synchronous Resonance Damping Control for Series-Compensated DFIG-Based Wind Farm With Improved Particle Swarm Optimization Algorithm," *IEEE Trans. Energy Convers.*, vol. 34, no. 2, pp. 849-859, 2019.

[164] P. W. Sauer and M. A. Pai, *Power system dynamics and stability*. Upper Saddle River, NJ, USA: Prentice-Hall,, 1998.

[165] H. Xin, L. Huang, L. Zhang, Z. Wang, and J. Hu, "Synchronous Instability Mechanism of P-f Droop-Controlled Voltage Source Converter Caused by Current Saturation," *IEEE Trans. Power Syst.*, vol. 31, no. 6, pp. 5206-5207, 2016.

[166] I. Abdulrahman, "MATLAB-Based Programs for Power System Dynamic Analysis," *IEEE Open Access J. Power Energy*, vol. 7, pp. 59-69, 2020.

[167] H. T. Nguyen, G. Yang, A. H. Nielsen, P. H. Jensen, and B. Pal, "Applying Synchronous Condenser for Damping Provision in Converter-Dominated Power System," *J. Mod. Power Syst. Clean Energy*, pp. 1-9, 2020.

[168] M. Edrah *et al.*, "Effects of POD Control on a DFIG Wind Turbine Structural System," *IEEE Trans. Energy Convers.*, 2020.

[169] M. Pai, *Energy function analysis for power system stability*. Springer Science & Business Media, 2012.

[170] C. D. Meyer, *Matrix analysis and applied linear algebra*. Siam, 2000.

[171] S. Wang, J. Hu, X. Yuan, and L. Sun, "On Inertial Dynamics of Virtual-Synchronous-Controlled DFIG-Based Wind Turbines," *IEEE Trans. Energy Convers.*, vol. 30, no. 4, pp. 1691-1702, 2015.

[172] A. Roscoe *et al.*, "Response of a grid forming wind farm to system events, and the impact of external and internal damping," *IET Renewable Power Gener.*, vol. 14, no. 19, pp. 3908-3917, 2020.

[173] B. Tian, X. Mo, Y. Shen, W. Lei, and P. Xu, "Prospect and key techniques of Global Energy Interconnection Zhangjiakou Innovation Demonstration Zone," *Global Energy Interconnection*, 2018.

[174] National Grid ESO, *Minimum Specification Required for Provision of GB Grid Forming (GBGF) Capability (formerly Virtual Synchronous Machine/VSM Capability)*. Jun. 23, 2021. [Online]. Available: https://www.nationalgrideso.com/industry-information/codes/grid-code-old/modifications/gc0137-minimum-specification-required.

LIST OF PUBLICATIONS

Journal papers:

[1] **Min Zhao**, Hang Yin, Ying Xue, Xiao-Ping Zhang, Yuanliang Lan, "Coordinated Damping Control Design for Power System with Multiple Virtual Synchronous Generators Based on Prony Method," *IEEE Open Access Journal of Power and Energy*, revised and under review.

[2] **Min Zhao**, Xiao-Ping Zhang, Ying Xue, "Sub-synchronous Stability Analysis of PMSG-Based Wind Farm with Series-Compensated Network," *IEEE Access*, under review.

[3] **Min Zhao**, Xiao-Ping Zhang, Ying Xue, "Analysis of Virtual Synchronous Machine Control on Power System Forced Oscillation," *IEEE Access*, under review.

Conference papers:

[4] Min Zhao, H. Yin, Y. Xue and X. Zhang, "The impact on Power System with Wind Integration from Multiple Virtual Synchronous Machines", *2019 IEEE International Conference on Systems, Man and Cybernetics (SMC)*. 2019, pp. 1068-1073, doi: 10.1109/SMC.2019.8914561

APPENDIX

TABLE A-1
PARAMETERS OF SINGLE PMSG (VALUES IN PU IF NOT SPECIFIED)

PSMG-based wind turbine	Value
Rated power	2.5 MW
Rated voltage	0.69 kV
DC-link capacitor V_{dc}	1.5 kV
DC-link capacitor C_{dc}	110 mF
Stator inductance L_{sd}, L_{sq}	0.4896, 0.5396
Stator resistance R_s	0.0179
Rotor flux linkage ψ_f	1.0
Converter inductance L_c	0.1980
Converter resistance R_c	0.0079

TABLE A-2
PARAMETERS OF AC NETWORK (VALUES IN PU IF NOT SPECIFIED)

Symbol	Value
Rated power	100 MVA
Rated voltage	220 kV
Line inductance L_g	0.4
Line resistance R_g	0.07
Compensation level	32.5%

TABLE A-3
PARAMETERS OF CONTROLLERS (VALUES IN PU IF NOT SPECIFIED)

RSC controller	Value
k_{p1}, k_{i1}	2.0, 5.0
k_{p2}, k_{i2}	10, 100
GSC controller (Vector current control)	**Value**
k_{p3}, k_{i3}	0.25, 25
k_{p4}, k_{i4}	0.2, 20
k_{p5}, k_{i5}	0.4758, 3.2655
GSC controller (VSM control)	**Value**
H, K_d	5, 50
K, D_q	10, 5
L_v, R_v	0.1, 0.01

TABLE A-4
PARAMETERS OF VSM CONTROLLER WITH VIRTUAL IMPEDANCE[90, 135]

H	7 s	K	5 pu
K_d	35 pu	D_q	10 pu
L_v	0.3 pu	R_v	0.1 pu
D_p	20 pu		